Republic of Iraq
Ministry of Higher Education
And Scientific Research
University of Babylon
College of Materials Engineering
Department of Metallurgical Engineering

Effect of (Zr,Mo) on Microstructure and Properties of NiTi Shape Memory Biomedical Alloys

A Thesis

Submitted to the Department of Metallurgical Engineering of College of Materials Engineering University of Babylon in Partial Fulfillment of the Requirements for the Degree of Master in Materials Engineering/Metallurgical

By

Nareeman Yaseen Ali Abod

Supervised by

Prof.Dr.Jassim Mohammed Salman Al-Murshdy

2021 A.D 1443 A.H

بسم الله الرحمن الرحيم

(أَللَّهُ لَا إِلَهَ إِلَّا هُوَ الْحَيُّ الْقَيُّومُ لَا تَأْخُذُهُ سِنَةٌ وَلَا نَوْمٌ لَهُ مَا فِي السَّمَاوَاتِ وَمَا فِي الْأَرْضِ مَنْ ذَا الَّذِي يَشْفَعُ عِنْدَهُ إِلَّا بِإِذْنِهِ يَعْلَمُ مَا بَيْنَ أَيْدِيهِمْ وَمَا خَلْفَهُمْ وَلَا يُحِيطُونَ بِشَيْءٍ مِنْ عِلْمِهِ إِلَّا بِمَا شَاءَ وَسِعَ كُرْسِيُّهُ السَّمَاوَاتِ وَالْأَرْضَ وَلَا يَئُودُهُ حِفْظُهُمَا وَهُوَ الْعَلِيُّ الْعَظِيمُ)

صدق الله العظيم

سورة البقرة ، الآية (255)

Abstract

The shape memory alloys properties of nickel titanium (NiTi) were first discovered in the early 1960s, as shape memory alloys had many applications, NiTi alloys have been increasingly considered in external and internal biomedical devices, for example cardiac stent wires, orthodontics, vascular and bone fractures, fixing plates and screws, self-expanding urinary tracts. NiTi shape memory alloy was prepared from elemental nickel and titanium powders by powder metallurgy Technique, at 800 MPa compacting pressure, 950 ˚C temperature and10^{-3} torr vacuum atmosphere.

In order to evaluate the NiTi performances conclude several characterization such as X-ray diffraction analysis XRD, Scanning electron microscopy (SEM) with EDS, micro hardness, electrochemical test in solution Ringer solution.

The results upon XRD analysis revealed that Ni-Ti were completely changed into NiTi (both cubic and monoclinic phases) and Ni_3Ti phase but When zirconium was added at a rate of 3%, a compound appeared, which is Ni_7Zr_2. The samples are ground in a dry atmosphere and the samples are polished after sintering.optical microscopy, x-ray diffraction techniques ,micro hardness test was conducted using Brinell hardness machine. It was observed that as the Zr content is increased, the hardness values increased. For instance, equal at 30% of Ni Ti had a hardness of 127.05 which increased significantly as Zr content was increased to 30 at % . Increase in hardness also suggests that the workability . It was observed that as the Mo content is increased, the hardness values increased. For instance, Ni Ti had a hardness of 127.05 which increased was increased to 40at%. In the optical microscope and SEM, bright areas, and dark areas appear. This confirms the phases appearing in XRD, which are in the dark areas Ni_3Ti and the bright areas NiTi. Due to molybdenum, optical microscopy

reveals surface characteristics such as open pores and grain borders, as well as the distinction between the phases NiTi and Ni_3Ti.

The corrosion of NiTi alloys showed significant improvement after Mo and Zr addition in ringer solution. It was demonstrated that more considerable progress with the acquisition of the(1,2&3)wt% Zr was (87,89 &57)%respectively in Ringer solution. While with the addition of (1,2&3)wt%of Mo the improvement percentage in Ringer was (50,16&8)%), respectively. However, the Zr additive result to the base alloy gives excellent properties.

The improvement of wear rate for NiTi When adding Mo& Zr under load 15N , When adding Mo, the weight loss is less than when adding Zr and weight loss increases with increases time.

List of symbols

Abbreviations	Description	Unit
XRD	X-Ray Diffraction	
SEM	Scanning Electron Microcopy	
EDS	Energy Dispersive Spectroscopy	
SMA	Shape Memory Alloy	
NiTi	Nickel-Titanium	
PM	Powder Metallurgy	
A_f	Reverse (austenite) transformation final temperature up on heating	**°C**
A_s	Reverse (austenite) transformation start temperature up on heating	**°C**
B19'	Martensite Phase	
B2	Austenite Phase	
Icorr.	Corrosion Current Density	**µA/cm²**
M_f	Martensite final temperature up on cooling	
M_S	Martensite start temperature up on cooling	
Nitinol	Nickel-Titanium in Naval Ordnance Laboratory	
O.C.P.	Open Circuit Potential	**Mv**
SME	Shape Memory Effect	**%**
S.R.	Shape recovery	**%**
A_F	Reverse(austenite) transformation final up on heating	
A_S	Reverse(austenite) transformation start up on heating	

LOM	Light Optical Microscope	
Ti	Titanium	
Ni	Nickel	
Zr	Zirconium	
Mo	Molybdenum	
db	Average impression diameter before heating	**M**
da	Average impression diameter after heating	**M**
CR	Corrosion Rate	
NASA	National Aeronautics Space Adminstration	
EAM	Embedded Atom Method	

List of Tables

Chapter Two : **Theoretical Part & Literature Review**	
Table (2-1): Some of the typical properties of these alloys	13
Chapter Three : **Experimental Work**	
Table (3.1): The percentage of elements used in current study	37
Table (3.2): The Purity and the Average Particle Size of the Powders Used	41
Table (3.3): Chemical Composition Ringer's Solution	48

Chapter Four : Result and Discussion	
Table (4-1) illustrated the chemical composition for A alloy.	61
Table (4-2) illustrated the chemical composition for B alloy.	62
Table (4-3) illustrated the chemical composition for C alloy	63
Table (4-4) illustrated the chemical composition for D alloy.	64
Table (4-5) illustrated the chemical composition for E alloy.	65
Table (4-6) illustrated the chemical composition for F alloy.	66
Table (4-7) illustrated the chemical composition for G alloy.	67
Table (4-8): Corrosion Current (Icorr.), and Corrosion Rate (C.R.) for All Alloys in Ringer Solution at 37±1°C	71

Chapter One

Introduction

1.1 Introduction

Shape memory alloys (SMAs) are known primarily for one fundamental and unique property, the ability to remember and recover from large strains without permanent deformation. Shape memory alloys can exist in two different temperature-dependent crystal structures (phases) called lower temperature phase (martensite) and higher temperature phase (austenite). Unlike most conventional metals that recover less than 1% strain before plastic deformation, shape-memory alloys SMAs undergo a diffusionless, thermoelastic martenstic phase transformation that enables the material to deform via a twinning process rather than the conventional dislocation slip mechanism and allows complete recovery of strains as large as 8% [1,2].

Two separate mechanical effects characterize the response of shape memory alloys; stress effect (pseudoelasticity) and thermal effect (SME). In pseudoelasticity, or superelasticity martensite reverts to the austenite phase upon unloading without heating. On the other hand, thermal effect requires heating to recover the martensite phase to the austenite phase because the deformation is irreversible. Thermal effect can also be thermally induced, in this case, the structure consists of thermally induced martensite [3].

NiTi shape memory alloys are the most important group of shape memory alloys. The chemical composition of NiTi shape memory alloys are ranges from(53-57)wt% nickel balance titanium [3,4].

There are many commercial applications of NiTi shape memory alloys. These alloys exhibit strong shape memory effect and pseudoelastic

behavior, which are completely new properties compared to the conventional metal alloys. These new properties make this material ideal for a variety of applications. It also exhibits resistance to corrosion and is biocompatible, making it suitable for use in different fields of biomedical applications such as (cardiovascular, orthodontics, orthopedics and neurosurgery) [5,6].

Recently, the production of NiTi shape memory alloys (SMAs) as porous materials has received considerable interest due to their porous structures and extraordinary mechanical characteristics similar to those of some natural biomaterials for hard tissue implants [7].The porous nature of the material enables the existing bone tissue to migrate inward, increasing bonding strength. Furthermore, the implant properties can be engineered to match those of the bone[8].

The main concern of using Nitinol medical application is the dissolution of free nickel ions which are toxic and may even cause carcinogenic effects. This harmful metal release can be precluding an appropriate surface modification [9].

Nitinol Corrosion resistance is mainly effected by its surface condition chemistry .Ti is very active element and when nitinol is in contact with even a weak oxidizing enviro with nitinol, a very thin native passive layer dominated by titanium dioxide forms on the surface of Nitinol.

1.2. Processing of Nitinol

Various methods for producing conventional porous metals and alloys currently exist, including casting, metallic deposition, and powder metallurgy. One casting technique commonly used for producing metal foams includes the injection of gas into a metal melt. Other methods employ powder metallurgy techniques including conventional sintering,

Self-propagating High-temperature Synthesis (SHS), and sintering at elevated pressure using a Hot Isostatic Press (HIP)[5].

Due to the high melting temperature (1310°C) and relatively high density of NiTi (6.45 g/cm3), conventional fabrication techniques of casting NiTi from a melt can be difficult due to the reactivity of the melt that often results in segregation defects[5] . In addition, it can be seen in the phase diagram of NiTi that the B2 phase region is very narrow at temperatures below 950°C and NiTi alloys have a tendency to decompose upon cooling, forming other stable intermetallics such as Ni_3Ti and $NiTi_2$, which do not exhibit the shape memory characteristics of binary NiTi. These difficulties have influenced to utilize powder metallurgy techniques to prepare porous samples of NiTi SMA in the present study. Powder metallurgy offers the opportunity of employing either elemental or pre-alloyed starting powders. However, additional processing techniques required for producing pre-alloyed NiTi powders are both difficult and expensive. For this reason, binary NiTi SMA mainly fabricated from elemental powders using the powder metallurgy techniques[6].

1.3 Biocompatibility

Biocompatibility is the ability of a material to perform with a condign Host response in a specific application. And Biomaterials are the materials which used in medicine and dentistry and they become in contact with living tissue as a body implants or medical devices. There are very demanding requisites for a material to be used as biomaterial. It must have special mechanical, physical and chemical properties. However, the first and the most urgent requirement is material biocompatibility with the human body [6].

The NiTi alloy is one of the most popular SMAs (shape memory alloys) in bioengineering applications owing to its biocompatibility and its other remarkable properties. Titanium is well recognized to be biocompatible with long-term corrosion resistance. In contrast to Ti, Ni release from the surface of NiTi implants has been a concerning issue because the dissolution and concentration of Ni ions or wear debris above a certain amount an adverse effects like as allergenicity, toxicity and potential carcinogenic effects [8].

Because NiTi is an intermetallic compound, The bonding force of nickel to titanium is very strong in NiTi making a nickel ion release from NiTi to the surrounding biological environment slight, Furthermore, NiTi is a self passivating material, i.e., it forms a stable nickel-free surface TiO2 layer that protects the base material from general corrosion, although the very little Ni leaching it is necessary to apply a certain surface Treatments to eliminate or minimize the amount of Ni leaching from the surface of NiTi but even a very small amount could produce a harmful effect (Ni amount in human body should not exceed 5mg/L). Implant to negligible amounts[9].

1.4 The objectives of the current study

The aim of the research is to study:

1- Improving the properties of the shape memory alloy by adding molybdenum (Mo) and zirconium (Zr).
2- refing the granule size and improve hardness .

Chapter Two

Theoretical Part& Literature Review

2.1. Introduction.

This chapter involves the theoretical part of shape memory alloys in many relating fields, these include: NiTi alloy system ; phase diagram and martensitic transformations for such alloys; powder metallurgy process and its affecting variables on the properties of these alloys; and using of chemical machining in preparing of the alloys.

2.2 The Memory Alloys.

Mechanical properties of shape-memory alloys (SMAs) are typically represented by the characteristic stress–strain curve, which forms a hysteresis loop in a loading, unloading and shaperecovering process. To represent the deformation behavior of SMAs, various constitutive equations have been developed, and prediction of the macroscopic behavior has been possible using finite-element simulations.[10]

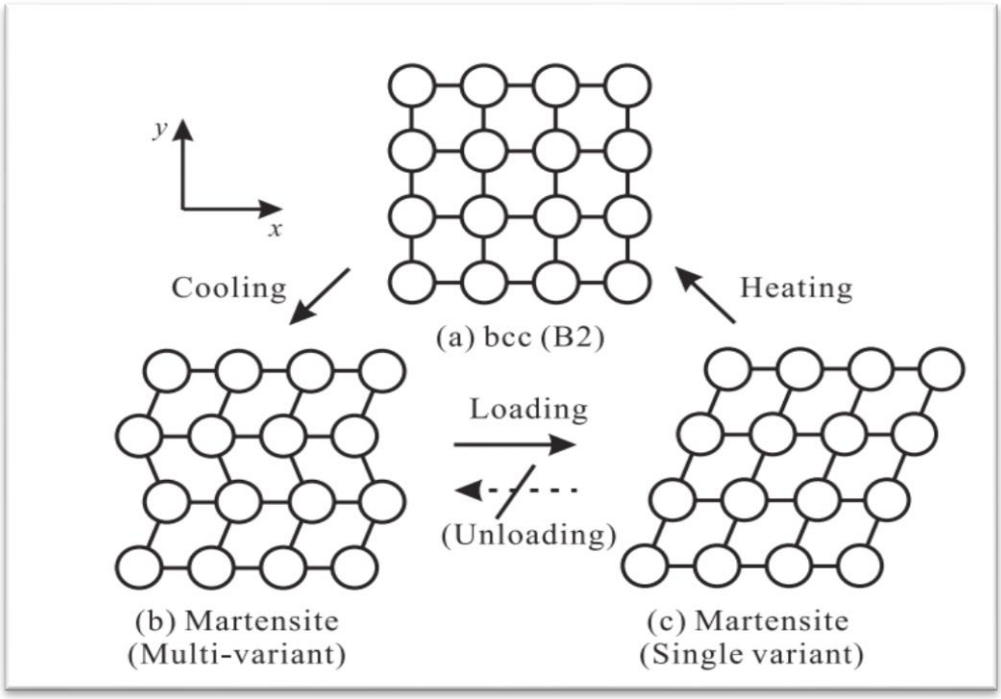

Figure (2-1) Schematic illustration of deformation and shape recovery of a SMA[10].

The atomistic behavior leading to the deformation and shape-recovery is explained on the basis of the phase transformation between austenite and martensite phases and the characteristics of the crystal structure. One well-known atomistic mechanism is illustrated in Fig. 1a. The stable phase depends on the temperature, and phases at high and low temperature are body-centered cubic (bcc or B2) and martensite, respectively. The martensite phase consists of many *variants*, and each variant has a directional unit cell. In Fig. 1(b), for example, a unit cell of the martensite is illustrated as a box leaning in the positive or negative direction along the *x*-axis. Cells leaning in the same direction constitute a layer, and the direction of the lean alternates between layers. the layer is called a variant, although a realistic variant is defined as a rather larger domain. The martensite phase is generated by cooling the B2 structure shown in Figure (2-1) (a). Randomly orientated variants are then generated, as shown in Figure (2-1) (b). some of the layers change their orientation, as shown in Figure (2-1) (c). This structural change induces macroscopic deformation. When the external shear load is released, the strain does not return to the original state except for slight elastic recovery. When the specimen is heated to the transformation temperature, the martensite transforms into the B2 structure, and martensite appears again with cooling of the specimen. Since the B2 structure is cubic, the shape of the unit cell is independent of the orientation of the martensite layers. Therefore, [11] the specimen macroscopically regains its original shape. This mechanism is well known but has not been fully verified since direct observation of dynamic behavior in a wide range of temperatures is difficult. Therefore, computer simulation is expected to provide evidence for and further extend the mechanism. The molecular dynamics method has become a powerful and effective tool to investigate material properties and dynamic behavior on an atomistic scale, and it has also been applied in the case of

SMAs. The stable structure of Ni_3Al, for instance, was investigated by Foiles and Daw [12] using an interatomic potential based on the embeddedatom method (EAM) with suitable parameters [13]. The phase stability and transformation between B2 and martensite structures in NiAl was also reproduced using the EAM potential as reported by Rubini and Ballone [14]. then utilized the EAM potential to demonstrate the shape-memory behavior of Ni-Al alloy in terms of a small single crystal [15] the size dependency and the polycrystalline model Ozgen and Adiguzel also investigated the shape-memory behavior of Ni-Al alloy using a Lennard-Jones [16]). In addition, for Ni-Ti alloy, martensitic transformation was simulated by Sato et al. [17]. It was also reported by Kastner [18] that the shape-memory effect can be represented even by a two-dimensional model with a general LJ potential on the basis of thermodynamical discussion on the effect of temperature on the phase transformation. For a more practical purpose, Park et al. demonstrated shape-memory and pseudoelastic behavior during uniaxial loading of an fcc silver nanowire, and discussed the effect of the initial defects and mechanism of twin-boundary propagation [18].

2.3 Properties of SMA:

2. 3.1 Shape memory effect:

During martensitic phase transformation the molecular structure is twinned. On a macroscopic scale the size and shape of undeformed martensite phase is same as the cubic austenitic phase. The temperature at which starting and finishing of both parent austenitic phase and daughter martensitic phase has characterized by the following variables Ms, Mf, As, Af . Ms is the martensite start temperature upon cooling and Mf is the martensite finish temperature upon cooling, during heating AS and Af are the temperatures of the austenite starts and finishes. The loading quantity of SMA increases with the four variables (Ms, Mf, As& Af), shape memory effect (SME) is noticed when SMA temperature is below Mf , when the alloy

is in deformed martensite, SMA will be recovered the original shape by heating the specimen above Af as shown figure (2-2) and (2-3).

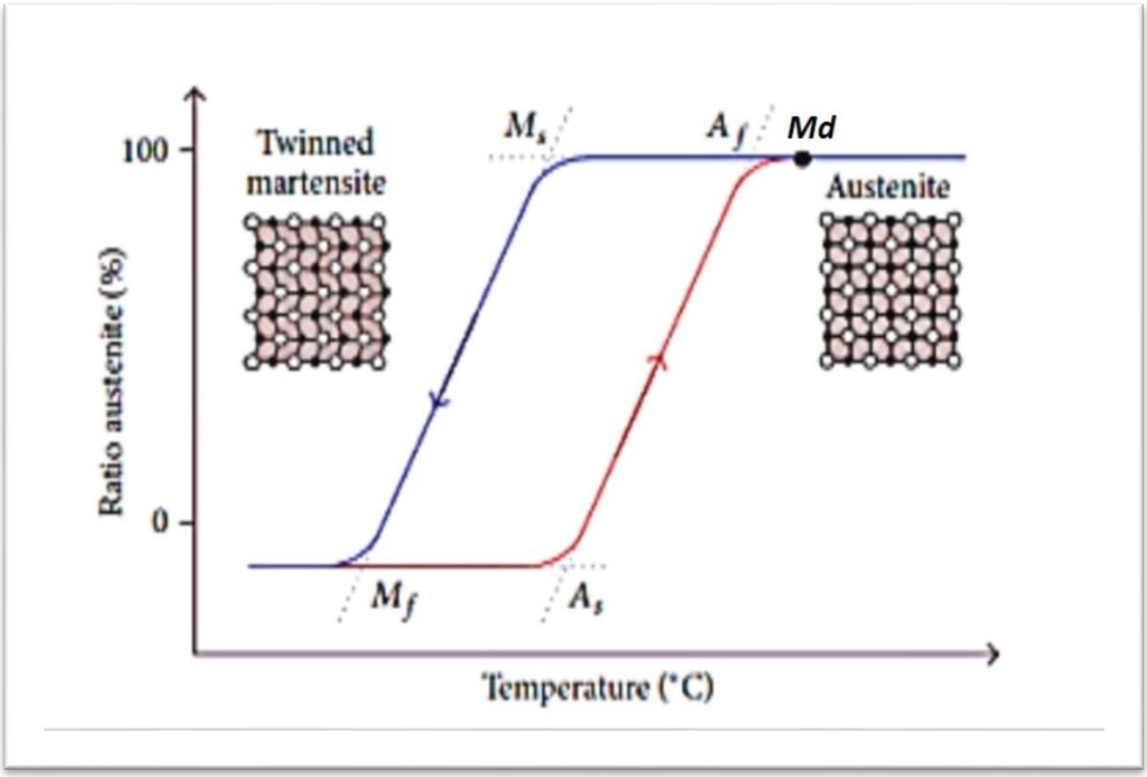

Figure (2-2) ;Temperature Hysteresis in SMA [19].

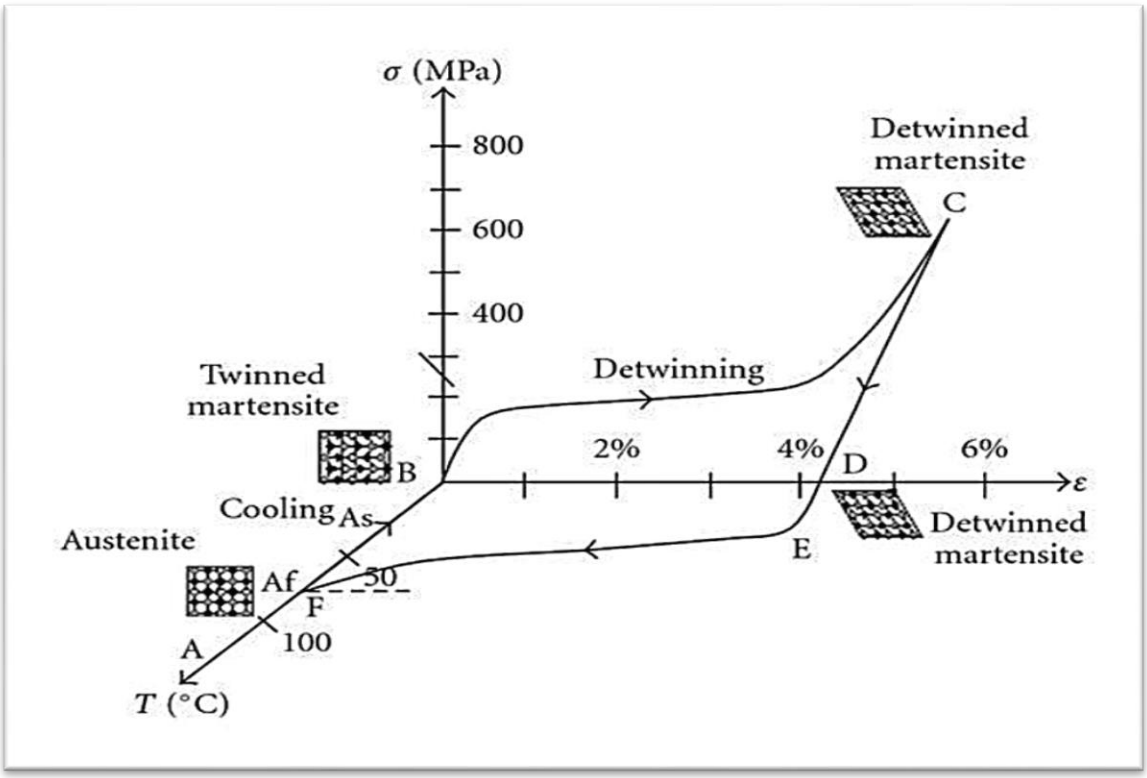

Figure (2-3) ; Stress-strain temperature of NiTi SMA [20].

Normally SME refers to the one-way SME in which external load makes to include de-twinning brings the SMA in to a current distorted structure that can be regain on heating above Af .In this type there is no transformation strains are induced during cooling, it resumes its original shape and rigidity when heated to its higher temperature form (austenite). This is called the one-way shape memory effect. The ability of shape memory alloys to recover a original shape upon heating above the transformation temperatures and to return to a certain alternate Shape upon cooling is known as the two-way shape memory effect. Two-way SME is the one in which transformation strains are persuaded during heating or cooling of SMA Two-way SME is not an essential, but a developed characteristic[21]. Two-way memory is exceptional. There is also an all-round shape memory effect, which is a special case of the two-way shape memory effect [22].

2.3.2 Pseudo elasticity:

Super elasticity or pseudo elasticity of SMA involves stress induced strain recovery upon unloading at a temperature above Af . In general super elastic thermo mechanical loading path starts at zero stress state where de-twinned martensite is stable examples of this characteristic are isothermal (constant temperature) and isobaric (constant pressure) loading paths indicated in Figure (2-4)&(2-5). For achieving the required constant stress by austenite is not shown in the constant pressure path. The point which we remember is the constant temperature conditions carry out only by quasi-static loading which we can treat as small strain increments. During phase transformation, there is a dissipation of latent heat which was generated during quasi-static process. For easy understanding this review paper concentrates mostly constant pressure and constant temperature loading paths will be considered [23].

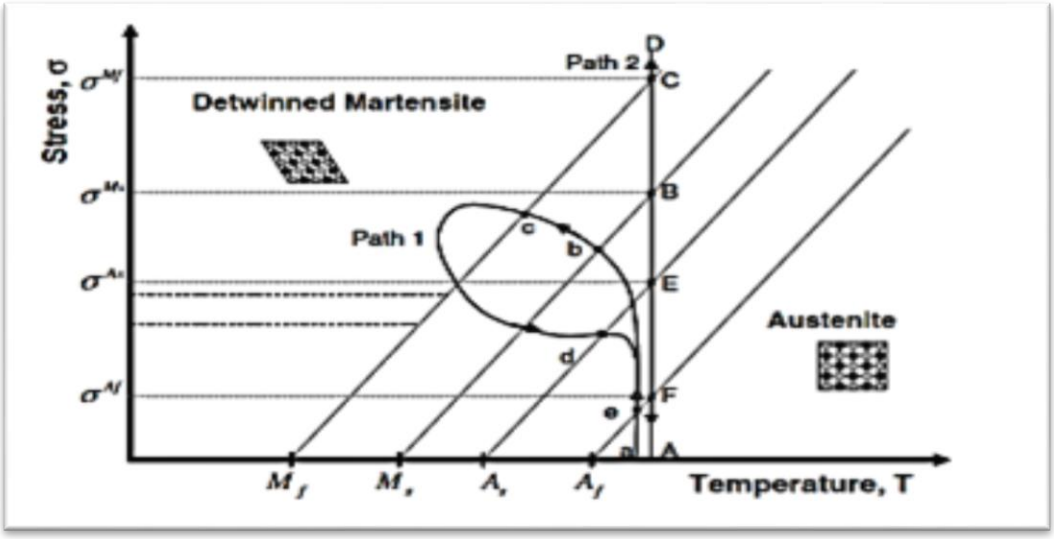

Figure (2-4);phase diagram and two possible[23].

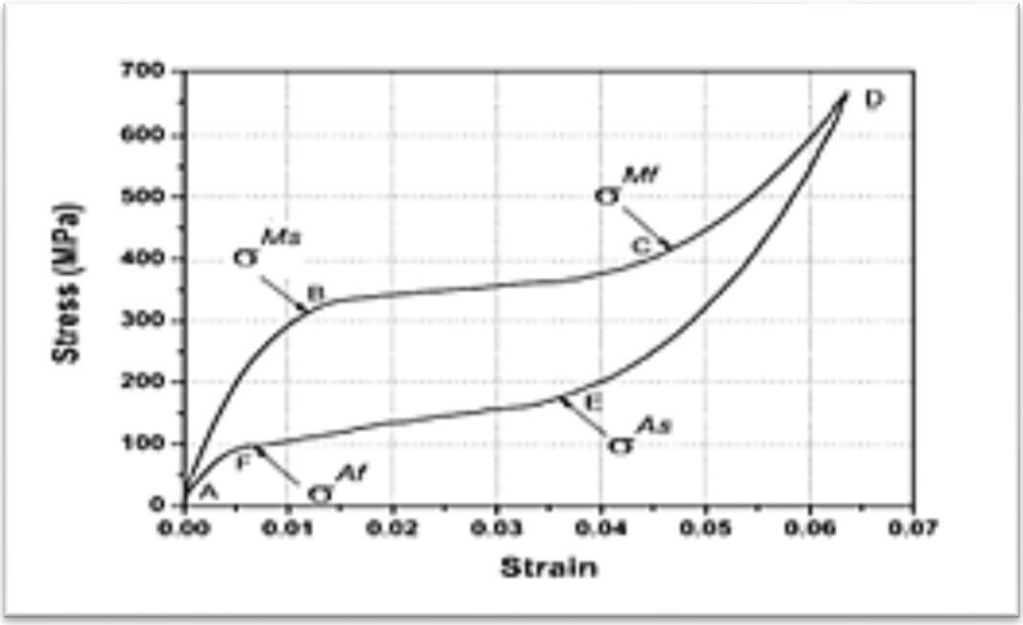

Figure (2-5);SMA pseudoelastic loading cycle

pseudoelastic loading paths [23].

During loading at a temperature above Mf the transformation occurred at critical stress levels from austenite to martensite that stress is called as Transformation stress (a-b). This phase transformation usually occurs during (b-c) path. During thermo elastic critical stress level large in elastic strains are going to be developed. If the load increased further de twinned martensite region (c-d) does not produce any more phase transformation, during multi-axial loading there may be re-orientation of martensite twins will occur. At

point (d) there will be Reverse transformation (RT) from martensite to austenite which will leads to recovery of in elastic strains. At point (e) there will be a complete transformation from martensite to austenite and the final element of the loading path (e-a) is identified by regaining of thermo elastic strains which leads to zero macroscopic strains upon completion of the path. This transformation process concludes in a hysteresis which returns the energy dissipated in the cycle.

2.3.3 Damping properties:

It is very important property for all the materials which are going to use in any specific application.SMA having high damping capacity compared to the remaining materials. Damping property mainly deals with the dissipation of mechanical energy in to heat. The numerous interfaces, which exist during martensitic transformation between austenite and martensite, different martensite variants, the boundaries obtained during twinning of martensite instead of thermo elastic transformation. There will be occurrence of many irreversible events like production defects, dislocation movements etc. hysteresis observed during pseudo elastic characteristic is one of the energy dissipation. The ratio of dissipated energy to the total energy obtained during transformation cycle for isotropic materials will develop. This ratio depends on excitation frequency, temperature, amplitude. A novel material like SMA mainly depends on operating and transformation temperatures as shown Figure(2-6).[24]

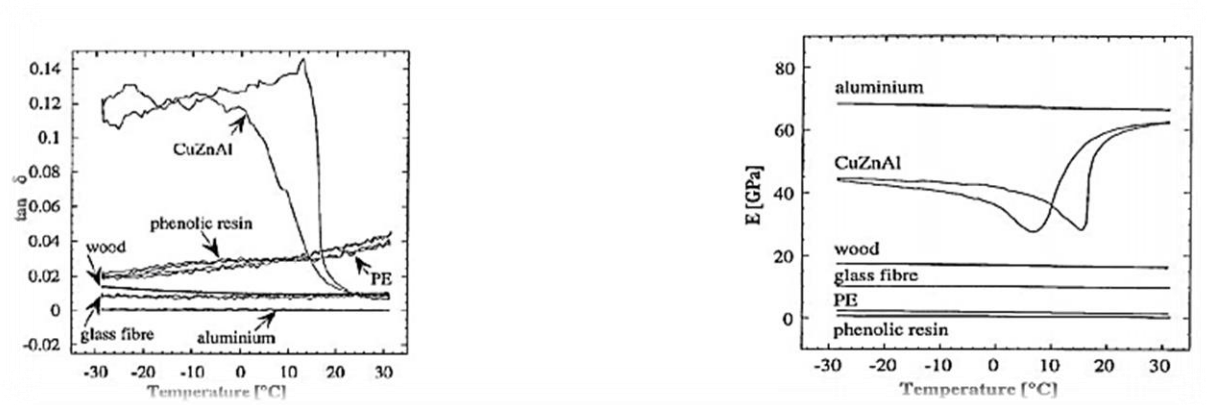

Figure(2-6); Damping factor Vs temperature , Elastic modulus vs. temperature for an frequency of 13Hz for an frequency of 13Hz and and strain amplitude of 10-4 [24] strain amplitude of 10-4

The properties of SMA are determined by their composition and the most commercially adopted shape memory alloys are NiTi (Nitinol) and the Cu-based alloys like Cu-Zn-Al and Cu-Al-Ni. Some of the typical properties of these alloys are listed in below table. [24]

Table (2-1): Some of the typical properties of these alloys[24].

	Nitinol (Ni-Ti)	Cu-Zn-Al	Cu-Al-Ni
Melting temperature(^{0}C)	1300	950-1020	1000-1050
Density (gcm^{-3})	6.45	7.64	7.12
Resistivity(μΩcm)	70-100	8.5-9.7	11-13
Thermal conductivity (W cm^{-1}per^{0}C)	18	120	30-43
Young's modulus (Gpa)	83(austenite) 26-48(martensite)	72(beta phase) 70(martensite)	85(beta phase) 80 (martensite)
Yield strength (Mpa)	195-690(austenite) 70-140 (martensite)	350 (beta phase) 80 (martensite)	400 (beta phase) 130 (martensite)
Ultimate tensile strength (Mpa)	895	600	500-800
Shape memory strain (% maximum)	8.5	4	4
Transformation range (^{0}C)	-200-110	<120	<200
Transformation hysteresis (^{0}C)	30-50	15-25	15-20

2.4 Applications of Shape Memory Alloys

In 1932 smart alloy or shape memory alloy was first discovered by Arne Olander [25], while, Vernon was the first one described the term shape – memory in 1941 . However, the importance of shape memory alloys was not recognized until the shape memory effect was discovered by William

Buehler and Frederick wang in 1962, when they described it in a nickel – titanium alloys (nitinol) [26]. Since then, shape memory alloys have been used for engineering and technical applications in numerous commercial fields; for examples, in automotive [27] , biomedical [28] , aerospace [29], robotics [30], consumer products and industrial applications [31] and fashion [32]. In general, the SMAs applications can be divided into four groups depending on their key function of their unique properties, which are shape memory effect and superelasticity [33]. Table (2-1) Shows the types of shape memory applications [34]. This review focuses on applications of shape memory alloys particularly biomedical, robotic, automotive and aerospace applications.

2.4.1 Biomedical Applications

The materials used for vivo application which are touch with human tissue should have unique properties to meet this requirements, for example, these materials must have biological reliability – biological compatibility, free toxicity, perfect corrosion resistance, and accuracy of mechanical properties [35]. Since the discovery of shape memory effect in NiTi alloys in 1962, they proposed to use this shape memory alloy in biomedical applications [36]. Due to the unique properties of Ni-Ti shape memory alloy (SMA), shape memory effect (SME), shape effect (SE), and a very good corrosion resistance, Ni-Ti shape memory alloys are often used as prosthesis materials in the human body[37]. The application areas available with various size and shape, range from dental arch wire not directly in tough with blood flow in the human organism to stents used to stabilize damaged blood vessels as shown in figure (2-7) [38]. Furthermore, shape memory alloys are used in medical devices in different areas such as orthopedics [39], neurology[40], cardiology and interventional radiology [41]. In addition they are used in stents [42], endodontics [43], eyeglass frames [44], guide wires [45], aneurism treatments [46] and medical tweezers [47], sutures [48], anchors

for attaching tendon to bone [49], implants Figure (2-8) shows example of using shape memory alloy in catheter – based surgeries [50]. NiTi shape memory alloy coiled spring can be used as a micro – muscle fiber as you can see in figure (2-9) [51]. The researchers developed mechanical circulation using shape memory alloys fiber to assist patients with heart diseases as you can see in figure (2-10) [52].

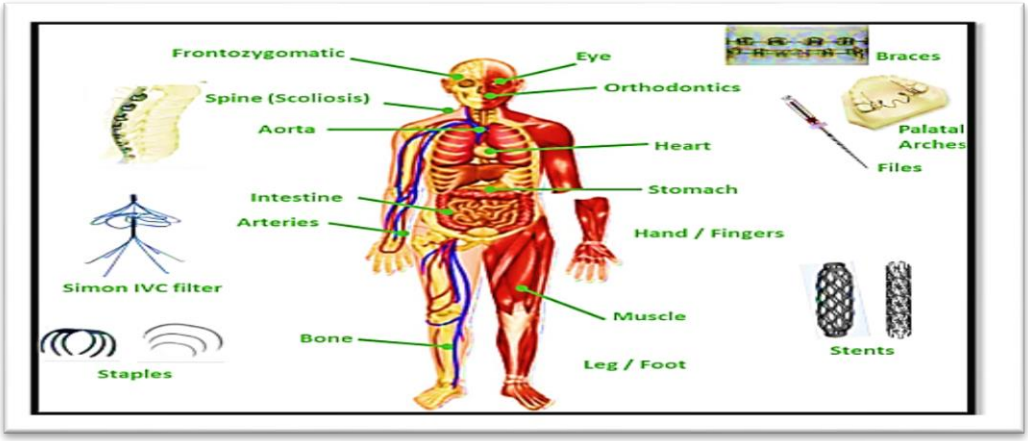

Figure (2-7) Potential and existing shape memory alloy applications in biomedical domain [38].

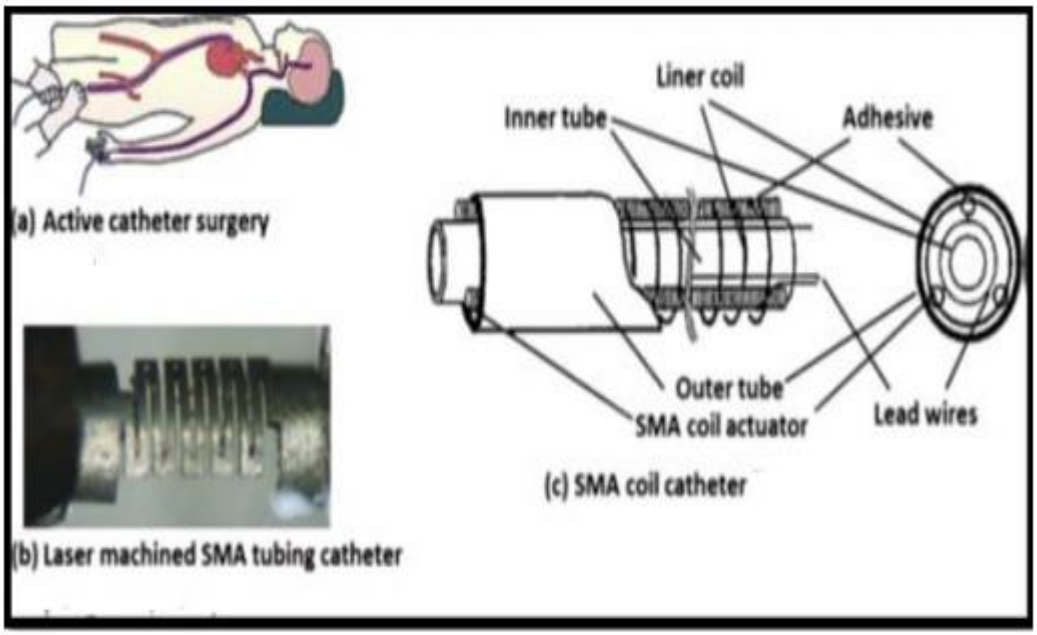

Figure (2-8) Shape memory alloy active catheter [50].

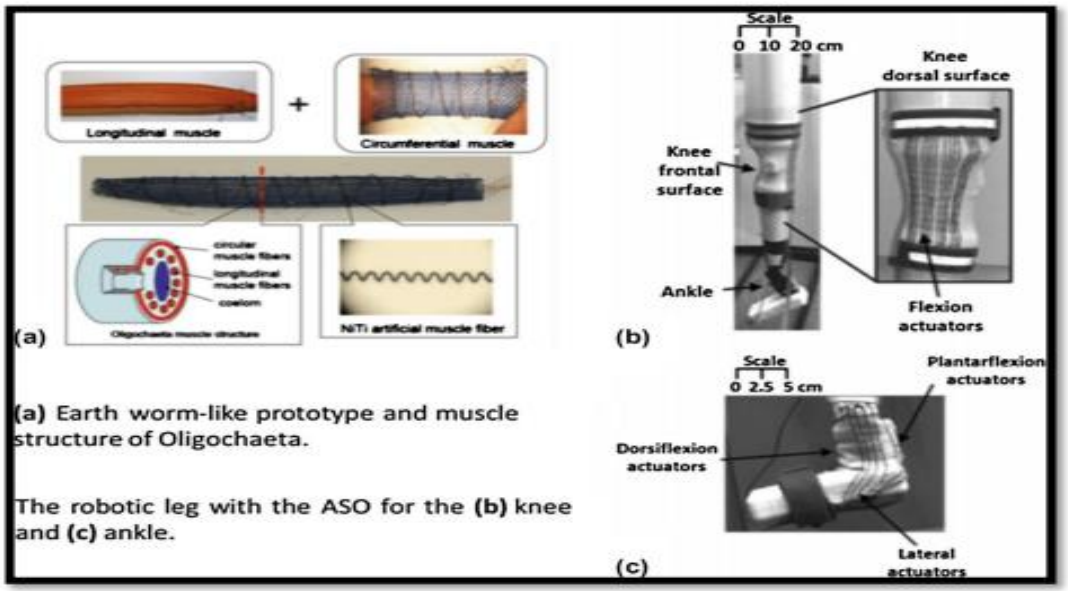

Figure (2-9) Muscle like NiTi shape memory alloy [51].

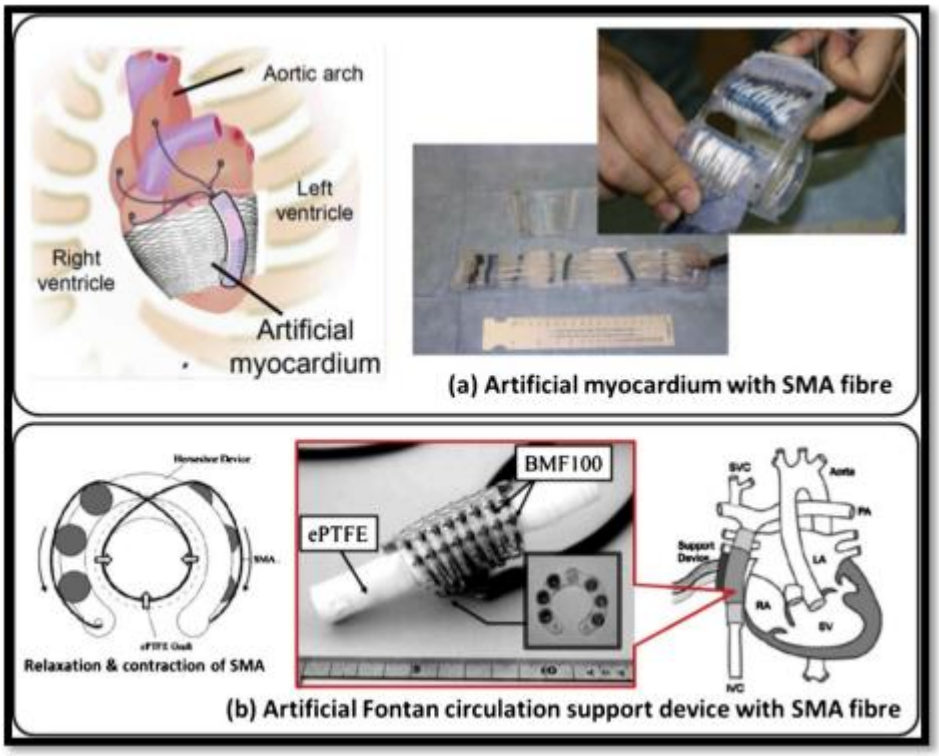

Figure (2-10) Artificial heart support device with shape memory fiber [52].

2.4.2 Robotic Applications

Shape memory alloys have been used in robotic application since 1980s [53]. However, the robots can be divided into several groups depending on their movement techniques and applications, for example jumper, crawler,

fish, walker, flower, medical and biomimetic robotic hand [54]. Figure (2-11) shows the different kinds of shape memory alloys in the robotic applications [55]. Today, numerous works carried out on robotics have focused on biologically inspired and humanoid robots [56]. These robots can be used to solve problems which are challenges for humans, for example can be used in underwater, space, air and land to provide pertinent information from these environments which is difficult to get by humans [57]. Recently, sever flying robots with shape memory alloys have been developed, for example Bat Robot [45] and BATMAV Robot [57]. A dragonfly shown in figure 6 with a 44 cm length and a 63 cm wingspan was developed by Festo Group [48]. The dragonfly is known as BionicOpter see figure (2-12), the dragon equipped with four actuators shape memory alloys to control the movement dragonfly tail up and down and dragonfly head from side to side [58]. The dragonfly has thirteen degrees of freedom, can hover in maneuver in all direction and in mid – air [58].

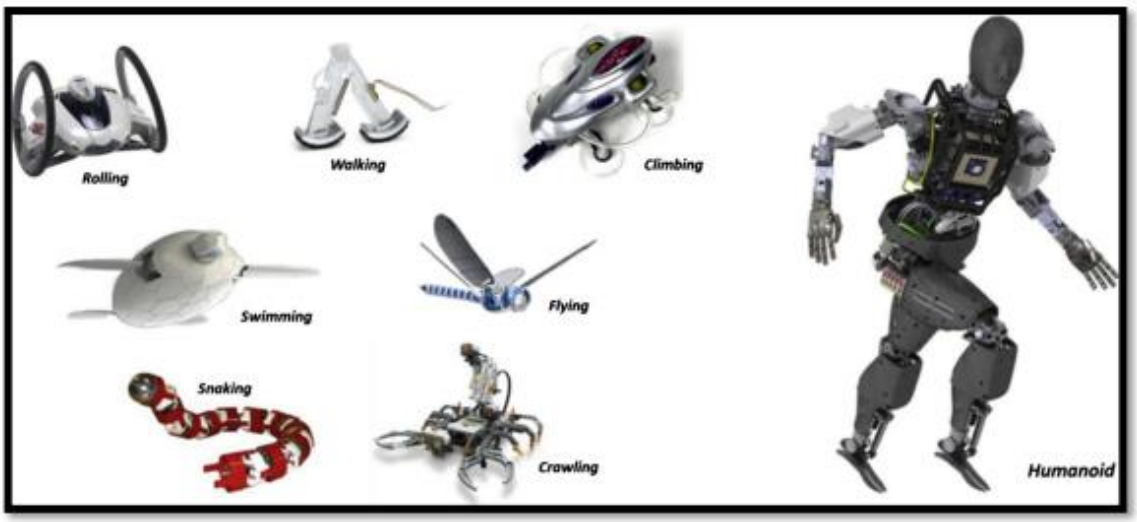

Figure (2-11) Potential and Existing shape memory alloys applications in robotic domain [55].

Figure (2-12) Festo BionicOpter - inspiration dragonfly flight [58].

2.4.3 Automotive Applications

Nowadays, the number of sensors and actuators are growing tremendously due to the request for reliable, convenient and good performance in modern vehicles [58]. Therefore, these offer a wide range for shape memory alloys to use in the automotive industry as shown in figure (2-13) [59]. There are numerous possibility applications for shape memory alloys in automotive industry which have been proposed, but very few of them have been used in practical applications due to the limited range of operating temperature compared with shape memory alloy transformation temperatures [55]. In addition, there are other limitations for example hysteresis width, stability and lifetime [60]. However, shape memory alloys can be used in the mirror system in modern vehicles due to the versatility of shape memory alloy as shown in figure (2-14) [61]. Furthermore, figure (2-15) shows the emerging General Motors shape memory alloys applications [62]. Recently, several other shape memory alloy applications for automotive industry have been developed and they can be found in the literature [63- for examples, tumble flaps actuator, micro – scanner system, pop – up bonnet and side mirror actuator as you can see in figure (2-14) [63]. It is well known that the stander transformation temperatures of NiTi shape memory alloy are at range temperatures – 40 ◦ C to approximately + 110 ◦ C [63]. In contrast, the stander operating temperature range for automotive application is between –

40 ° C to approximately +125 ◦ C as shown in figure (2-15) [64]. Therefore, the majority of the practical applications of shape memory alloys are covered by NiTi shape memory alloy [65]. However, from the figure (2-15) and in order to act properly the shape memory alloys should exhibit a martensite transformation temperature above maximum operating temperatures as shown in the figure (2-14) the red dotted lines. Moreover, there are many kinds of high temperatures shape memory alloys. But these alloys are of high cost for automotive industry [66]. Although, the Cu-Al-Ni shape memory alloys exhibits martensitic transformation temperatures up to 200 ◦ C, these materials are unstable, brittle, exhibit low fatigue strength and cannot be used for multiple cyclic operations [65]

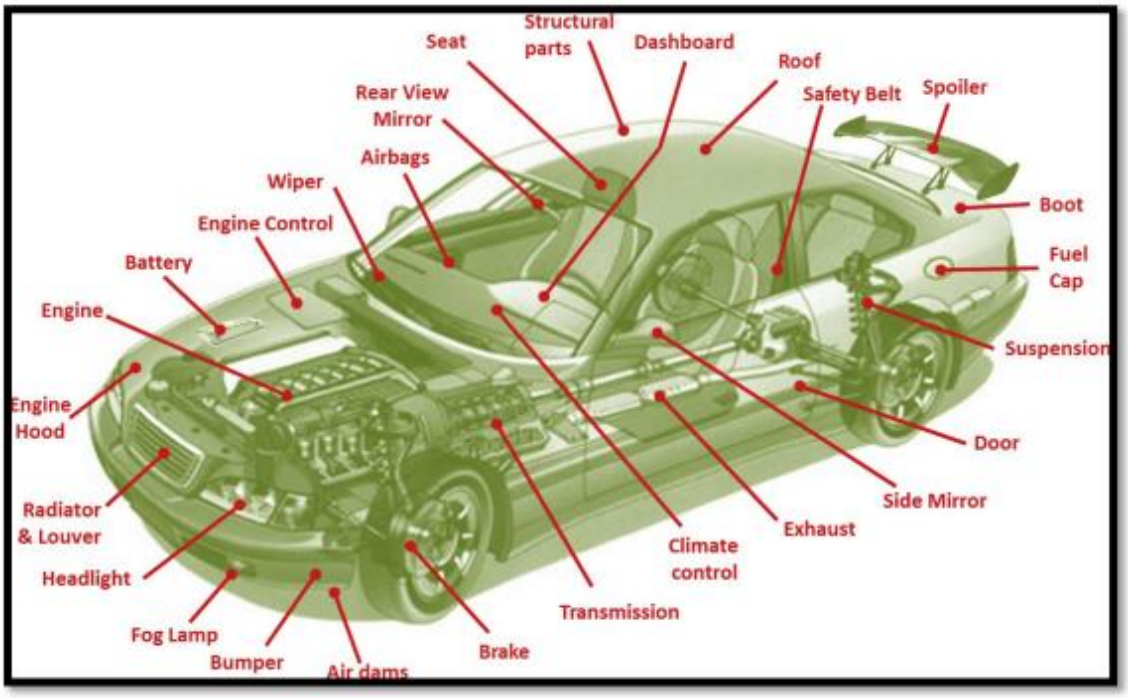

Figure(2-13) Existing and potential shape memory applications in the automotive domain [59].

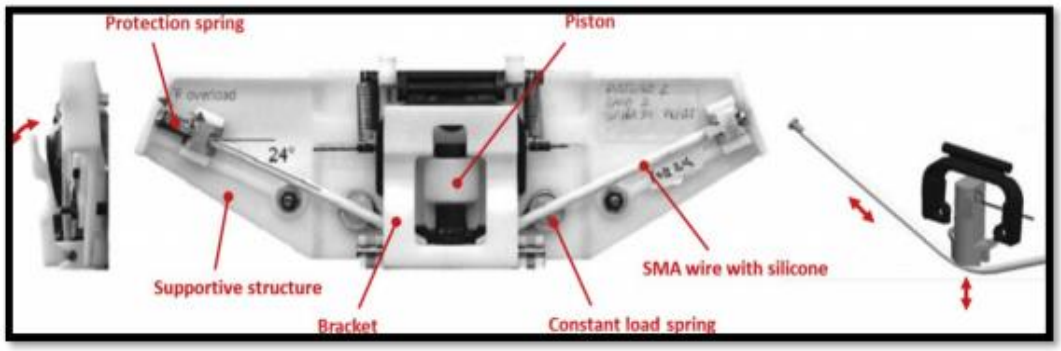

Figure (2-14) EAGLE mirror prototype [61].

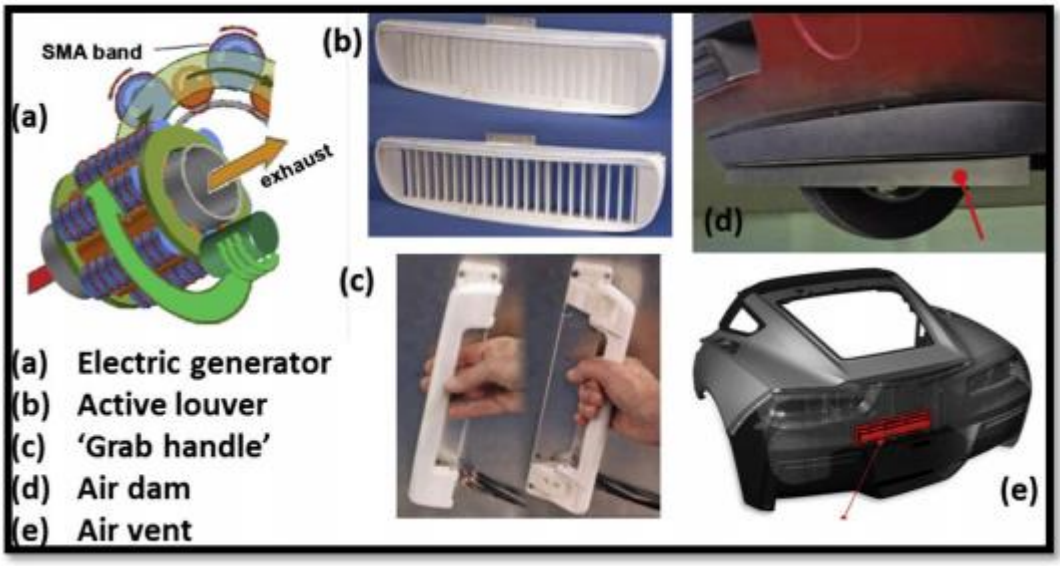

Figure(2-15) Emerging General Motors Shape Memory Alloy [63].

2.4.5 Aerospace Applications

SMAs have been used in aerospace since 1970s when used in hydraulic line coupling which is used in the F-14 fighter jets [62]. Since this time and due to the unique properties of SMAs many aerospace researchers have proposed to use this material for solving engineering issues in the aerospace manufacture[67]. In the 1990s, numerous works carried out on aerospace industry such as Advanced Research Projects Agency (DARPA) program for aircraft smart wings [66], the Smart Aircraft and Marine Propulsion System Demonstration (SAMPSON) program for jet engines[67] and another program can be seen in literatures [68]. The Boeing company has improved an active device based on SMA technology programs which is VGC, a

variable geometry chevron on a 77-300 ER with GE90-115B jet engine, this device has the ability to minimize noise through take- off, figure 12 shows Boeing variable geometry chevron [69]. Then, after the VGC success, many companies such as Boeing, DARPA, NASA and other have been introduced more SMAs based on technology programs in order to use SMAs in aerospace industry [70].Figure (2-16) shows the possibility SMAs applications in the aerospace industry [66].

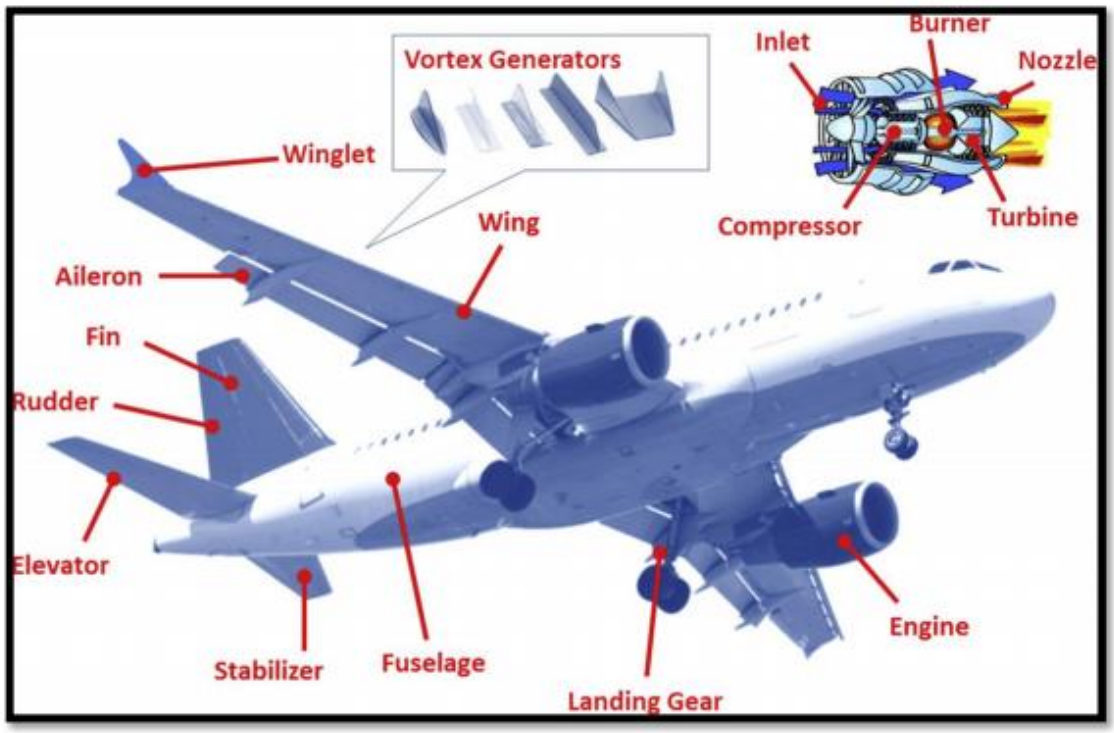

Figure(2-16) Existing and potential shape memory alloys applications in the airspace domain [64].

2.5 Phase Diagrams for NiTi Alloy

The Ni-Ti phase diagram shows a number of different transformations, a few of which are important during the sintering of Ni-Ti alloys. These are the eutectoid (β-Ti Æ α-Ti+Ti2Ni) and the eutectic (liquid Æ β-Ti+Ti2Ni) transformations which take place at 765 °C and 942°C, respectively Figure (2-18). The reaction between Ti and Ni is exothermic, so it has the possibility of self-sustaining synthesis. This means that there is an ignition temperature at which the reaction can be initiated and then it will continue by itself.

Combustion synthesis of NiTi is therefore possible. NiTi shows a relatively low heat of formation (ΔHq= 67kJ/mol)6 . Preheating of the sample mixture is necessary for self-sustaining synthesis, promoting transient melt formation9 . In addition, it has been reported that NiTi synthesis from elemental powder mixtures leads to the formation of other intermetallic compounds like Ti2Ni, Ni3Ti, Ni4Ti3 and Ni3Ti2 10–12. Among them, Ti_2Ni and Ni_3Ti are relatively more stable than NiTi thermodynamically, and therefore it is difficult to avoid their presence in the microstructure during the synthesis of a NiTi alloy[71]

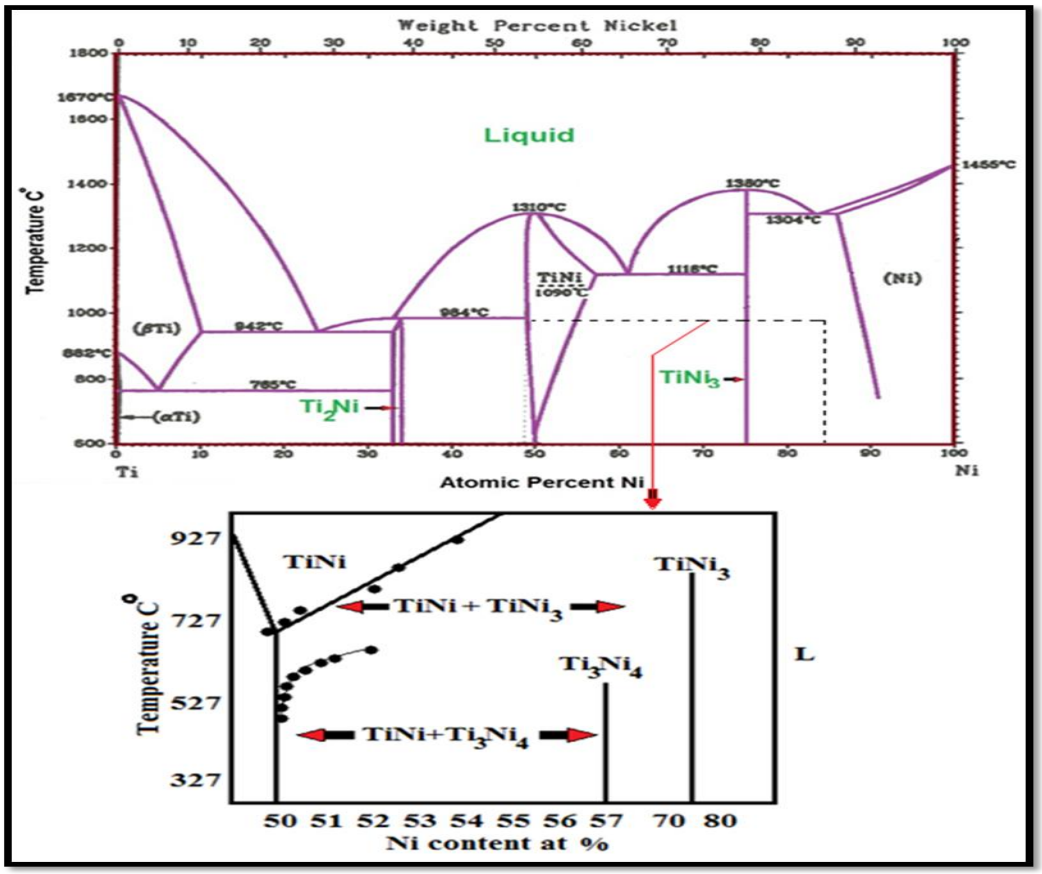

Figure (2.18): Nickel-Titanium Phase Diagram [71].

2.6 Transformation temperatures.

From the B2 phase stability regime, the B2 structure starts to transform into the B19Š martensite phase at Ms (the martensite start temperature) on cooling. The volume transformed into the martensite is a function of

temperature. Holding at any temperature below Ms for any length of time does not cause the formation of more "athermal" martensite. The parent B2 phase is completely transformed into the product B19 martensite for temperatures below Mf (the martensite finish temperature).[72] If the transformation process includes the R-phase, the start and the end temperatures of the transformation from the austenite to R-phase are denoted by Rs and Rf , respectively. On heating, the reverse transformation from B2 austenite to B19 martensite phase takes place. The temperature, at which the reverse transformation begins, is denoted As. Similarly, the last remnant of martensite disappears at the temperature Af . There is transformation temperature hysteresis such that As > Mf and Af > Ms. If the reverse transformation includes the R-phase, corresponding transformation temperature are denoted A_{RS} and A_{RF} on heating. The magnitude of thermal hysteresis of the B19Š phase transformation is much larger (one order of magnitude higher) compared with the magnitude of the thermal hysteresis of the R-phase transformation [73]. There is a strong composition dependence of the B19Š-Phase transformation temperatures (PTTs), see Figure (2-19) the PTTs decrease signiĄcantly with increasing concentration of Ni atoms in the Ni-rich NiTi-phase [74]. The PTTs can change by about 20°C per added 0.1 at% Ni [75]

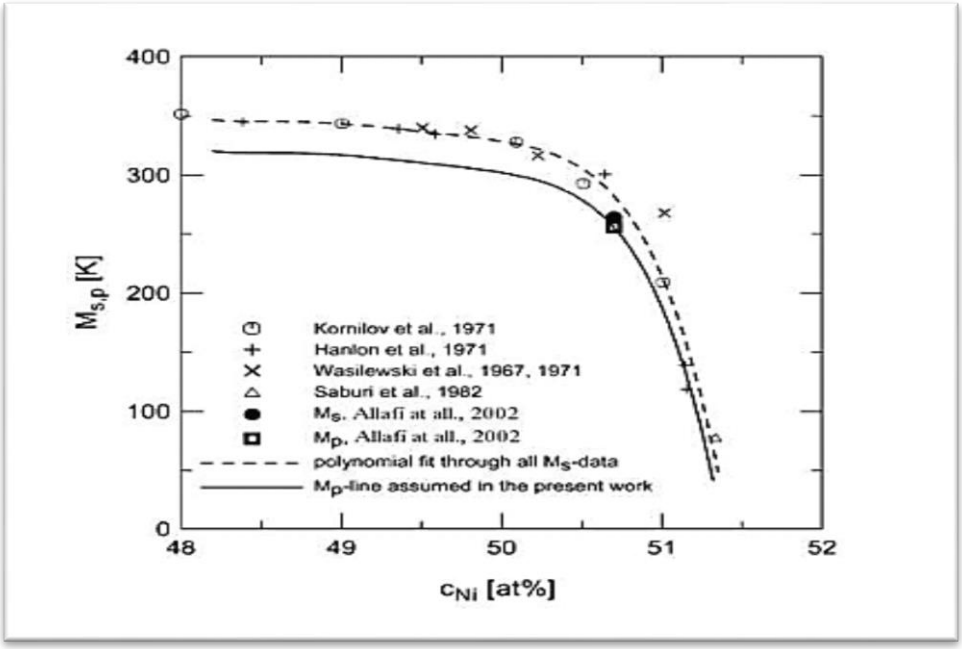

Figure (2-19): Relation between nickel content M_S, M_P temperatures [75].

martensitic transformations can be triggered by external applied stress according to the Clausius-Clapeyron type relationship. The highest temperature at which martensite phase can form under applied stress is denoted Md [76]. Md is the temperature above which the chemical driving force becomes so small that nucleation of martensite cannot be mechanicaly induced [75]. In the following section I will introduce a SMA phase diagram of one-step martensitic transformation in temperature-stress coordinates, where a dependence of transformation temperatures on applied stress can be seen.

2.7 Mechanical properties of NiTi SMA

Like most SMAs, NiTi alloys show marked differences in mechanical behavior depending upon whether they are tested in the martensitic or austenitic state. The martensitic stress - strain curve can be divided into three well defined regions, see Figure (2.20). An initial low plateau results from the stress induced growth of one martensitic orientation at the expense of the

adjacent. At higher stresses there is a second region that is linear, although not purely elastic [76].

The transition to the third region is a result of the onset of irreversible plastic deformation, as in the case of yielding of all conventional metals. The length of the martensitic plateau in the stress - strain curve extends typically to around 5% - 6%. However, depending on the details of the alloy and its prior thermomechanical history. The plateau can vary from a continuous curve with an inflection point to a clear horizontal with a sharp yield point.

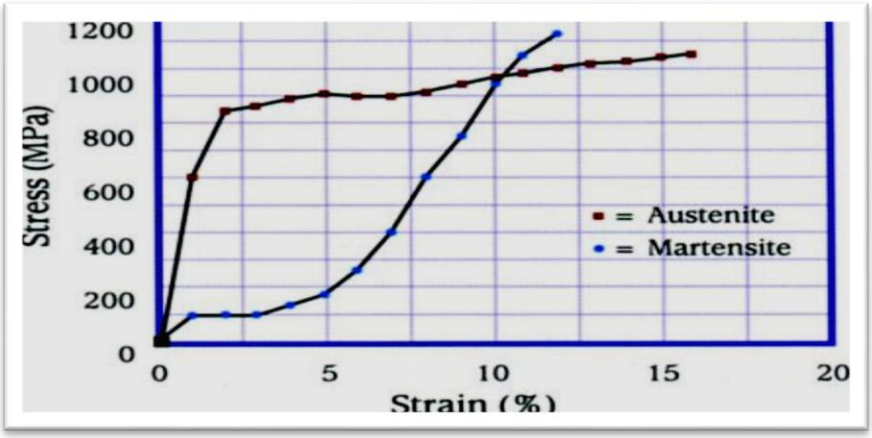

Fig.(2.20) Stress-strain curve for a Ni-Ti-10%Cu alloy in the austenitic and martensitic conditions [76].

2.8 the effect of alloying elements on the shape memory alloys

2.8.1 Molybedum (Mo)

Molybdenum metal is usually produced by powder metallurgy techniques in which Mo powder is hydrostratically compacted and sintered at about 2100°C. Hot working is done in the 870-1260°C range. Moly forms a volatile oxide when heated in air above about 600°C and therefore high temperature applications are limited to non-oxidizing or vacuum environments. [77]. The addition of Mo reduces the hardness of the alloy compared with the master sample. The porosity percentage decreases with increase in Mo percentage.The corrosion rate decreases with increase in Mo percentage in Ringer solution . [78]

2.8.2.Zirconium(Zr).

Zirconium is a neutral element when dissolved in Ti. Zirconium belongs to Group 4 (according to the new IUPAC name) in the Periodic Table, which is the same as Titanium and hafnium, have similar chemical structure and properties. Thus, they have been recognized as non-toxic and non-allergic. Zirconium is a transition metal with an atomic number of 40 and an atomic weight of 91.22 amu. As a greyish-white lustrous metal, Zirconium has exceptionally high melting (1857 °C) and boiling (4409 °C) points. Zirconium has excellent resistance to Corrosion, similar to Titanium and is highly biocompatible [79]. Since both metal surfaces form a stable oxide layer on their surface within nanoseconds when exposing to oxygen. Thus, the oxidation passivates the materials. However, Zirconium could not be used in dentistry in its pure form. An extensive review article [98] suggested that Zirconium implants had a lesser degree of osseointegration than titanium analogue using removal torque tests. Some surface modifications could restructure the implant that could remove torque test values comparable with the titanium implants.Although the removal torque test values highly depend solely on the surface structure (in terms of mechanical retention and biological interaction) than on the implant material itself [80], the atomic structural arrangement allows the torque performance in metal alloys better than in ceramics. The reason for using a zirconia implant is merely due to improvement in esthetic qualities in dental restorations. Thus, the development of Ti-alloys is still viable and active [81].

2.9 Literature Review

Vojtěch (2010) [96] studied the influence of heat treatment of shape memory NiTi alloy on its mechanical properties , the aim is to determin the mechanical properties of nitinol short-time heat treated at around 500°C. The temperature of 500°C was selected, because in manufacture of stents, shape setting is a step generally performed at about 500°C. It has been found that heat treatments of the straight annealed nitinol wire at moderate temperatures strongly influences its tensile strength and transformation stress. Annealing temperatures between 410-460°C improve the strength to some extent. At 12 higher temperatures above 485°C, the wire behaves in an opposite manner,

i.e. strength reduces. The observed development of mechanical properties and transformation behavior is related to precipitation processes occurring in the wire during heat treatment.

In 2010 Flamini et.al [97] electrodeposited a polyprypol (PPY) film on to Nickel - Titanium alloy (NiTi) employing sodium bis (2- ethylhexyl) sulfosuccinate (Aerosol Otor Aot) solutions. The results showed that the polymer has improved corrosion performance of the coated samples in chloride solution and the polymer improves the corrosion performance at the open circuit potential and at potentials where the bare substrate suffers pitting attack. The improvement in both adhesion and corrosion performance was discussed considering substrate / polymer interaction, over oxidation of PPy and the role played by AOT .

In 2012 ,. Tawhid Ezaz et al ,. [98] Dislocation slip in B2 NiTi is studied with atomistic simulations in conjunction with transmission electron microscopy (TEM). The atomistic simulations examine the generalized stacking fault energy (GSFE) curves for the {0 1 1}, f211g and {0 0 1} planes. The slip directions considered are h100i, h111i and h011i. The results show the smallest energy barriers for the (0 1 1)[1 0 0] case, which is

consistent with the experimental observations of dislocation slip reported in this study. To our knowledge, slip on the (0 1 1)½11 1 system is illustrated for the first time in our TEM findings, and atomistic simulations confirm that this system has the second lowest energy barrier. Specimens that underwent thermal cycling and pseudoelasticity show dislocation slip primarily in the austenite domains while the bulk of martensite domains does not display dislocations. The results are discussed via calculation of the ideal slip nucleation stress levels for the five potential slip systems in austenite

In 2015 ,. Kamal Kumar et al ,. **[99]**Nitinol (NiTi) is categorized as a smart material which is highly recognized material for medical and other engineering applications. The behaviour of NiTi can be modified by altering the composition, modifying the porosity and applying external thermal and mechanical treatment. Due to high composition sensitivity, there are several impediments in fabrication of NiTi with conventional techniques which impel the use of additive manufacturing methods. But due to very high cost of equipments, these processes have not been commercialized till now. This paper presents a review on applications, manufacturing NiTi alloy and its various production routes from conventional to rapid prototyping, porous NiTi, effect of additives on properties of the alloy and its challenges.

In 2016 ,. CNaresh et al ,.[100] Shape memory alloys (SMAs) are the special materials that have the ability to return to a predetermined shape when heated. When this alloy is in below transformation temperature it undergoes low yield strength and will deform easily into any new shape which it will retain, if this alloy is heated above its transformation temperature it changes its crystal lattice structure which returns to its real shape .SMAs are remarkably different from other materials are primarily due to shape memory effect (SME) and pseudoelasticity which are related with the specific way the phase transformation occurs, biocompatibility, high specific strength, high corrosion resistance, high wear resistance and high

anti-fatigue property. SMA are used in many applications such as aerospace, medical, automobile, tubes, controllers for hot water valves in showers, petroleum industry, vibration dampers, ball bearings, sensors, actuators, miniature grippers, micro valves, pumps, landing gears, eye glass frames, Material for helicopter blades, sprinklers in fine alarm systems packaging devices for electronic materials, dental materials, etc. This paper focuses on introducing shape memory alloy and their applications in past, present and in future, also revealed the concept and mechanism of shape memory materials for a particular requirement. Properties of SMAs, behaviour and characteristics of SMA, summary of recent advances and new application opportunities are also discussed.

In 2016 ,. Aun Nawaz Khan et al ,. [101] Shape Memory Alloys (SMA) are unique class of alloys which possess various engineering applications. One such SMA is Nickel–Titanium (Nitinol) shape memory alloy. The problem, however with Nickel is that the metal may leach out in form of toxic Ni2+ ions. The latter may prove costly when used in various applications. To increase the corrosion resistant properties of Nitinol and to evaluate its shape memory properties, small amount of Zirconium i.e. 5 and 10 at % are added into the existing Nitinol system. Buttons of Nitinol and Nickel–Titanium with Zirconium additions are made using the button arc furnace. For the characterization of the alloys, various techniques including Energy Dispersive Spectroscopy (EDS), Back Scattering Electron (BSE) imaging, Differential Scanning Calorimetry (DSC) have been performed. Thework conducted reveals that addition of Zirconium in Nitinol has marked influence on microstructure, shape memory properties, transformation temperature, hardness values, and corrosion properties of the alloy.

In 2017 ,. Hossein Sina et al ,. [102] The present study focuses on *in situ* as well as *ex situ* studies on the sintering of pre-compacted powder mixtures of 50at% Nickel-50at%Titanium. *In situ* studies were carried out by monitoring

the changes in morphology of the fracture surface of the compact continuously during heating in the hot stage of an environmental scanning electron microscope. Results on the initiation of sintering and its variation with the particle size of reactants are presented. Differential Scanning Calorimetry and X-ray diffraction studies have also been made to characterize the formation of intermetallic compounds during the progress of sintering

In 2017 ,. Yulong Liang et al,.[103] investigated Based on ternary Ni45Ti51.8Fe3.2 (at %) shape memory alloy (SMA), Nb and Ta elements are added to an NiTiFe SMA by replacing Ni element, and consequently quaternary Ni44Ti51.8Fe3.2Nb1 and Ni44Ti51.8Fe3.2Ta1 (at %) SMAs are fabricated. The microstructure, mechanical property, and phase transformation of NiTiFeNb and NiTiFeTa SMAs are further investigated. Ti2Ni and β-Nb phases can be observed in NiTiFeNb SMA, whereas Ti2Ni and Ni3Ti phases can be captured in NiTiFeTa SMA. As compared to NiTiFe SMA, quaternary NiTiFeNb and NiTiFeTa SMAs possess the higher strength, since solution strengthening plays a considerable role. NiTiFeNb and NiTiFeTa SMAs exhibit a one-step transformation from B2 austenite to B19’ martensite during cooling, but they experience a two-step transformation of B19’-R-B2 during heating**.**

In 2017 ,. M Losertová et al ,. [104]Superelastic behavior of off-stoichiometric NiTi alloys is significantly affected by microstructure changes due to heat treatment. Applying appropriate thermal treatments important effects on microstructural changes, transformation temperatures and thermomechanical properties of final NiTi products can be achieved. The experimental samples of NiTi alloy with 55.8 wt.% Ni were submitted to heat treatment and the microstructures before and after the treatment were observed. The thermal regimes consisted of annealing treatment at 600 °C for 1 hour followed by water quenching and of ageing at eight different

temperatures (250, 270, 290, 300, 350, 400, 450 and 500 °C) for 30 minutes. Microstructure features studied by means of optical and scanning electron microscopies, EDX microanalyses, X-ray diffraction analyses and microhardness measurement, have shown that higher ageing temperatures led to microstructure changes and corresponding increase in microhardness.

In 2017 ,. CENGIZ TATAR and ZÜLKÜF YILDIRIM ,. [**105]** The effect of hydrostatic pressure on the behaviour of reverse and forward transformation temperatures and physical properties of NiTi shape memory alloy has been investigated. The transformation temperatures and physical properties of the alloy change with applied pressure. It has been clearly seen from differential scanning calorimetry that with the increase of applied pressure, while *A*s, *A*f and *M*f transformation temperatures decrease, *M*s value increases. Moreover, it is obvious that with the increase of applied pressure, Gibbs free energy increases by 5.2883 J, while elastic energy increases by 1.4687 J. In addition, entropy of the alloys decreases by 0.2335 J *(*g ◦C*)*-1 with applied pressure. Additionally, it is evident from the scanning electron microscopy images of the samples that there is an obvious difference in the grain sizes of the unpressured sample and the samples on which pressure is applied, the sizes being 10–100 and 30–150 μm, respectively

In 2018 ,. Shih-Fu Ou et al ,. [106]In this study, an optimal selective laser melting (SLM) process for manufacturing dense NiTi alloy with pseudoelasticity and shape-memory capability was proposed. The microstructure, phase-transformation temperature, shape memory capability, and pseudoelasticity were investigated by scanning electron microscopy, X-ray diffraction, differential scanning calorimetry, and bending and tensile tests. NiTi powder with a particle size > 45 μm was selected for the subsequent SLM process, because it exhibited a Ni/Ti ratio of ~1 and a lower oxygen content than powders with smaller particle sizes. A thin-walled disk

(0.48 mm thick) and cuboid samples (5 mm thick) were prepared for investigating the variation in the homogeneity of the microstructure. The thin-walled SLM-NiTi sample exhibited a marginally inhomogeneous microstructure between layers, and defects existed in the previously formed side. The cuboid SLM-NiTi sample was fabricated without undesirable secondary phases, and it exhibited a 100% shape-recovery rate under 2% bending strain and completely pseudoelastic under 3% strain. Also, the SLM-NiTi exhibited lower phase-transformation temperatures and a broader phase-transformation range than the original NiTi. The phase-transformation range can be reduced by annealing.

In 2019 Lai-Chang Zhang and Liang-Yu Chen [107] Compared with stainless steel and Co–Cr-based alloys, Ti and its alloys are widely used as biomedical implants due to many fascinating properties, such as superior mechanical properties, strong corrosion resistance, and excellent biocompatibility. After briefly introducing several most commonly used biomedical materials, this article reviews the recent development in Ti alloys and their biomedical applications, especially the low-modulus β-type Ti alloys and their design methods. This review also systemically investigates the recently attractive progress in preparation of biomedical Ti alloys, including additive manufacturing, porous powder metallurgy, and severe plastic deformation, applied in the manufacturing and the influenced microstructures and properties. Nevertheless, there are still some problems with the long-term performance of Ti alloys, and therefore several surface modification methods are reviewed to further improve their biological activity, wear resistance, and corrosion resistance. Finally, the biocompatibility of Ti and its alloys is concluded. Summarizing the findings from literature, future prediction is also conducted.

In 2021 *Shahad Raheem* ,.[108] Ti-15Mo Alloy is an attractive source for use as a biomaterial due to its outstanding corrosion resistance and its good

mix of mechanical properties such as fatigue, stiffness, and wear resistance. In this work, Ti -15Mo- X(In or Zr) alloy was processed through powder metallurgy to obtain a biomechanically compatible alloy for biomedical implantation. First, titanium, molybdenum, and additive (Indium or zirconium) powders in different composition (0.5,1, 1.5,2 wt.%) However, the Zr additive result to the base alloy gives excellent properties: porosity tends to decrease than when adding indium, and their values (10.8-15.5%). Also, its show excellent mechanical properties: compressive strength increase due to decrease the amount of the porosity in range (374-563), and the elastic modulus is around (82-62 Gpa), wear rate resistance its show a significant improvement reached to 86.5 % under load 20N load, while 76.% at load 40 N, the hardness value in a range (340-420 HB). The corrosion of Ti-15Mo alloy showed significant improvement after In and Zr's addition in artificial saliva and Hank's solutions. It was demonstrated that more considerable progress with the acquisition of the 2wt% In was 59%, 78% in Hank's and Saliva solution, respectively. While with the addition of 2wt.% of Zr, the improvement percentage in Hank's and artificial saliva was 73%,91%, respectively **.**

Chapter Two

Theoretical Part& Literature Review

2.1. Introduction.

This chapter involves the theoretical part of shape memory alloys in many relating fields, these include: NiTi alloy system ; phase diagram and martensitic transformations for such alloys; powder metallurgy process and its affecting variables on the properties of these alloys; and using of chemical machining in preparing of the alloys.

2.2 The Memory Alloys.

Mechanical properties of shape-memory alloys (SMAs) are typically represented by the characteristic stress–strain curve, which forms a hysteresis loop in a loading, unloading and shaperecovering process. To represent the deformation behavior of SMAs, various constitutive equations have been developed, and prediction of the macroscopic behavior has been possible using finite-element simulations.[10]

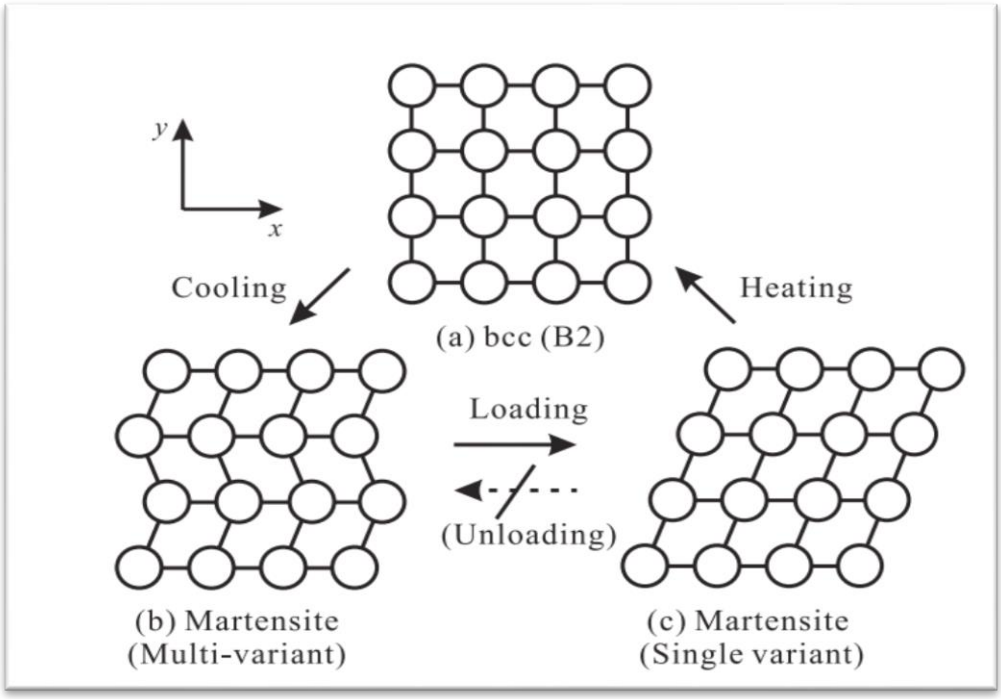

Figure (2-1) Schematic illustration of deformation and shape recovery of a SMA[10].

The atomistic behavior leading to the deformation and shape-recovery is explained on the basis of the phase transformation between austenite and martensite phases and the characteristics of the crystal structure. One well-known atomistic mechanism is illustrated in Fig. 1a. The stable phase depends on the temperature, and phases at high and low temperature are body-centered cubic (bcc or B2) and martensite, respectively. The martensite phase consists of many *variants*, and each variant has a directional unit cell. In Fig. 1(b), for example, a unit cell of the martensite is illustrated as a box leaning in the positive or negative direction along the *x*-axis. Cells leaning in the same direction constitute a layer, and the direction of the lean alternates between layers. the layer is called a variant, although a realistic variant is defined as a rather larger domain. The martensite phase is generated by cooling the B2 structure shown in Figure (2-1) (a). Randomly orientated variants are then generated, as shown in Figure (2-1) (b). some of the layers change their orientation, as shown in Figure (2-1) (c). This structural change induces macroscopic deformation. When the external shear load is released, the strain does not return to the original state except for slight elastic recovery. When the specimen is heated to the transformation temperature, the martensite transforms into the B2 structure, and martensite appears again with cooling of the specimen. Since the B2 structure is cubic, the shape of the unit cell is independent of the orientation of the martensite layers. Therefore, [11] the specimen macroscopically regains its original shape. This mechanism is well known but has not been fully verified since direct observation of dynamic behavior in a wide range of temperatures is difficult. Therefore, computer simulation is expected to provide evidence for and further extend the mechanism. The molecular dynamics method has become a powerful and effective tool to investigate material properties and dynamic behavior on an atomistic scale, and it has also been applied in the case of

SMAs. The stable structure of Ni_3Al, for instance, was investigated by Foiles and Daw [12] using an interatomic potential based on the embeddedatom method (EAM) with suitable parameters [13]. The phase stability and transformation between B2 and martensite structures in NiAl was also reproduced using the EAM potential as reported by Rubini and Ballone [14]. then utilized the EAM potential to demonstrate the shape-memory behavior of Ni-Al alloy in terms of a small single crystal [15] the size dependency and the polycrystalline model Ozgen and Adiguzel also investigated the shape-memory behavior of Ni-Al alloy using a Lennard-Jones [16]). In addition, for Ni-Ti alloy, martensitic transformation was simulated by Sato et al. [17]. It was also reported by Kastner [18] that the shape-memory effect can be represented even by a two-dimensional model with a general LJ potential on the basis of thermodynamical discussion on the effect of temperature on the phase transformation. For a more practical purpose, Park et al. demonstrated shape-memory and pseudoelastic behavior during uniaxial loading of an fcc silver nanowire, and discussed the effect of the initial defects and mechanism of twin-boundary propagation [18].

2.3 Properties of SMA:

2. 3.1 Shape memory effect:

During martensitic phase transformation the molecular structure is twinned. On a macroscopic scale the size and shape of undeformed martensite phase is same as the cubic austenitic phase. The temperature at which starting and finishing of both parent austenitic phase and daughter martensitic phase has characterized by the following variables Ms, Mf, As, Af . Ms is the martensite start temperature upon cooling and Mf is the martensite finish temperature upon cooling, during heating AS and Af are the temperatures of the austenite starts and finishes. The loading quantity of SMA increases with the four variables (Ms, Mf, As& Af), shape memory effect (SME) is noticed when SMA temperature is below Mf , when the alloy

is in deformed martensite, SMA will be recovered the original shape by heating the specimen above Af as shown figure (2-2) and (2-3).

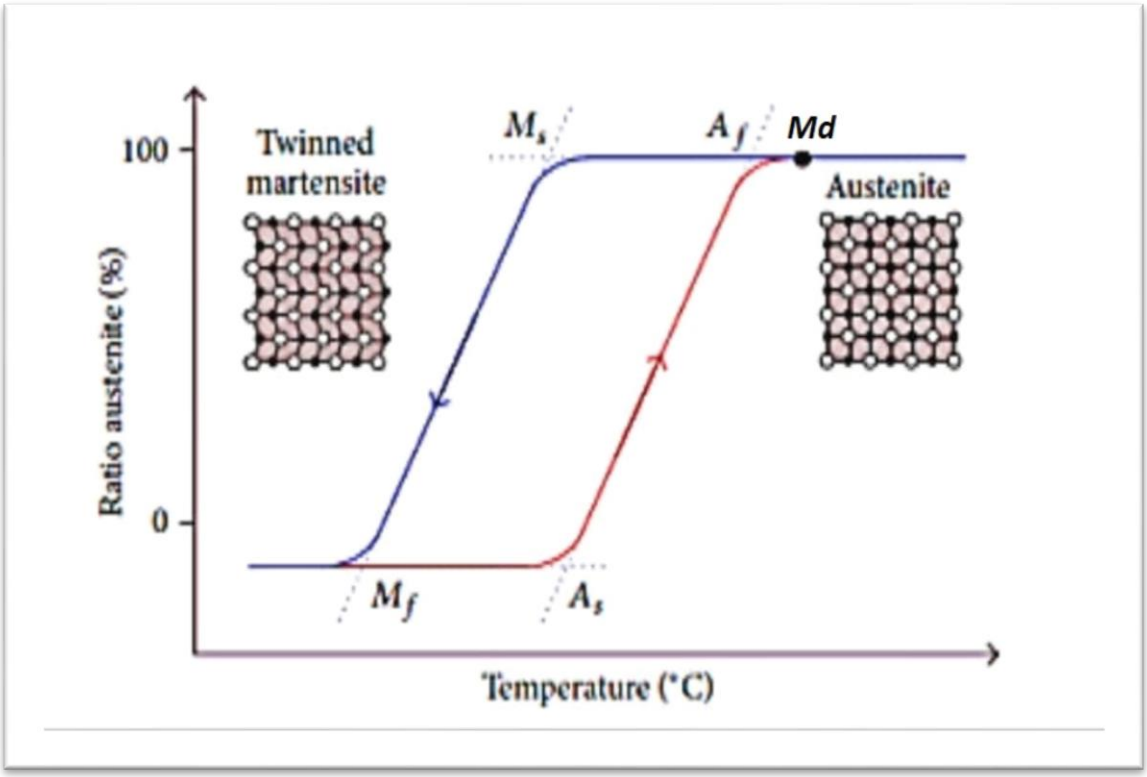

Figure (2-2) ;Temperature Hysteresis in SMA [19].

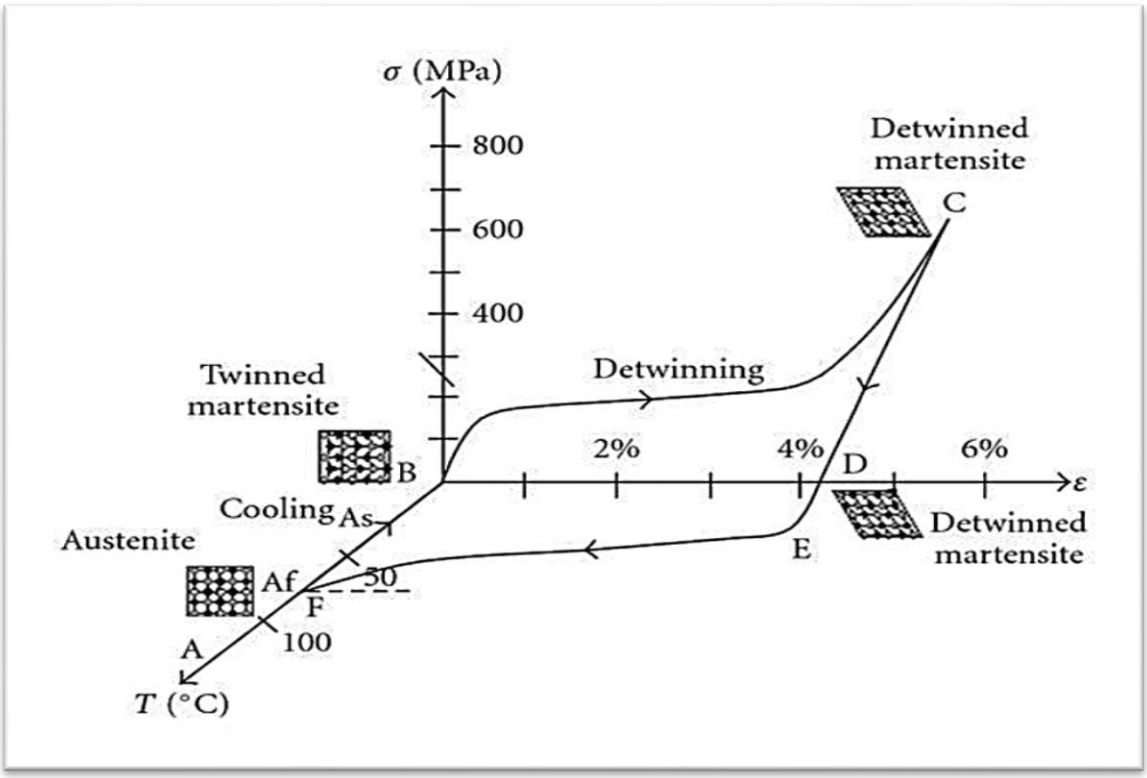

Figure (2-3) ; Stress-strain temperature of NiTi SMA [20].

Normally SME refers to the one-way SME in which external load makes to include de-twinning brings the SMA in to a current distorted structure that can be regain on heating above Af .In this type there is no transformation strains are induced during cooling, it resumes its original shape and rigidity when heated to its higher temperature form (austenite). This is called the one-way shape memory effect. The ability of shape memory alloys to recover a original shape upon heating above the transformation temperatures and to return to a certain alternate Shape upon cooling is known as the two-way shape memory effect. Two-way SME is the one in which transformation strains are persuaded during heating or cooling of SMA Two-way SME is not an essential, but a developed characteristic[21]. Two-way memory is exceptional. There is also an all-round shape memory effect, which is a special case of the two-way shape memory effect [22].

2.3.2 Pseudo elasticity:

Super elasticity or pseudo elasticity of SMA involves stress induced strain recovery upon unloading at a temperature above Af . In general super elastic thermo mechanical loading path starts at zero stress state where de-twinned martensite is stable examples of this characteristic are isothermal (constant temperature) and isobaric (constant pressure) loading paths indicated in Figure (2-4)&(2-5). For achieving the required constant stress by austenite is not shown in the constant pressure path. The point which we remember is the constant temperature conditions carry out only by quasi-static loading which we can treat as small strain increments. During phase transformation, there is a dissipation of latent heat which was generated during quasi-static process. For easy understanding this review paper concentrates mostly constant pressure and constant temperature loading paths will be considered [23].

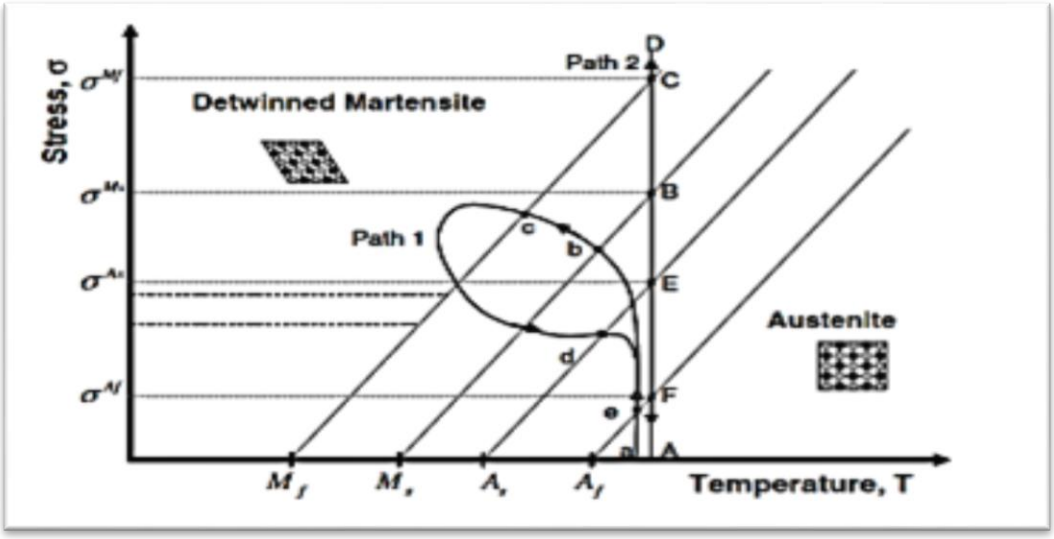

Figure (2-4);phase diagram and two possible[23].

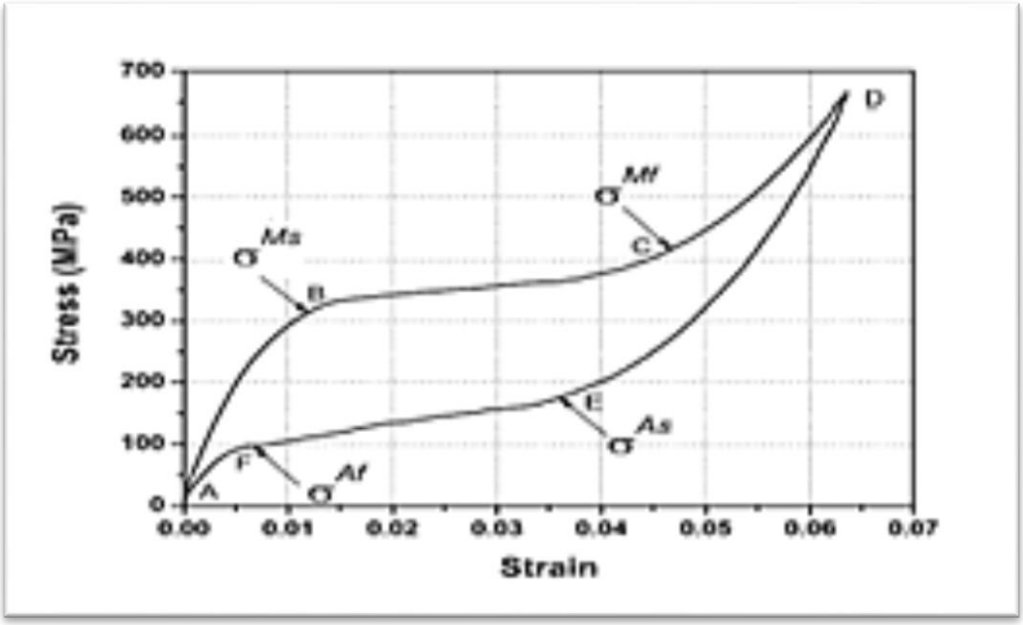

Figure (2-5);SMA pseudoelastic loading cycle

pseudoelastic loading paths [23].

During loading at a temperature above Mf the transformation occurred at critical stress levels from austenite to martensite that stress is called as Transformation stress (a-b). This phase transformation usually occurs during (b-c) path. During thermo elastic critical stress level large in elastic strains are going to be developed. If the load increased further de twinned martensite region (c-d) does not produce any more phase transformation, during multi-axial loading there may be re-orientation of martensite twins will occur. At

point (d) there will be Reverse transformation (RT) from martensite to austenite which will leads to recovery of in elastic strains. At point (e) there will be a complete transformation from martensite to austenite and the final element of the loading path (e-a) is identified by regaining of thermo elastic strains which leads to zero macroscopic strains upon completion of the path. This transformation process concludes in a hysteresis which returns the energy dissipated in the cycle.

2.3.3 Damping properties:

It is very important property for all the materials which are going to use in any specific application.SMA having high damping capacity compared to the remaining materials. Damping property mainly deals with the dissipation of mechanical energy in to heat. The numerous interfaces, which exist during martensitic transformation between austenite and martensite, different martensite variants, the boundaries obtained during twinning of martensite instead of thermo elastic transformation. There will be occurrence of many irreversible events like production defects, dislocation movements etc. hysteresis observed during pseudo elastic characteristic is one of the energy dissipation. The ratio of dissipated energy to the total energy obtained during transformation cycle for isotropic materials will develop. This ratio depends on excitation frequency, temperature, amplitude. A novel material like SMA mainly depends on operating and transformation temperatures as shown Figure(2-6).[24]

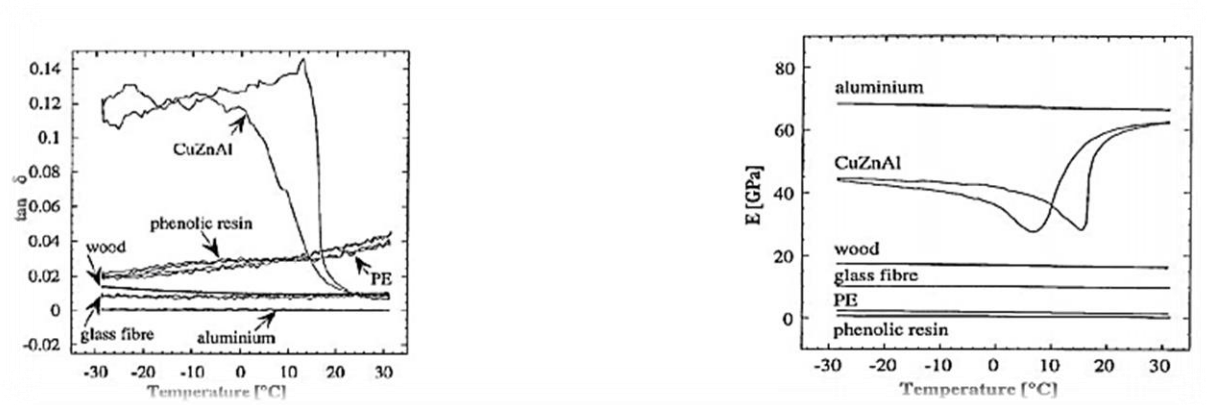

Figure(2-6); Damping factor Vs temperature , Elastic modulus vs. temperature for an frequency of 13Hz for an frequency of 13Hz and and strain amplitude of 10-4 [24] strain amplitude of 10-4

The properties of SMA are determined by their composition and the most commercially adopted shape memory alloys are NiTi (Nitinol) and the Cu-based alloys like Cu-Zn-Al and Cu-Al-Ni. Some of the typical properties of these alloys are listed in below table. [24]

Table (2-1): Some of the typical properties of these alloys[24].

	Nitinol (Ni-Ti)	Cu-Zn-Al	Cu-Al-Ni
Melting temperature(^{0}C)	1300	950-1020	1000-1050
Density (gcm^{-3})	6.45	7.64	7.12
Resistivity(μΩcm)	70-100	8.5-9.7	11-13
Thermal conductivity (W cm^{-1}per^{0}C)	18	120	30-43
Young's modulus (Gpa)	83(austenite) 26-48(martensite)	72(beta phase) 70(martensite)	85(beta phase) 80 (martensite)
Yield strength (Mpa)	195-690(austenite) 70-140 (martensite)	350 (beta phase) 80 (martensite)	400 (beta phase) 130 (martensite)
Ultimate tensile strength (Mpa)	895	600	500-800
Shape memory strain (% maximum)	8.5	4	4
Transformation range (^{0}C)	-200-110	<120	<200
Transformation hysteresis (^{0}C)	30-50	15-25	15-20

2.4 Applications of Shape Memory Alloys

In 1932 smart alloy or shape memory alloy was first discovered by Arne Olander [25], while, Vernon was the first one described the term shape – memory in 1941 . However, the importance of shape memory alloys was not recognized until the shape memory effect was discovered by William

Buehler and Frederick wang in 1962, when they described it in a nickel – titanium alloys (nitinol) [26]. Since then, shape memory alloys have been used for engineering and technical applications in numerous commercial fields; for examples, in automotive [27] , biomedical [28] , aerospace [29], robotics [30], consumer products and industrial applications [31] and fashion [32]. In general, the SMAs applications can be divided into four groups depending on their key function of their unique properties, which are shape memory effect and superelasticity [33]. Table (2-1) Shows the types of shape memory applications [34]. This review focuses on applications of shape memory alloys particularly biomedical, robotic, automotive and aerospace applications.

2.4.1 Biomedical Applications

The materials used for vivo application which are touch with human tissue should have unique properties to meet this requirements, for example, these materials must have biological reliability – biological compatibility, free toxicity, perfect corrosion resistance, and accuracy of mechanical properties [35]. Since the discovery of shape memory effect in NiTi alloys in 1962, they proposed to use this shape memory alloy in biomedical applications [36]. Due to the unique properties of Ni-Ti shape memory alloy (SMA), shape memory effect (SME), shape effect (SE), and a very good corrosion resistance, Ni-Ti shape memory alloys are often used as prosthesis materials in the human body[37]. The application areas available with various size and shape, range from dental arch wire not directly in tough with blood flow in the human organism to stents used to stabilize damaged blood vessels as shown in figure (2-7) [38]. Furthermore, shape memory alloys are used in medical devices in different areas such as orthopedics [39], neurology[40], cardiology and interventional radiology [41]. In addition they are used in stents [42], endodontics [43], eyeglass frames [44], guide wires [45], aneurism treatments [46] and medical tweezers [47], sutures [48], anchors

for attaching tendon to bone [49], implants Figure (2-8) shows example of using shape memory alloy in catheter – based surgeries [50]. NiTi shape memory alloy coiled spring can be used as a micro – muscle fiber as you can see in figure (2-9) [51]. The researchers developed mechanical circulation using shape memory alloys fiber to assist patients with heart diseases as you can see in figure (2-10) [52].

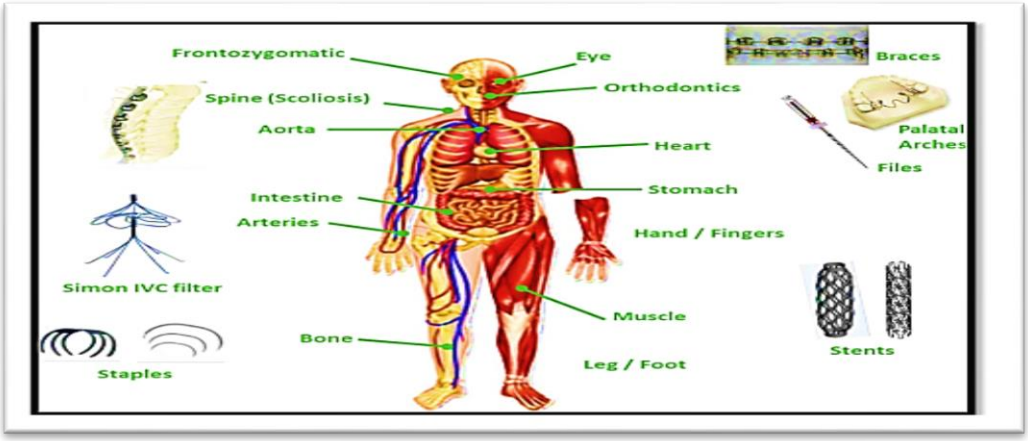

Figure (2-7) Potential and existing shape memory alloy applications in biomedical domain [38].

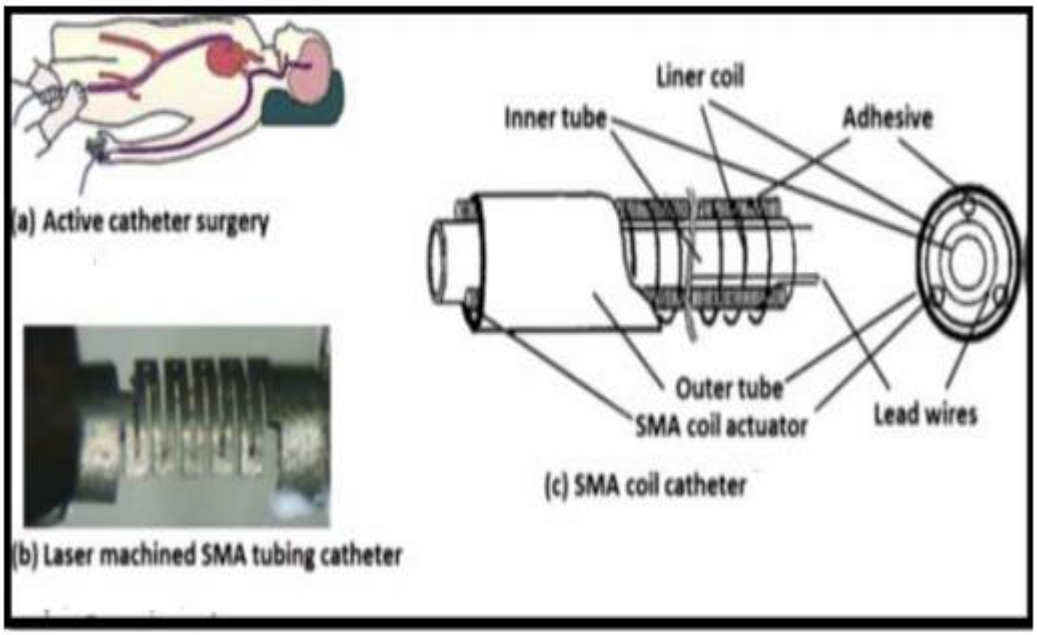

Figure (2-8) Shape memory alloy active catheter [50].

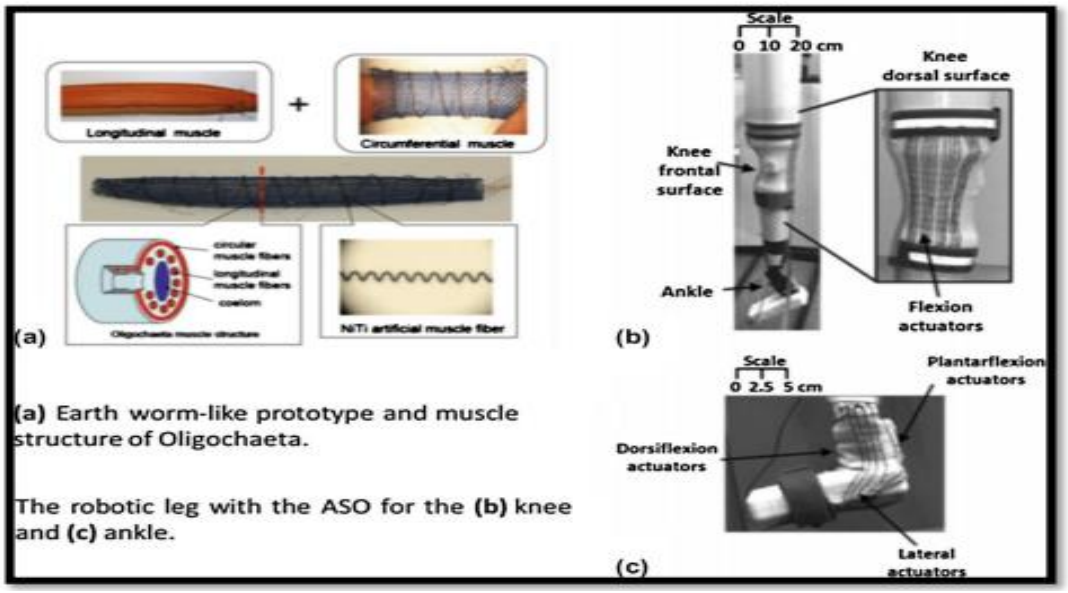

Figure (2-9) Muscle like NiTi shape memory alloy [51].

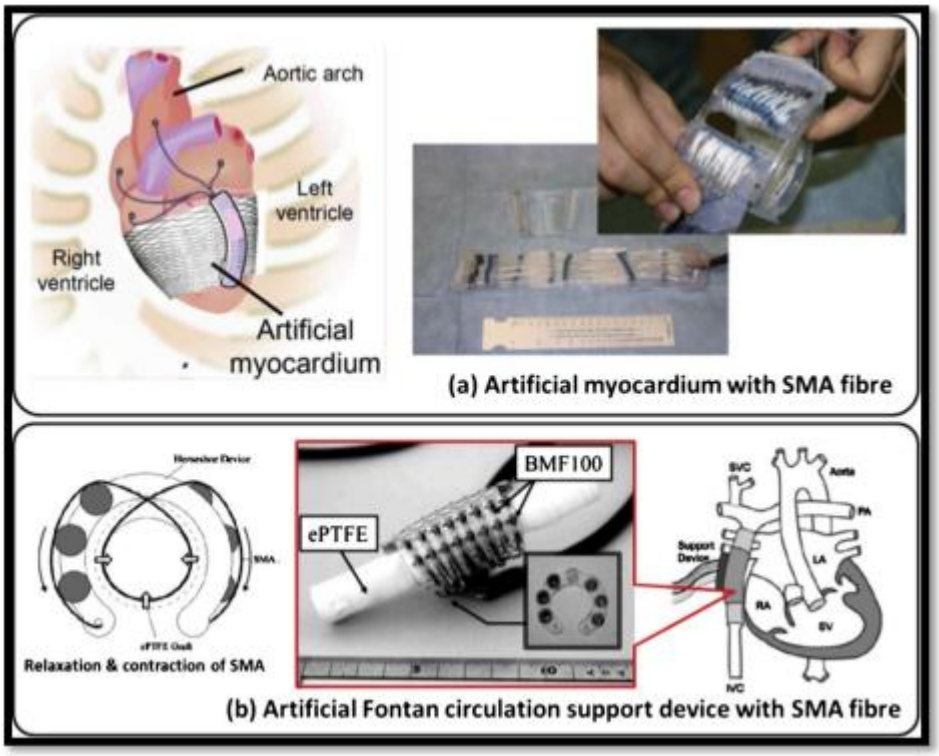

Figure (2-10) Artificial heart support device with shape memory fiber [52].

2.4.2 Robotic Applications

Shape memory alloys have been used in robotic application since 1980s [53]. However, the robots can be divided into several groups depending on their movement techniques and applications, for example jumper, crawler,

fish, walker, flower, medical and biomimetic robotic hand [54]. Figure (2-11) shows the different kinds of shape memory alloys in the robotic applications [55]. Today, numerous works carried out on robotics have focused on biologically inspired and humanoid robots [56]. These robots can be used to solve problems which are challenges for humans, for example can be used in underwater, space, air and land to provide pertinent information from these environments which is difficult to get by humans [57]. Recently, sever flying robots with shape memory alloys have been developed, for example Bat Robot [45] and BATMAV Robot [57]. A dragonfly shown in figure 6 with a 44 cm length and a 63 cm wingspan was developed by Festo Group [48]. The dragonfly is known as BionicOpter see figure (2-12), the dragon equipped with four actuators shape memory alloys to control the movement dragonfly tail up and down and dragonfly head from side to side [58]. The dragonfly has thirteen degrees of freedom, can hover in maneuver in all direction and in mid – air [58].

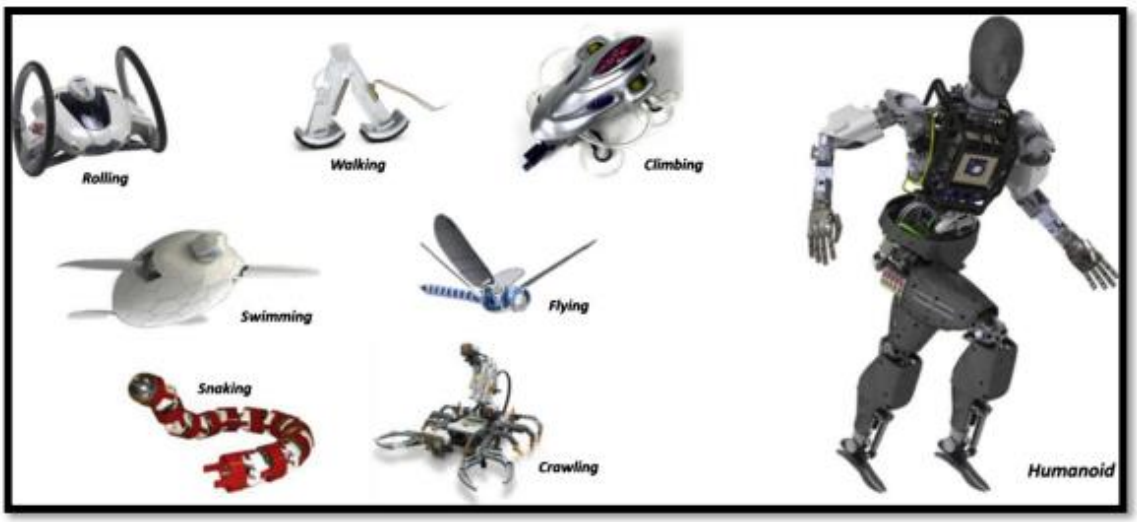

Figure (2-11) Potential and Existing shape memory alloys applications in robotic domain [55].

Figure (2-12) Festo BionicOpter - inspiration dragonfly flight [58].

2.4.3 Automotive Applications

Nowadays, the number of sensors and actuators are growing tremendously due to the request for reliable, convenient and good performance in modern vehicles [58]. Therefore, these offer a wide range for shape memory alloys to use in the automotive industry as shown in figure (2-13) [59]. There are numerous possibility applications for shape memory alloys in automotive industry which have been proposed, but very few of them have been used in practical applications due to the limited range of operating temperature compared with shape memory alloy transformation temperatures [55]. In addition, there are other limitations for example hysteresis width, stability and lifetime [60]. However, shape memory alloys can be used in the mirror system in modern vehicles due to the versatility of shape memory alloy as shown in figure (2-14) [61]. Furthermore, figure (2-15) shows the emerging General Motors shape memory alloys applications [62]. Recently, several other shape memory alloy applications for automotive industry have been developed and they can be found in the literature [63- for examples, tumble flaps actuator, micro – scanner system, pop – up bonnet and side mirror actuator as you can see in figure (2-14) [63]. It is well known that the stander transformation temperatures of NiTi shape memory alloy are at range temperatures – 40 ◦ C to approximately + 110 ◦ C [63]. In contrast, the stander operating temperature range for automotive application is between –

40 ° C to approximately +125 ◦ C as shown in figure (2-15) [64]. Therefore, the majority of the practical applications of shape memory alloys are covered by NiTi shape memory alloy [65]. However, from the figure (2-15) and in order to act properly the shape memory alloys should exhibit a martensite transformation temperature above maximum operating temperatures as shown in the figure (2-14) the red dotted lines. Moreover, there are many kinds of high temperatures shape memory alloys. But these alloys are of high cost for automotive industry [66]. Although, the Cu-Al-Ni shape memory alloys exhibits martensitic transformation temperatures up to 200 ◦ C, these materials are unstable, brittle, exhibit low fatigue strength and cannot be used for multiple cyclic operations [65]

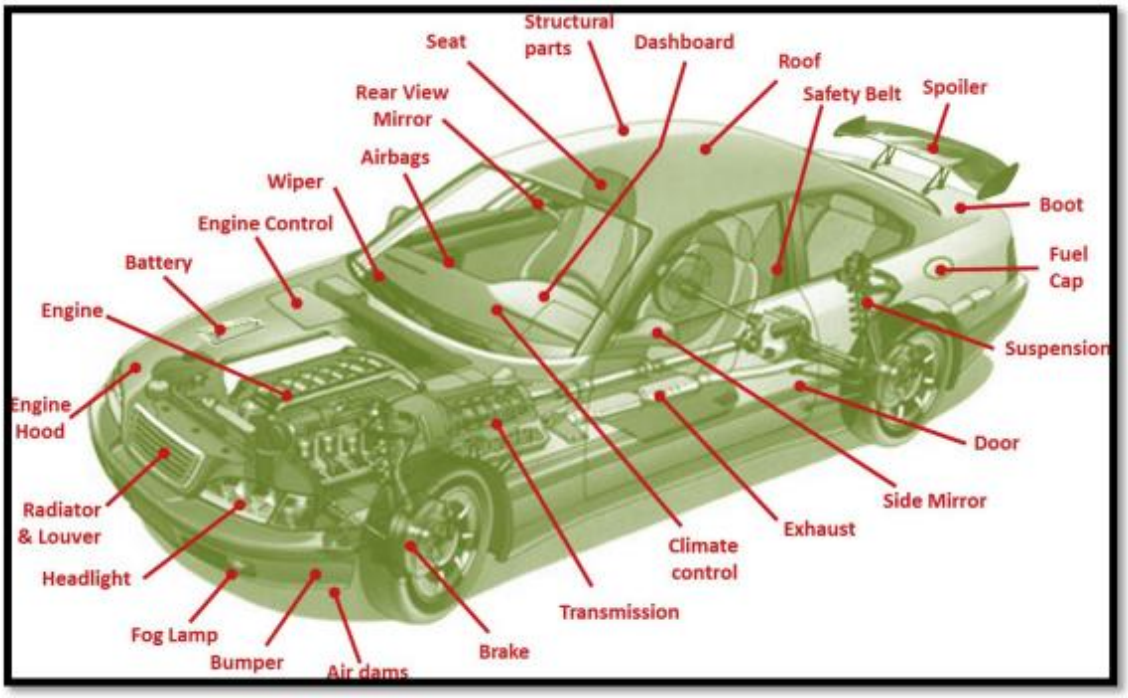

Figure(2-13) Existing and potential shape memory applications in the automotive domain [59].

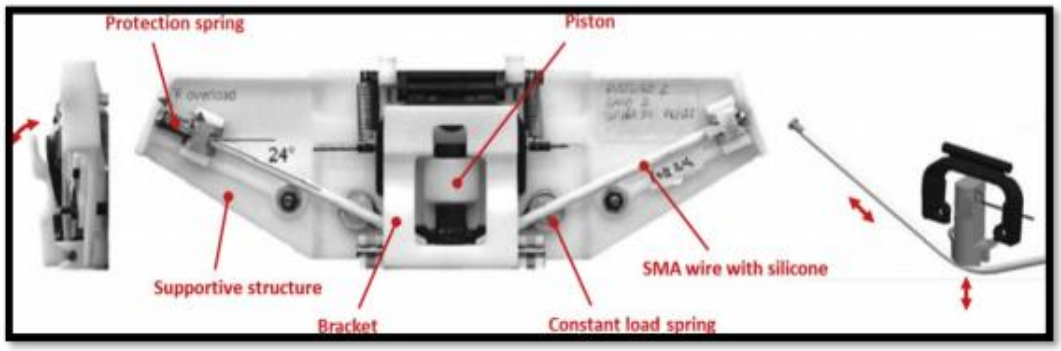

Figure (2-14) EAGLE mirror prototype [61].

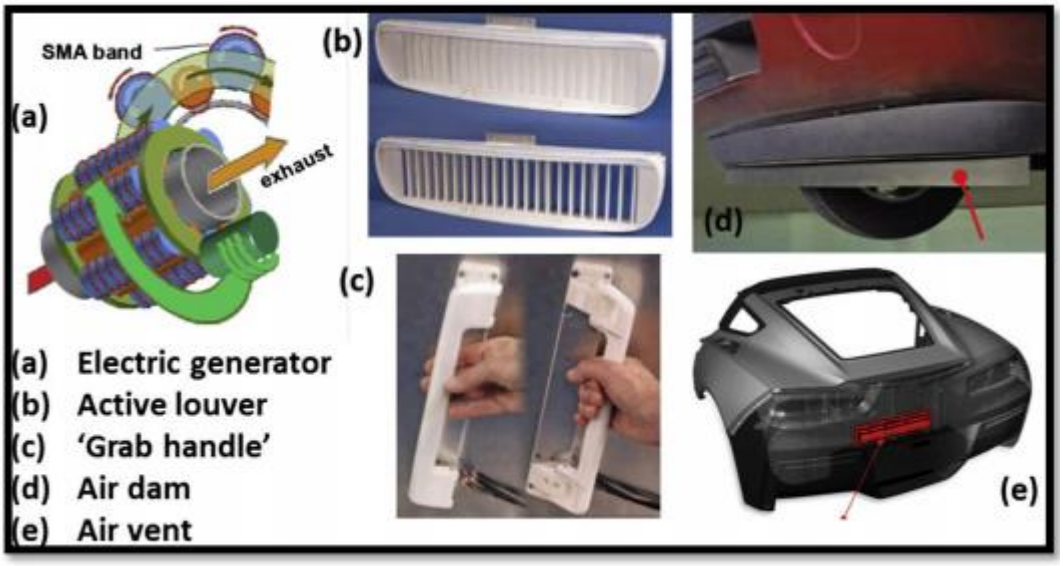

Figure(2-15) Emerging General Motors Shape Memory Alloy [63].

2.4.5 Aerospace Applications

SMAs have been used in aerospace since 1970s when used in hydraulic line coupling which is used in the F-14 fighter jets [62]. Since this time and due to the unique properties of SMAs many aerospace researchers have proposed to use this material for solving engineering issues in the aerospace manufacture[67]. In the 1990s, numerous works carried out on aerospace industry such as Advanced Research Projects Agency (DARPA) program for aircraft smart wings [66], the Smart Aircraft and Marine Propulsion System Demonstration (SAMPSON) program for jet engines[67] and another program can be seen in literatures [68]. The Boeing company has improved an active device based on SMA technology programs which is VGC, a

variable geometry chevron on a 77-300 ER with GE90-115B jet engine, this device has the ability to minimize noise through take- off, figure 12 shows Boeing variable geometry chevron [69]. Then, after the VGC success, many companies such as Boeing, DARPA, NASA and other have been introduced more SMAs based on technology programs in order to use SMAs in aerospace industry [70].Figure (2-16) shows the possibility SMAs applications in the aerospace industry [66].

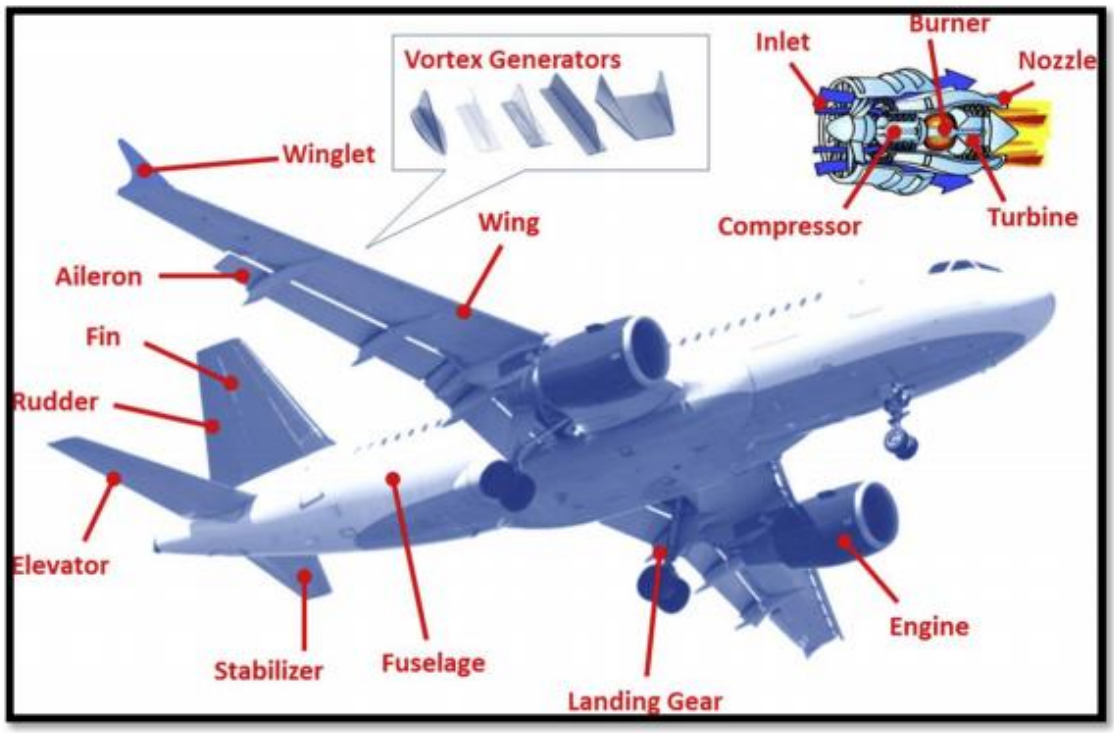

Figure(2-16) Existing and potential shape memory alloys applications in the airspace domain [64].

2.5 Phase Diagrams for NiTi Alloy

The Ni-Ti phase diagram shows a number of different transformations, a few of which are important during the sintering of Ni-Ti alloys. These are the eutectoid (β-Ti Æ α-Ti+Ti2Ni) and the eutectic (liquid Æ β-Ti+Ti2Ni) transformations which take place at 765 °C and 942°C, respectively Figure (2-18). The reaction between Ti and Ni is exothermic, so it has the possibility of self-sustaining synthesis. This means that there is an ignition temperature at which the reaction can be initiated and then it will continue by itself.

Combustion synthesis of NiTi is therefore possible. NiTi shows a relatively low heat of formation (ΔHq= 67kJ/mol)6 . Preheating of the sample mixture is necessary for self-sustaining synthesis, promoting transient melt formation9 . In addition, it has been reported that NiTi synthesis from elemental powder mixtures leads to the formation of other intermetallic compounds like Ti2Ni, Ni3Ti, Ni4Ti3 and Ni3Ti2 10–12. Among them, Ti_2Ni and Ni_3Ti are relatively more stable than NiTi thermodynamically, and therefore it is difficult to avoid their presence in the microstructure during the synthesis of a NiTi alloy[71]

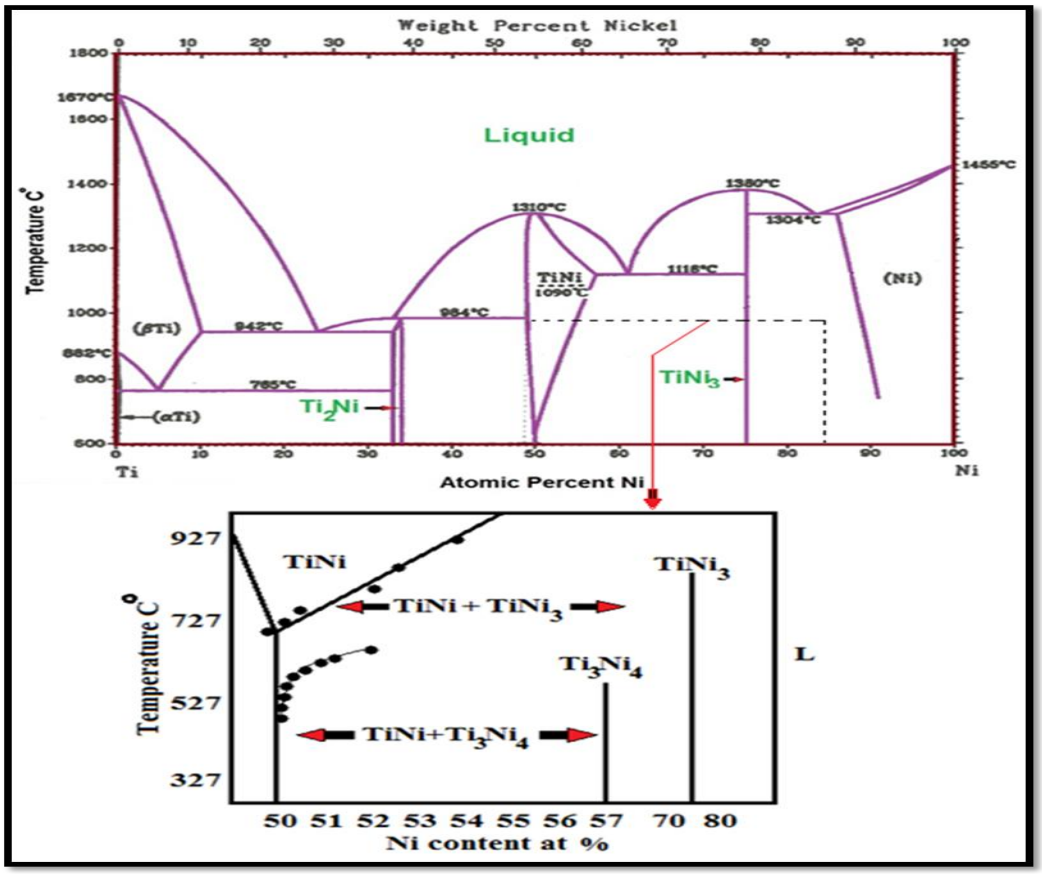

Figure (2.18): Nickel-Titanium Phase Diagram [71].

2.6 Transformation temperatures.

From the B2 phase stability regime, the B2 structure starts to transform into the B19Š martensite phase at Ms (the martensite start temperature) on cooling. The volume transformed into the martensite is a function of

temperature. Holding at any temperature below Ms for any length of time does not cause the formation of more "athermal" martensite. The parent B2 phase is completely transformed into the product B19 martensite for temperatures below Mf (the martensite finish temperature).[72] If the transformation process includes the R-phase, the start and the end temperatures of the transformation from the austenite to R-phase are denoted by Rs and Rf , respectively. On heating, the reverse transformation from B2 austenite to B19 martensite phase takes place. The temperature, at which the reverse transformation begins, is denoted As. Similarly, the last remnant of martensite disappears at the temperature Af . There is transformation temperature hysteresis such that As > Mf and Af > Ms. If the reverse transformation includes the R-phase, corresponding transformation temperature are denoted A_{RS} and A_{RF} on heating. The magnitude of thermal hysteresis of the B19Š phase transformation is much larger (one order of magnitude higher) compared with the magnitude of the thermal hysteresis of the R-phase transformation [73]. There is a strong composition dependence of the B19Š-Phase transformation temperatures (PTTs), see Figure (2-19) the PTTs decrease signiĄcantly with increasing concentration of Ni atoms in the Ni-rich NiTi-phase [74]. The PTTs can change by about 20°C per added 0.1 at% Ni [75]

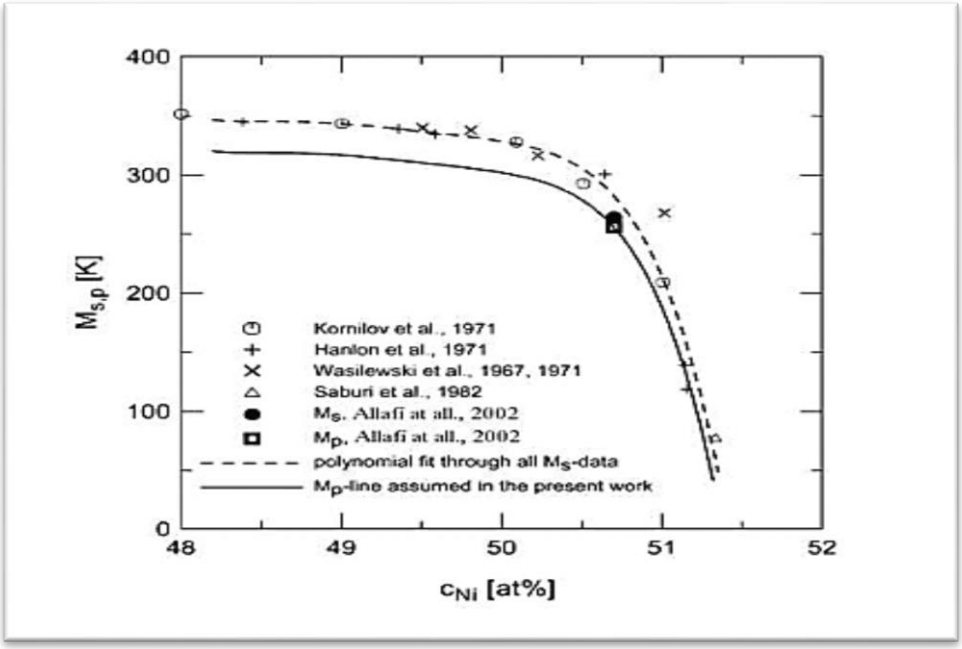

Figure (2-19): Relation between nickel content M_S, M_P temperatures [75].

martensitic transformations can be triggered by external applied stress according to the Clausius-Clapeyron type relationship. The highest temperature at which martensite phase can form under applied stress is denoted Md [76]. Md is the temperature above which the chemical driving force becomes so small that nucleation of martensite cannot be mechanicaly induced [75]. In the following section I will introduce a SMA phase diagram of one-step martensitic transformation in temperature-stress coordinates, where a dependence of transformation temperatures on applied stress can be seen.

2.7 Mechanical properties of NiTi SMA

Like most SMAs, NiTi alloys show marked differences in mechanical behavior depending upon whether they are tested in the martensitic or austenitic state. The martensitic stress - strain curve can be divided into three well defined regions, see Figure (2.20). An initial low plateau results from the stress induced growth of one martensitic orientation at the expense of the

adjacent. At higher stresses there is a second region that is linear, although not purely elastic [76].

The transition to the third region is a result of the onset of irreversible plastic deformation, as in the case of yielding of all conventional metals. The length of the martensitic plateau in the stress - strain curve extends typically to around 5% - 6%. However, depending on the details of the alloy and its prior thermomechanical history. The plateau can vary from a continuous curve with an inflection point to a clear horizontal with a sharp yield point.

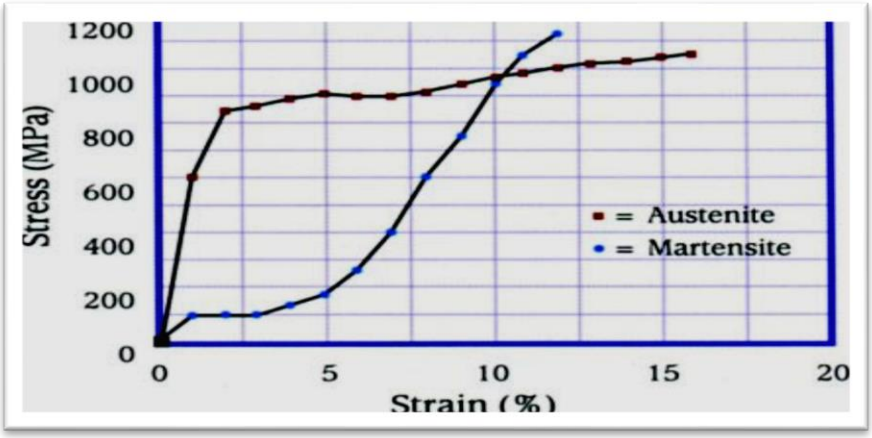

Fig.(2.20) Stress-strain curve for a Ni-Ti-10%Cu alloy in the austenitic and martensitic conditions [76].

2.8 the effect of alloying elements on the shape memory alloys

2.8.1 Molybedum (Mo)

Molybdenum metal is usually produced by powder metallurgy techniques in which Mo powder is hydrostratically compacted and sintered at about 2100°C. Hot working is done in the 870-1260°C range. Moly forms a volatile oxide when heated in air above about 600°C and therefore high temperature applications are limited to non-oxidizing or vacuum environments. [77]. The addition of Mo reduces the hardness of the alloy compared with the master sample. The porosity percentage decreases with increase in Mo percentage.The corrosion rate decreases with increase in Mo percentage in Ringer solution . [78]

2.8.2.Zirconium(Zr).

Zirconium is a neutral element when dissolved in Ti. Zirconium belongs to Group 4 (according to the new IUPAC name) in the Periodic Table, which is the same as Titanium and hafnium, have similar chemical structure and properties. Thus, they have been recognized as non-toxic and non-allergic. Zirconium is a transition metal with an atomic number of 40 and an atomic weight of 91.22 amu. As a greyish-white lustrous metal, Zirconium has exceptionally high melting (1857 °C) and boiling (4409 °C) points. Zirconium has excellent resistance to Corrosion, similar to Titanium and is highly biocompatible [79]. Since both metal surfaces form a stable oxide layer on their surface within nanoseconds when exposing to oxygen. Thus, the oxidation passivates the materials. However, Zirconium could not be used in dentistry in its pure form. An extensive review article [98] suggested that Zirconium implants had a lesser degree of osseointegration than titanium analogue using removal torque tests. Some surface modifications could restructure the implant that could remove torque test values comparable with the titanium implants.Although the removal torque test values highly depend solely on the surface structure (in terms of mechanical retention and biological interaction) than on the implant material itself [80], the atomic structural arrangement allows the torque performance in metal alloys better than in ceramics. The reason for using a zirconia implant is merely due to improvement in esthetic qualities in dental restorations. Thus, the development of Ti-alloys is still viable and active [81].

2.9 Literature Review

Vojtěch (2010) [96] studied the influence of heat treatment of shape memory NiTi alloy on its mechanical properties , the aim is to determin the mechanical properties of nitinol short-time heat treated at around 500°C. The temperature of 500°C was selected, because in manufacture of stents, shape setting is a step generally performed at about 500°C. It has been found that heat treatments of the straight annealed nitinol wire at moderate temperatures strongly influences its tensile strength and transformation stress. Annealing temperatures between 410-460°C improve the strength to some extent. At 12 higher temperatures above 485°C, the wire behaves in an opposite manner,

i.e. strength reduces. The observed development of mechanical properties and transformation behavior is related to precipitation processes occurring in the wire during heat treatment.

In 2010 Flamini et.al [97] electrodeposited a polyprypol (PPY) film on to Nickel - Titanium alloy (NiTi) employing sodium bis (2- ethylhexyl) sulfosuccinate (Aerosol Otor Aot) solutions. The results showed that the polymer has improved corrosion performance of the coated samples in chloride solution and the polymer improves the corrosion performance at the open circuit potential and at potentials where the bare substrate suffers pitting attack. The improvement in both adhesion and corrosion performance was discussed considering substrate / polymer interaction, over oxidation of PPy and the role played by AOT .

In 2012 ,. Tawhid Ezaz et al ,. [98] Dislocation slip in B2 NiTi is studied with atomistic simulations in conjunction with transmission electron microscopy (TEM). The atomistic simulations examine the generalized stacking fault energy (GSFE) curves for the {0 1 1}, f211g and {0 0 1} planes. The slip directions considered are h100i, h111i and h011i. The results show the smallest energy barriers for the (0 1 1)[1 0 0] case, which is

consistent with the experimental observations of dislocation slip reported in this study. To our knowledge, slip on the (0 1 1)½11 1 system is illustrated for the first time in our TEM findings, and atomistic simulations confirm that this system has the second lowest energy barrier. Specimens that underwent thermal cycling and pseudoelasticity show dislocation slip primarily in the austenite domains while the bulk of martensite domains does not display dislocations. The results are discussed via calculation of the ideal slip nucleation stress levels for the five potential slip systems in austenite

In 2015 ,. Kamal Kumar et al ,. **[99]**Nitinol (NiTi) is categorized as a smart material which is highly recognized material for medical and other engineering applications. The behaviour of NiTi can be modified by altering the composition, modifying the porosity and applying external thermal and mechanical treatment. Due to high composition sensitivity, there are several impediments in fabrication of NiTi with conventional techniques which impel the use of additive manufacturing methods. But due to very high cost of equipments, these processes have not been commercialized till now. This paper presents a review on applications, manufacturing NiTi alloy and its various production routes from conventional to rapid prototyping, porous NiTi, effect of additives on properties of the alloy and its challenges.

In 2016 ,. CNaresh et al ,.[100] Shape memory alloys (SMAs) are the special materials that have the ability to return to a predetermined shape when heated. When this alloy is in below transformation temperature it undergoes low yield strength and will deform easily into any new shape which it will retain, if this alloy is heated above its transformation temperature it changes its crystal lattice structure which returns to its real shape .SMAs are remarkably different from other materials are primarily due to shape memory effect (SME) and pseudoelasticity which are related with the specific way the phase transformation occurs, biocompatibility, high specific strength, high corrosion resistance, high wear resistance and high

anti-fatigue property. SMA are used in many applications such as aerospace, medical, automobile, tubes, controllers for hot water valves in showers, petroleum industry, vibration dampers, ball bearings, sensors, actuators, miniature grippers, micro valves, pumps, landing gears, eye glass frames, Material for helicopter blades, sprinklers in fine alarm systems packaging devices for electronic materials, dental materials, etc. This paper focuses on introducing shape memory alloy and their applications in past, present and in future, also revealed the concept and mechanism of shape memory materials for a particular requirement. Properties of SMAs, behaviour and characteristics of SMA, summary of recent advances and new application opportunities are also discussed.

In 2016 ,. Aun Nawaz Khan et al ,. [101] Shape Memory Alloys (SMA) are unique class of alloys which possess various engineering applications. One such SMA is Nickel–Titanium (Nitinol) shape memory alloy. The problem, however with Nickel is that the metal may leach out in form of toxic Ni2+ ions. The latter may prove costly when used in various applications. To increase the corrosion resistant properties of Nitinol and to evaluate its shape memory properties, small amount of Zirconium i.e. 5 and 10 at % are added into the existing Nitinol system. Buttons of Nitinol and Nickel–Titanium with Zirconium additions are made using the button arc furnace. For the characterization of the alloys, various techniques including Energy Dispersive Spectroscopy (EDS), Back Scattering Electron (BSE) imaging, Differential Scanning Calorimetry (DSC) have been performed. Thework conducted reveals that addition of Zirconium in Nitinol has marked influence on microstructure, shape memory properties, transformation temperature, hardness values, and corrosion properties of the alloy.

In 2017 ,. Hossein Sina et al ,. [102] The present study focuses on *in situ* as well as *ex situ* studies on the sintering of pre-compacted powder mixtures of 50at% Nickel-50at%Titanium. *In situ* studies were carried out by monitoring

the changes in morphology of the fracture surface of the compact continuously during heating in the hot stage of an environmental scanning electron microscope. Results on the initiation of sintering and its variation with the particle size of reactants are presented. Differential Scanning Calorimetry and X-ray diffraction studies have also been made to characterize the formation of intermetallic compounds during the progress of sintering

In 2017 ,. Yulong Liang et al,.[103] investigated Based on ternary Ni45Ti51.8Fe3.2 (at %) shape memory alloy (SMA), Nb and Ta elements are added to an NiTiFe SMA by replacing Ni element, and consequently quaternary Ni44Ti51.8Fe3.2Nb1 and Ni44Ti51.8Fe3.2Ta1 (at %) SMAs are fabricated. The microstructure, mechanical property, and phase transformation of NiTiFeNb and NiTiFeTa SMAs are further investigated. Ti2Ni and β-Nb phases can be observed in NiTiFeNb SMA, whereas Ti2Ni and Ni3Ti phases can be captured in NiTiFeTa SMA. As compared to NiTiFe SMA, quaternary NiTiFeNb and NiTiFeTa SMAs possess the higher strength, since solution strengthening plays a considerable role. NiTiFeNb and NiTiFeTa SMAs exhibit a one-step transformation from B2 austenite to B19’ martensite during cooling, but they experience a two-step transformation of B19’-R-B2 during heating**.**

In 2017 ,. M Losertová et al ,. [104]Superelastic behavior of off-stoichiometric NiTi alloys is significantly affected by microstructure changes due to heat treatment. Applying appropriate thermal treatments important effects on microstructural changes, transformation temperatures and thermomechanical properties of final NiTi products can be achieved. The experimental samples of NiTi alloy with 55.8 wt.% Ni were submitted to heat treatment and the microstructures before and after the treatment were observed. The thermal regimes consisted of annealing treatment at 600 °C for 1 hour followed by water quenching and of ageing at eight different

temperatures (250, 270, 290, 300, 350, 400, 450 and 500 °C) for 30 minutes. Microstructure features studied by means of optical and scanning electron microscopies, EDX microanalyses, X-ray diffraction analyses and microhardness measurement, have shown that higher ageing temperatures led to microstructure changes and corresponding increase in microhardness.

In 2017 ,. CENGIZ TATAR and ZÜLKÜF YILDIRIM ,. [**105]** The effect of hydrostatic pressure on the behaviour of reverse and forward transformation temperatures and physical properties of NiTi shape memory alloy has been investigated. The transformation temperatures and physical properties of the alloy change with applied pressure. It has been clearly seen from differential scanning calorimetry that with the increase of applied pressure, while *A*s, *A*f and *M*f transformation temperatures decrease, *M*s value increases. Moreover, it is obvious that with the increase of applied pressure, Gibbs free energy increases by 5.2883 J, while elastic energy increases by 1.4687 J. In addition, entropy of the alloys decreases by 0.2335 J *(*g ◦C*)*-1 with applied pressure. Additionally, it is evident from the scanning electron microscopy images of the samples that there is an obvious difference in the grain sizes of the unpressured sample and the samples on which pressure is applied, the sizes being 10–100 and 30–150 μm, respectively

In 2018 ,. Shih-Fu Ou et al ,. [106]In this study, an optimal selective laser melting (SLM) process for manufacturing dense NiTi alloy with pseudoelasticity and shape-memory capability was proposed. The microstructure, phase-transformation temperature, shape memory capability, and pseudoelasticity were investigated by scanning electron microscopy, X-ray diffraction, differential scanning calorimetry, and bending and tensile tests. NiTi powder with a particle size > 45 μm was selected for the subsequent SLM process, because it exhibited a Ni/Ti ratio of ~1 and a lower oxygen content than powders with smaller particle sizes. A thin-walled disk

(0.48 mm thick) and cuboid samples (5 mm thick) were prepared for investigating the variation in the homogeneity of the microstructure. The thin-walled SLM-NiTi sample exhibited a marginally inhomogeneous microstructure between layers, and defects existed in the previously formed side. The cuboid SLM-NiTi sample was fabricated without undesirable secondary phases, and it exhibited a 100% shape-recovery rate under 2% bending strain and completely pseudoelastic under 3% strain. Also, the SLM-NiTi exhibited lower phase-transformation temperatures and a broader phase-transformation range than the original NiTi. The phase-transformation range can be reduced by annealing.

In 2019 Lai-Chang Zhang and Liang-Yu Chen [107] Compared with stainless steel and Co–Cr-based alloys, Ti and its alloys are widely used as biomedical implants due to many fascinating properties, such as superior mechanical properties, strong corrosion resistance, and excellent biocompatibility. After briefly introducing several most commonly used biomedical materials, this article reviews the recent development in Ti alloys and their biomedical applications, especially the low-modulus β-type Ti alloys and their design methods. This review also systemically investigates the recently attractive progress in preparation of biomedical Ti alloys, including additive manufacturing, porous powder metallurgy, and severe plastic deformation, applied in the manufacturing and the influenced microstructures and properties. Nevertheless, there are still some problems with the long-term performance of Ti alloys, and therefore several surface modification methods are reviewed to further improve their biological activity, wear resistance, and corrosion resistance. Finally, the biocompatibility of Ti and its alloys is concluded. Summarizing the findings from literature, future prediction is also conducted.

In 2021 *Shahad Raheem* ,.[108] Ti-15Mo Alloy is an attractive source for use as a biomaterial due to its outstanding corrosion resistance and its good

mix of mechanical properties such as fatigue, stiffness, and wear resistance. In this work, Ti -15Mo- X(In or Zr) alloy was processed through powder metallurgy to obtain a biomechanically compatible alloy for biomedical implantation. First, titanium, molybdenum, and additive (Indium or zirconium) powders in different composition (0.5,1, 1.5,2 wt.%) However, the Zr additive result to the base alloy gives excellent properties: porosity tends to decrease than when adding indium, and their values (10.8-15.5%). Also, its show excellent mechanical properties: compressive strength increase due to decrease the amount of the porosity in range (374-563), and the elastic modulus is around (82-62 Gpa), wear rate resistance its show a significant improvement reached to 86.5 % under load 20N load, while 76.% at load 40 N, the hardness value in a range (340-420 HB). The corrosion of Ti-15Mo alloy showed significant improvement after In and Zr's addition in artificial saliva and Hank's solutions. It was demonstrated that more considerable progress with the acquisition of the 2wt% In was 59%, 78% in Hank's and Saliva solution, respectively. While with the addition of 2wt.% of Zr, the improvement percentage in Hank's and artificial saliva was 73%,91%, respectively **.**

Chapter Four

Results and Discussion

4.1 Introduction

This chapter presents the experimental results and their discussion which involves the properties related to the NiTi alloy samples prepared by powder metallurgy technique. This includes the effect of physical and mechanical properties It includes microstructure analysis done by SEM, phases analysis results from XRD technique, electrochemical test (Open Circuit Potential, Potentiodynamic polarization), mechanical properties tests which involved hardness, wear test .

4.2 Results Of The Metallography

4.2.1 X-Ray Diffraction

X-ray diffraction technique is one of analytical techniques that reveals information about the crystallographic structure, chemical composition, and physical properties of materials. This technique is based on observing the scattered intensity of an X-ray beam hitting a sample. An important parameter is the wavelengths; X-rays have wavelengths in the order of angstroms, in the range of typical interatomic distances in crystalline solids. For this reason, X-ray diffraction (XRD) has provided information regarding the crystallographic structures in material. But also, it can be used to determine molecular structures. X-ray diffraction provided important evidence of atoms. XRD directed at the solid provides the simplest way to determine interring atomic spacing. The intensity of the diffracted beams depends on the arrangement and atomic number, but also on the other parameters.

XRD can be used to describe the NiTi alloys as shown in figures [(4.1)-(4.4)] resulted in a three-phase structure through examination, they found

that the important phases that appeared are NiTi monoclinic phase, NiTi cubic phase and hexagonal Ni_3Ti phase for all alloys.

(the phases are determined manually, by referring to reference cards and literatures) shown in appendix.

The formation of Ni_3Ti might be attributed to the slow cooling of the samples inside furnace whereas, in the sintering conditions used throughout this work, the Gibbs free energies for Ni_3Ti was less than that for NiTi [114]. The suggested reactions during the process are as follows [115].

$Ni + Ti \rightarrow NiTi$ ΔG: - 67 KJ / mol …….. (4.1)

$Ni + Ti \rightarrow Ni_3Ti$ ΔG: - 140 KJ / mol …….. (4.2)

According to the binary phase diagram of NiTi system as shown in figure (2.19), NiTi and Ni_3Ti are stable compounds and reaction (4.2) is more thermodynamically favored than reaction (4.1).

Phases produced as a result of the sintering process which were investigated using the XRD technique. It can be seen from the figures that there are probably no pure metals present. This proves that the sintering time and temperature used in this work result in complete sintering reaction.

When zirconium was added at a rate of 3%, a compound appeared, which is Ni_7Zr_2 as shown in figure (4.2).

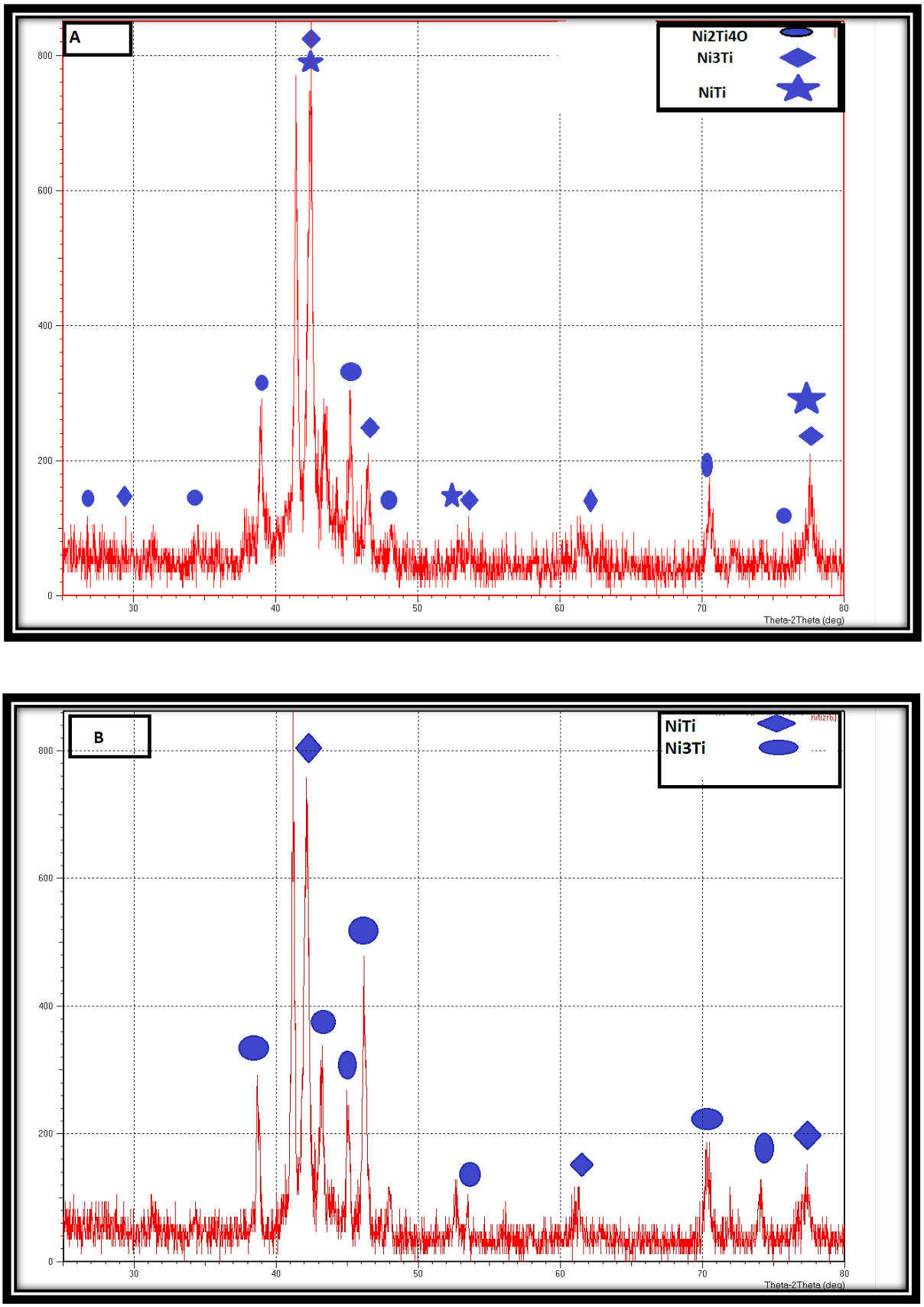

figure (4.1): X-Ray Diffraction A, B alloys

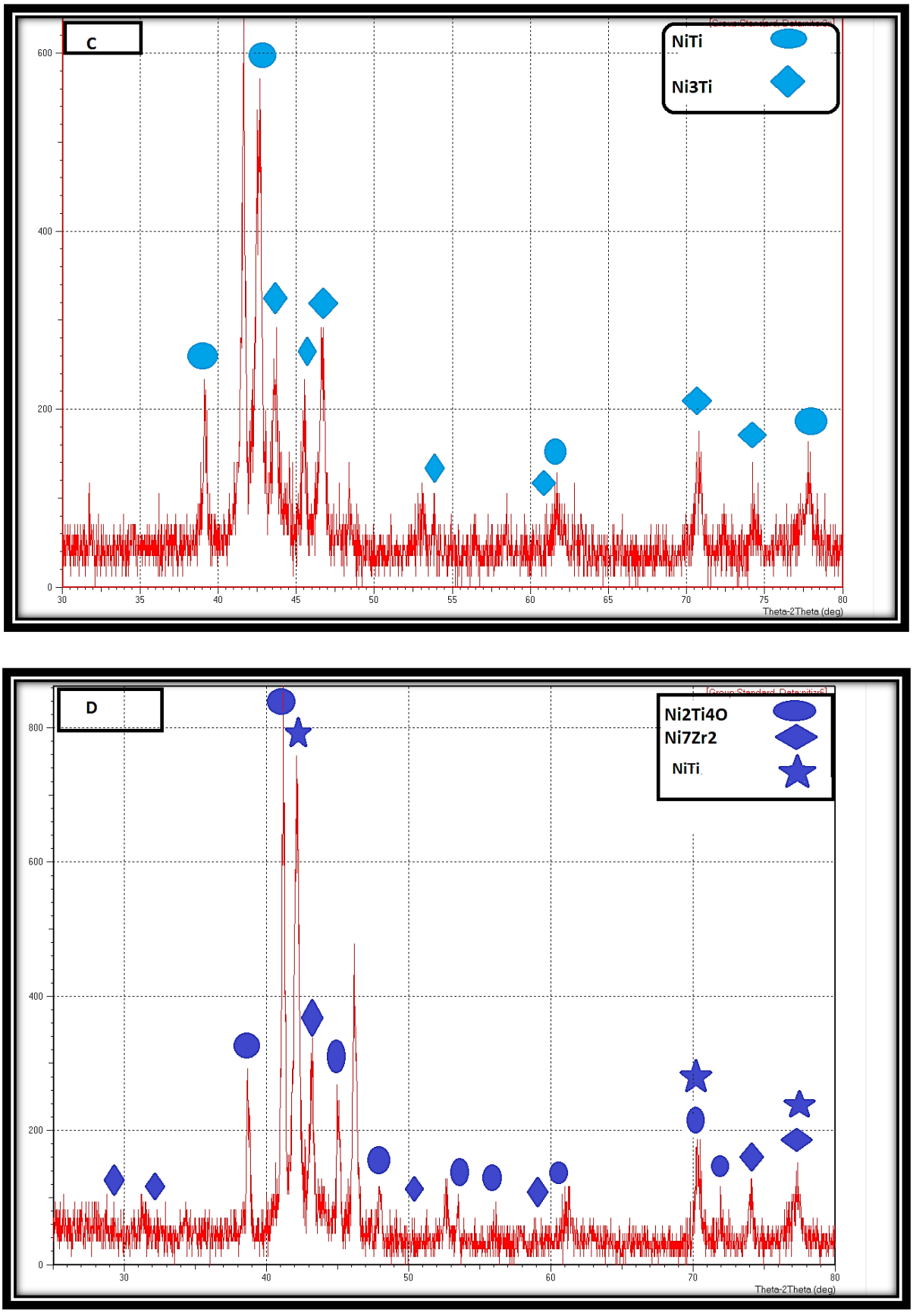

figure (4.2): X-Ray Diffraction C, D alloys

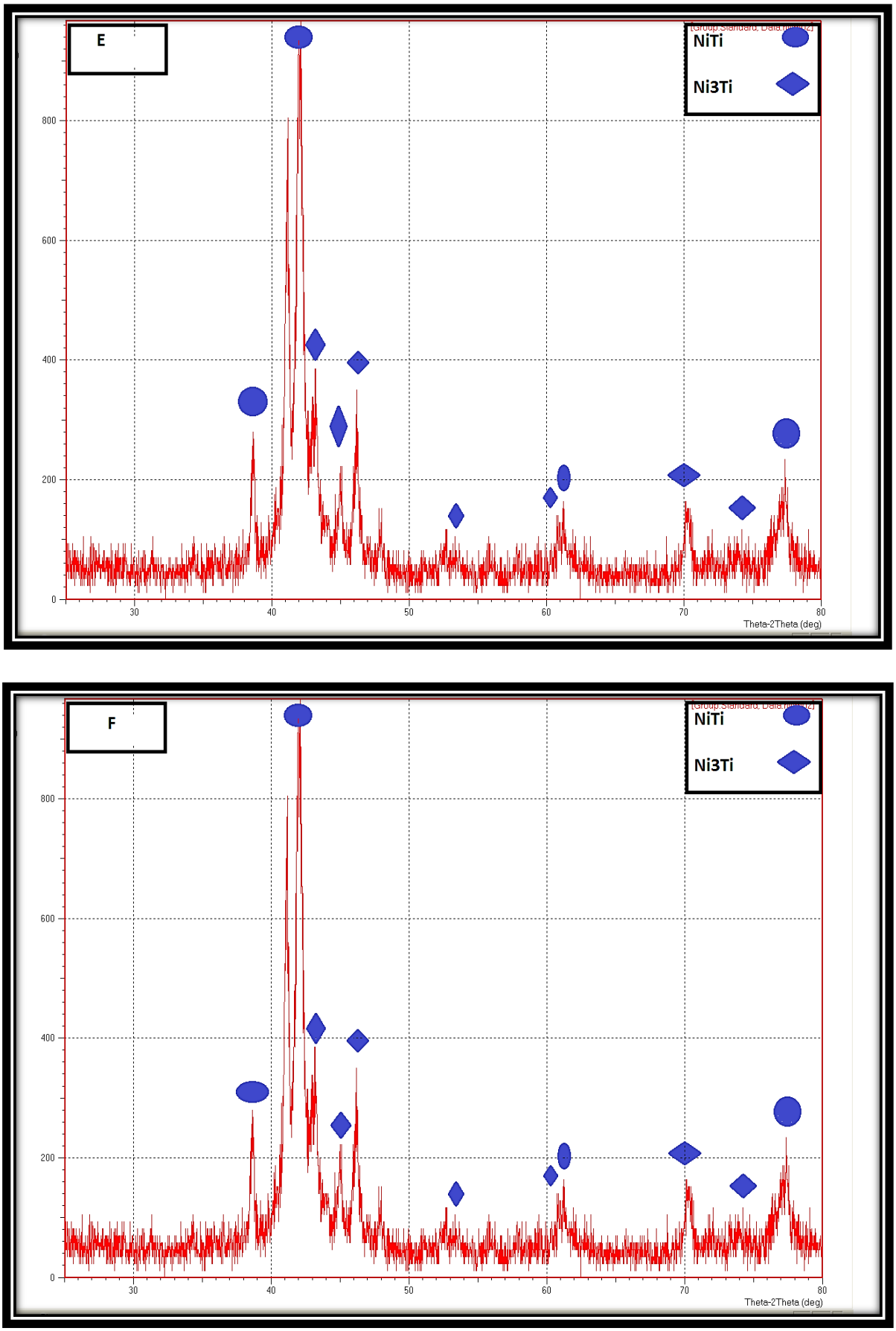

figure (4.3): X-Ray Diffraction E, F alloys

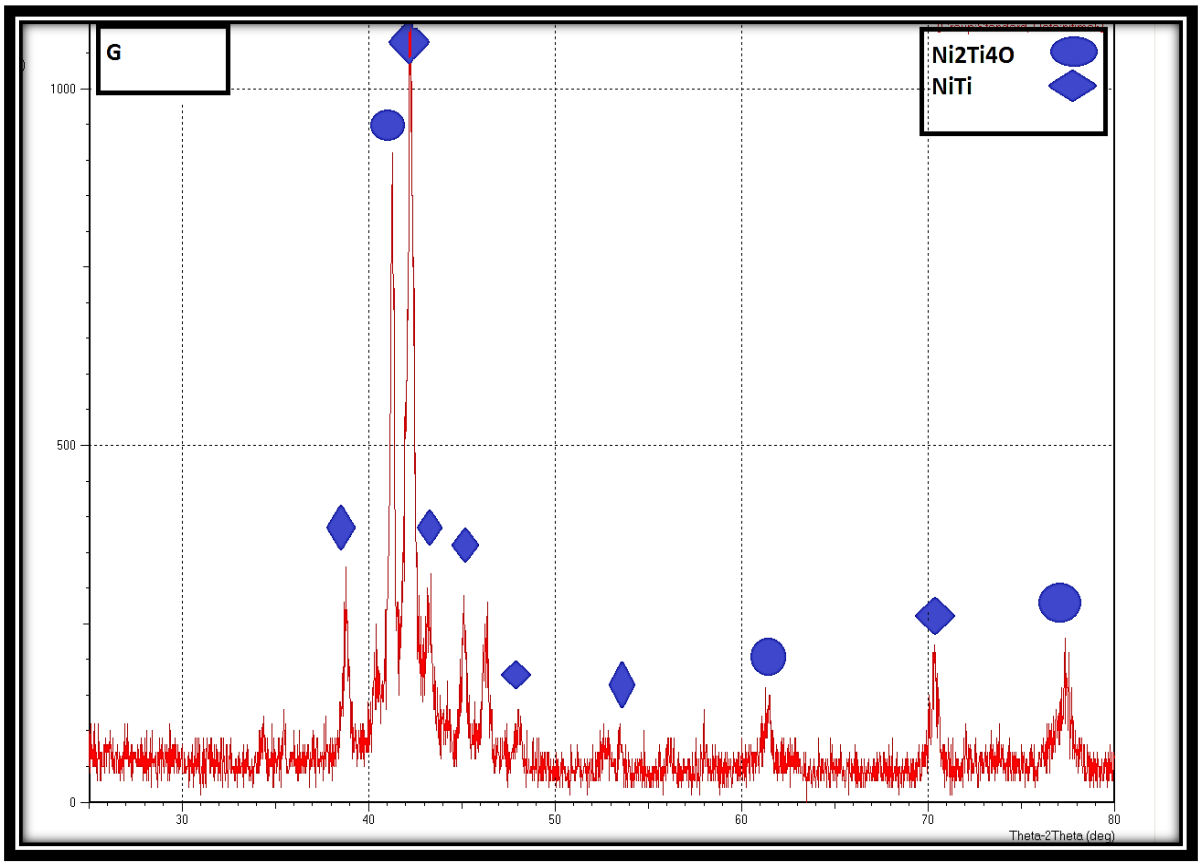

figure (4.4): X-Ray Diffraction G alloy

4.2.2 Optical Microscope

The microstructure of these alloys are fine grains for specimens. Sometime , reinforcement particle has been clear but others are not clear due to fine structures and probably due to type of used etching.

Figure (4.5), shows the microstructure in each samples with two magnifications. It is clear that the emergence of martensite phase B19 which is represented by the bright areas, while the shaded areas represent the appearance of the austenite phase B2, and the dark areas represent the presence of spaces or pores between the phases, and this is expected because the sample preparation process was done using powder metallurgical.

Microstructure of the sample however , varies greatly among different alloys and cannot be resolved by LOM Figure (4.5) indicated the optical microscopy images of bare samples which show the light optical microscopy

after etching. This image shows some features of the surface such as open pores and grain boundaries and also the phases NiTi and Ni_3Ti can be distinguished.[116]

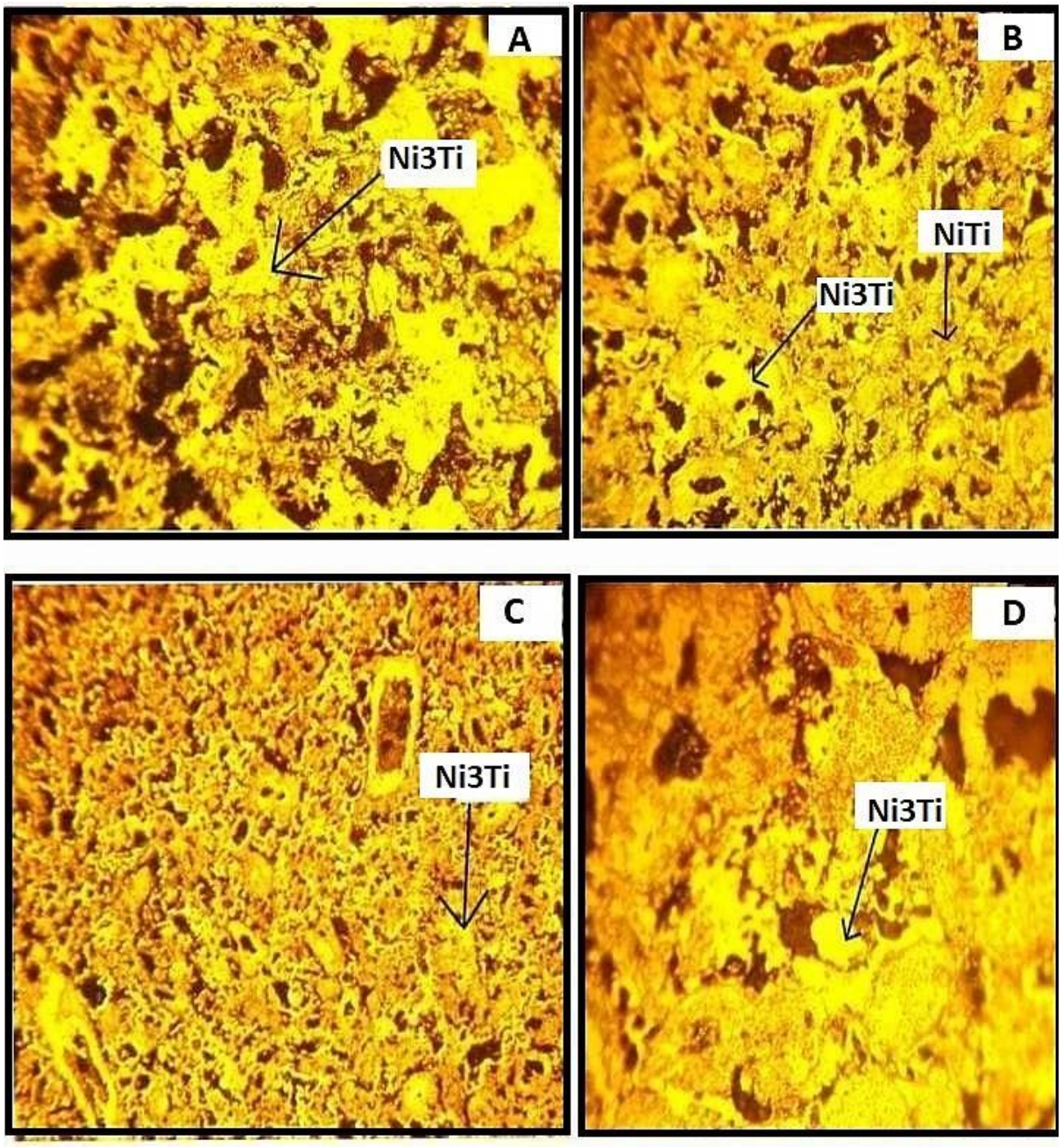

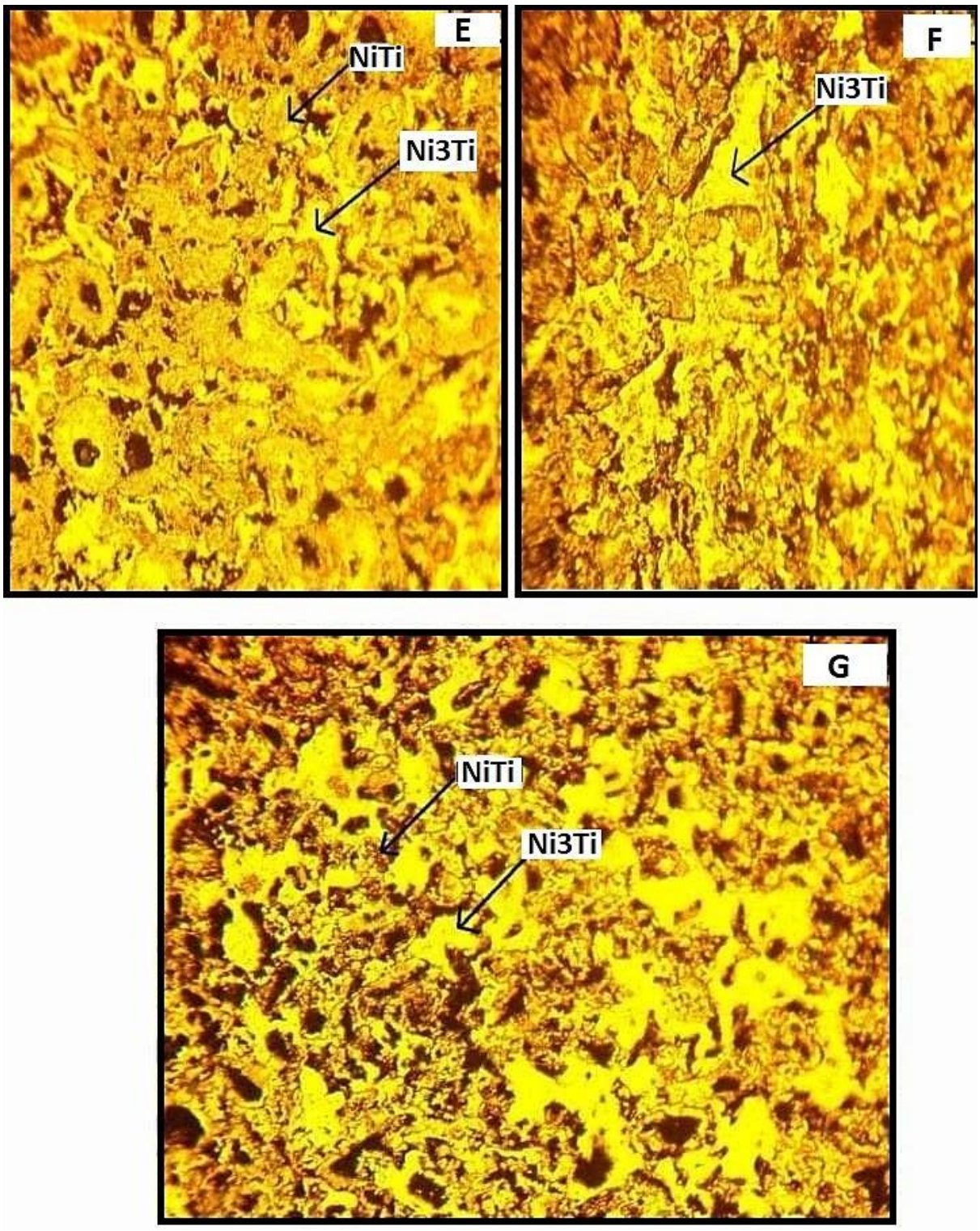

Fig(4.5) Shows optical microscopy alloys (A,B,C,D,E,F and G) after etching

4.2.3 Scanning Electron Microscopy

In SEM, a beam of relatively high-energy electrons is scanned across the sample's surface. The primary electrons penetrate the surface and transfer

energy to the material in a manner analogous to the way X rays and ions act in XPS and SIMS, respectively. In SEM, the incident electrons transfer sufficient energy for electrons (secondary electrons) to be emitted from the sample figures (4.6). The intensity of the secondary electrons primarily depends on the topography of the surface. By scanning the electron beam across the samples and determining the current generated from secondary electrons, images of the surface are obtained figures (4.6) Thus, in contrast to the methods described previously, which provide surface chemical information SEM generally gives images reflecting surface topography.

The microstructure image by (SEM) for prepared samples by powder metallurgy process has been shown in figure (4.6) .

The results appeared that reinforcement phase(NiTi) is formed near the pores in all specimen microstructures.

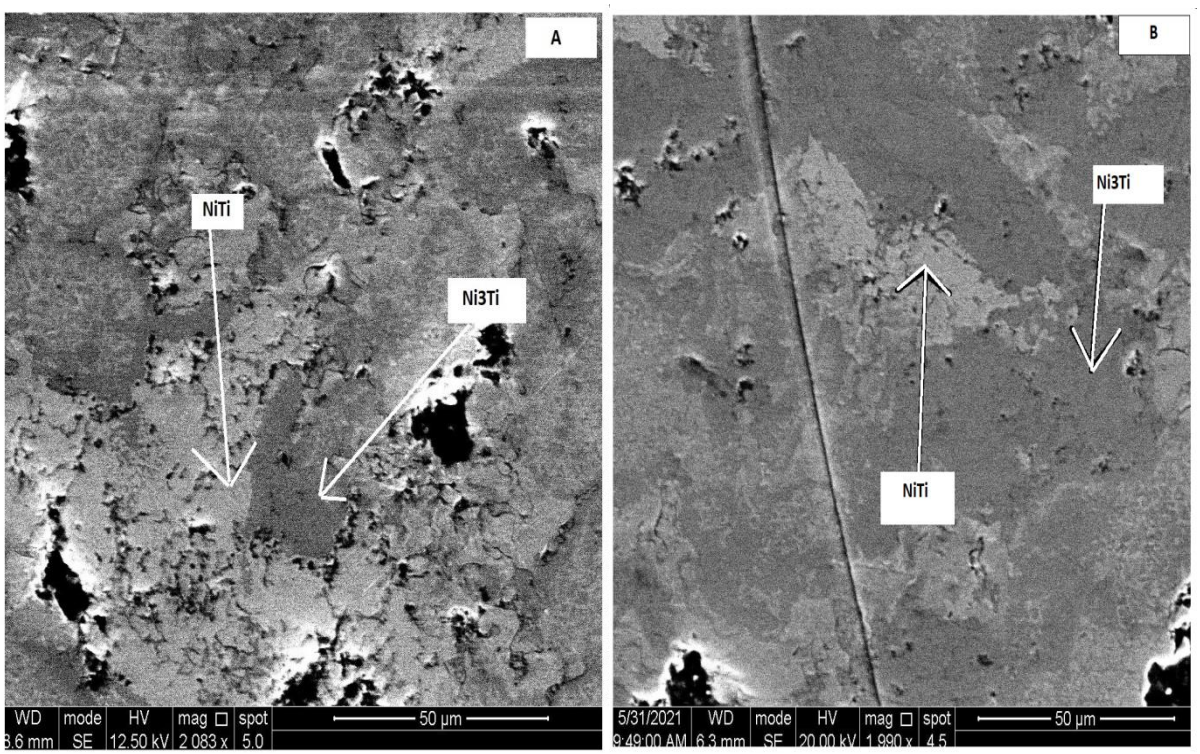

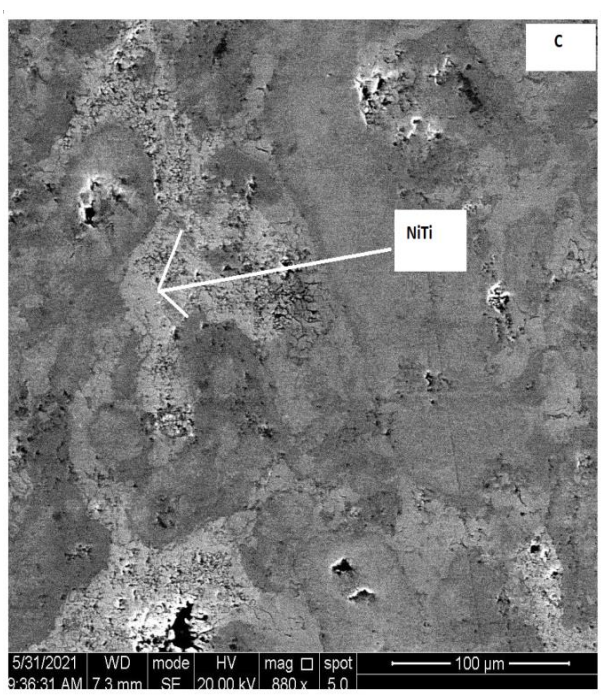
C
NiTi
5/31/2021 WD mode HV mag spot 100 µm
9:36:31 AM 7.3 mm SE 20.00 kV 880 x 5.0

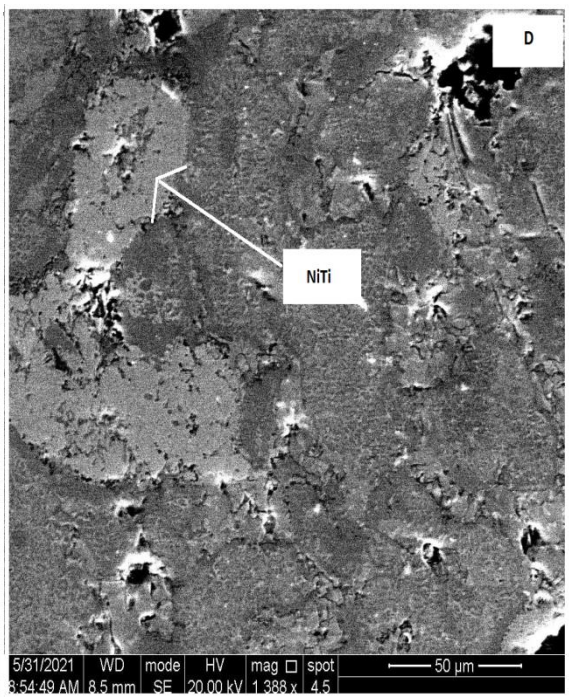
D
NiTi
5/31/2021 WD mode HV mag spot 50 µm
8:54:49 AM 8.5 mm SE 20.00 kV 1,388 x 4.5

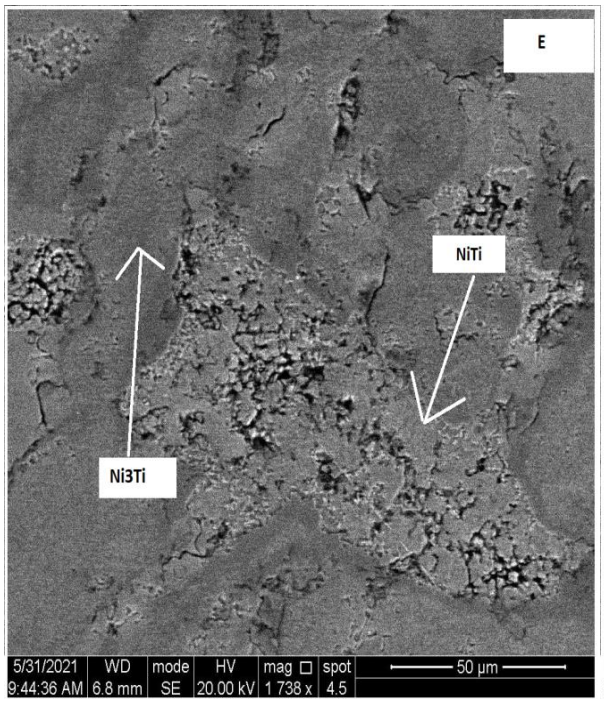
E
NiTi
Ni3Ti
5/31/2021 WD mode HV mag spot 50 µm
9:44:36 AM 6.8 mm SE 20.00 kV 1,738 x 4.5

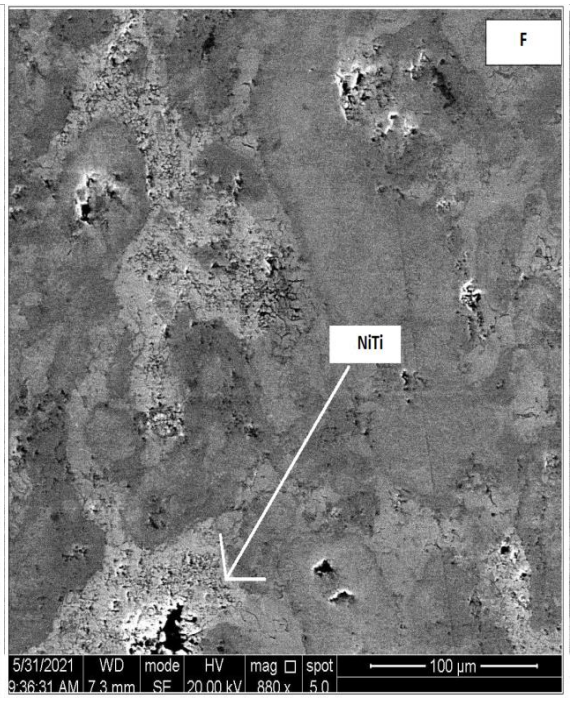
F
NiTi
5/31/2021 WD mode HV mag spot 100 µm
9:36:31 AM 7.3 mm SE 20.00 kV 880 x 5.0

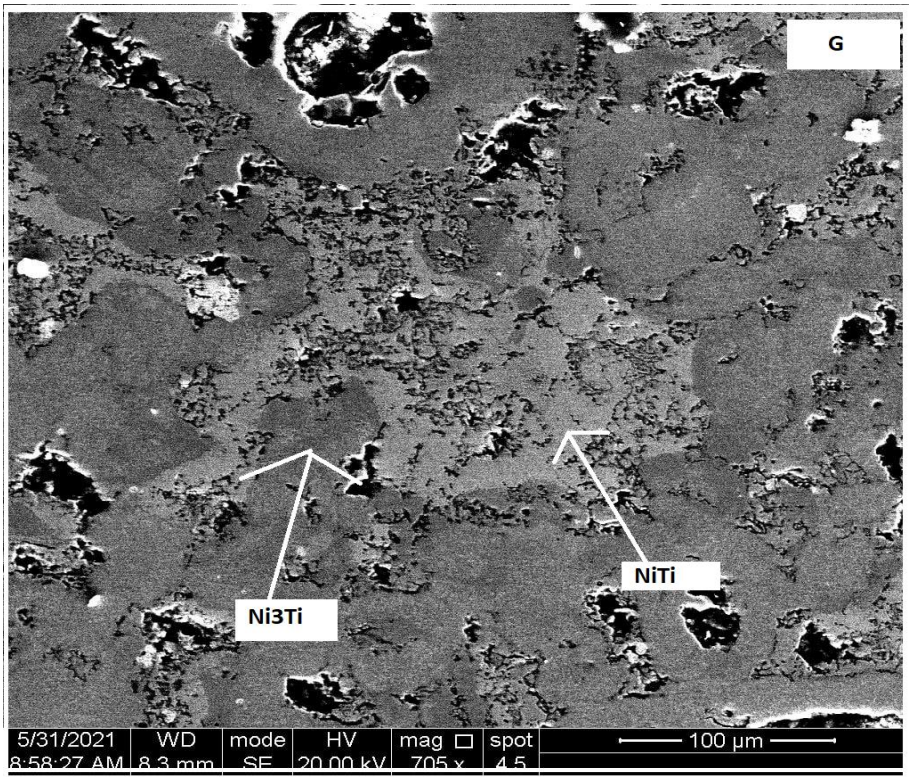

Figure (4-6): SEM Images for (A,B,C,D,E,F, and G) alloys.

4.2.4 Energy Dispersive X-Ray Analyzer (EDX)

The punctual chemical analysis by EDX aimed to determine microstructural details, quantitatively, through percentage values in weight, based on the choice of the best analysis points that would allow an understanding of the results obtained in terms of hardness. EDS technique was used to determine the mean value of chemical composition for micrograph of A alloy. Figure (4.7) shows the EDS spectrum and chemical composition of the A alloy . In the present study, A alloy sample was prepared to have % (45at Ti-55at Ni) which equates at %(34.10 Ni and 65.90 Ti) in EDS results as shown in figure (4.7). As can be seen, the results of EDS analysis were relatively close from the percentage of addition, because the values gained from EDS analysis do not cover the total area , only the spot where the electron stroke . Also the EDS shows no evidence of elements other than Ni and Ti.

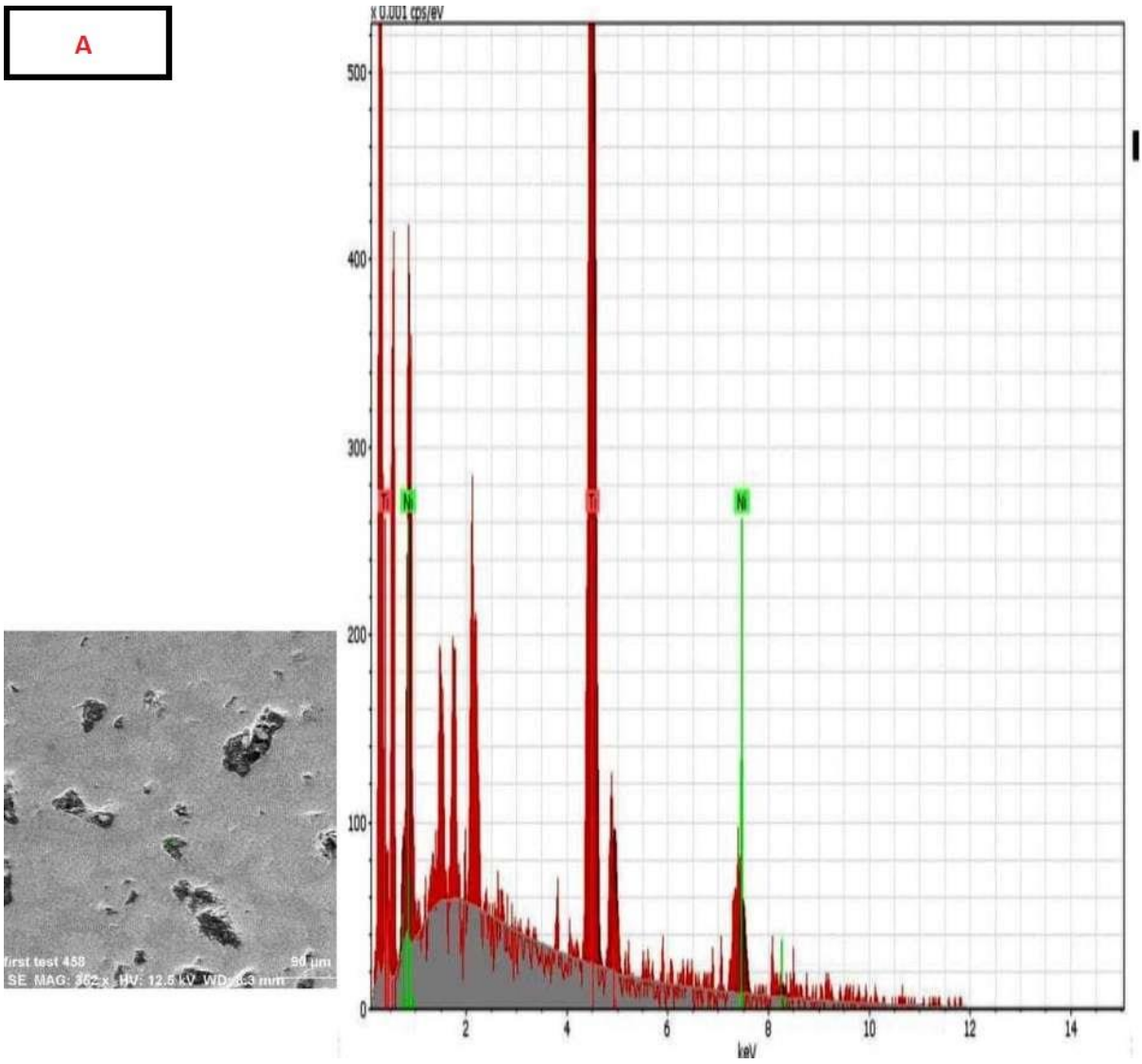

Figure (4-7): EDX for (A) alloy

Table (4-1) illustrated the chemical composition for A alloy.

Element	Wt.%	At.%	Wt%
Ti	65.90	70.32	1.81
Ni	34.10	29.68	2.34

Furthermore, the EDS results aid in verifying the purity of the initial elemental powders as well as the prevention of contamination of the powders during mixing and the production of sintering samples. The EDS Figs(4.8) to (4.9),(4.10) show no evidence of elements other than Ni , Ti and Zr EDS results indicate that there are no element present other than Ni ,Ti and Zr. These

results may be attributed to characteristic of EDS analysis which does not cover the total area, only the spot where the electron stroke. While Figures EDS (4.11) , (4.12)and(4.13). show no evidence of elements other than Ni , Ti and Mo EDS results indicate that there are no element present other than Ni ,Ti and Mo.

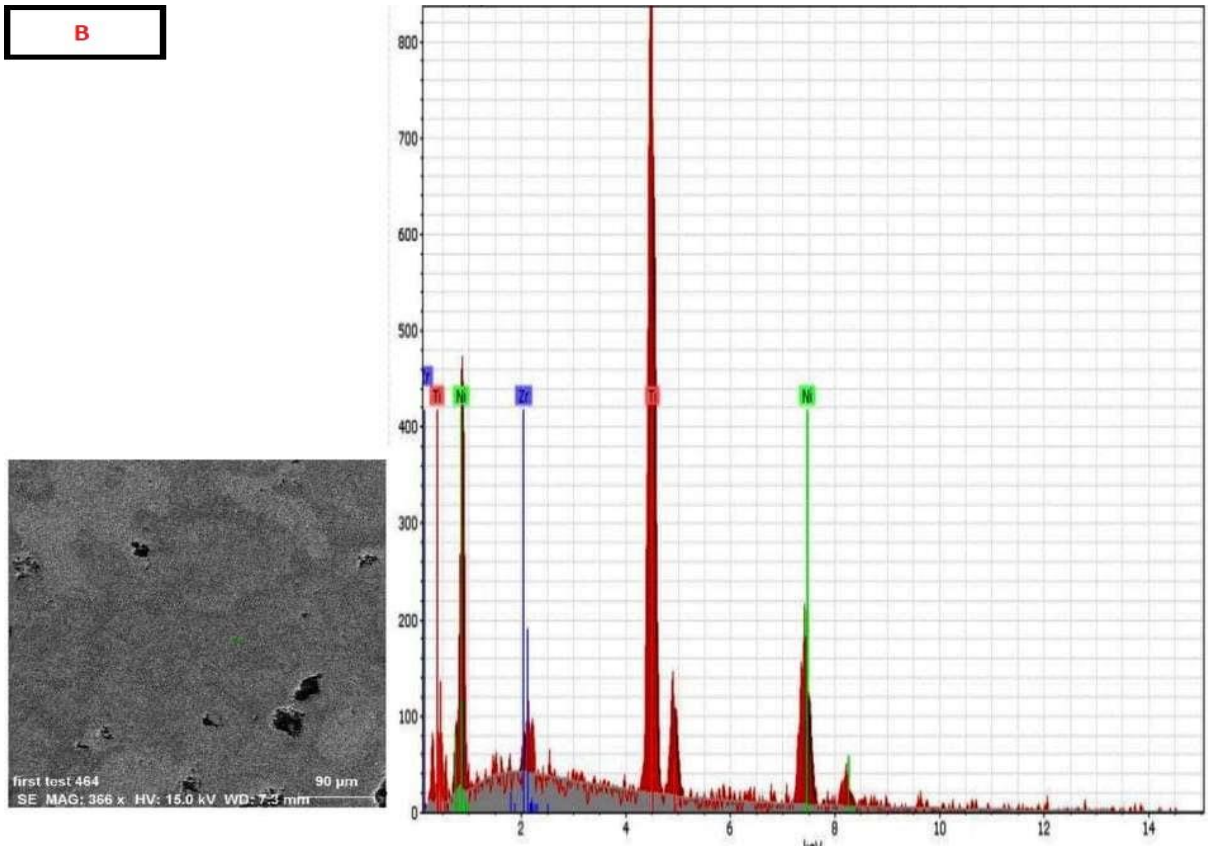

Figure (4-8): EDX for (B) alloy

Table (4-2) illustrated the chemical composition for B alloy.

Element	Wt%	At%	Wt%
Ti	57.72	63.13	1.75
Ni	39.59	35.33	2.07
Zr	2.69	1.54	0.28

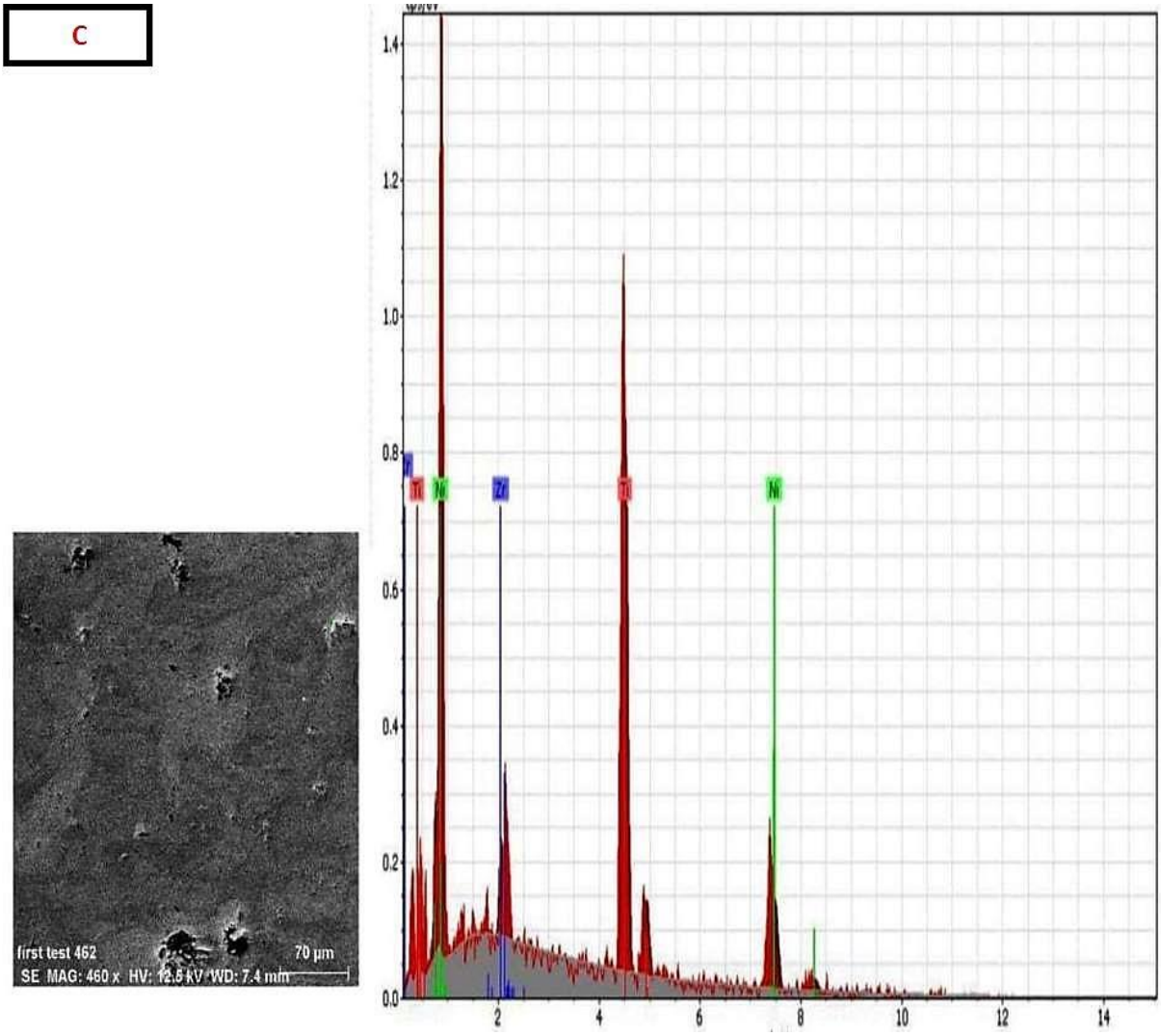

Figure (4-9): EDX for (C) alloy

Table (4-3) illustrated the chemical composition for C alloy.

Element	Wt%	At%	Wt%
Ti	49.15	55.17	1.32
Ni	45.55	41.71	2.19
Zr	5.30	3.12	0.29

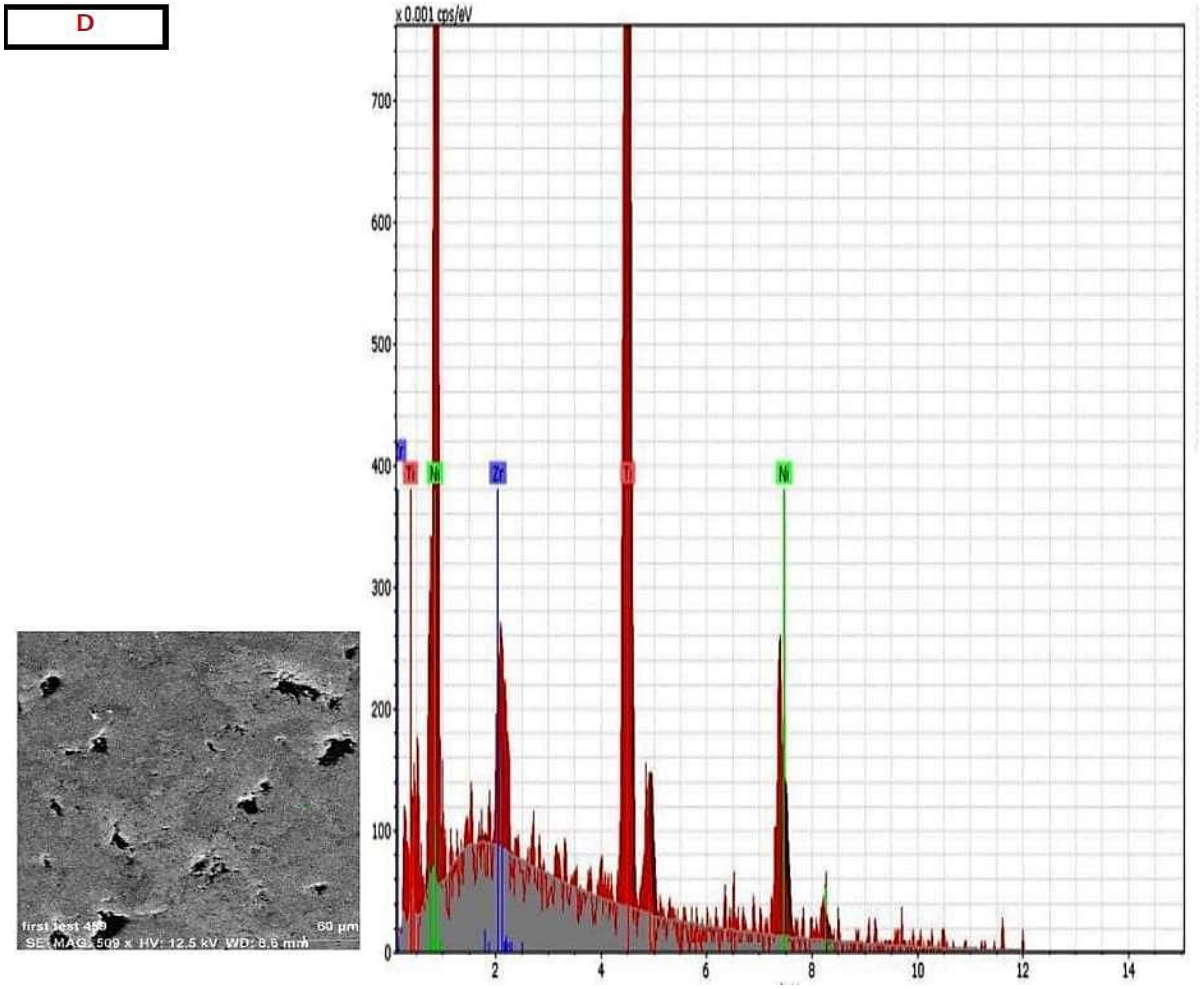

Figure (4-10): EDX for (D) alloy

Table (4-4) illustrated the chemical composition for D alloy.

Element	Wt%	At%	Wt%
Ti	50.98	57.07	1.82
Ni	43.39	39.62	3.12
Zr	5.63	3.31	0.44

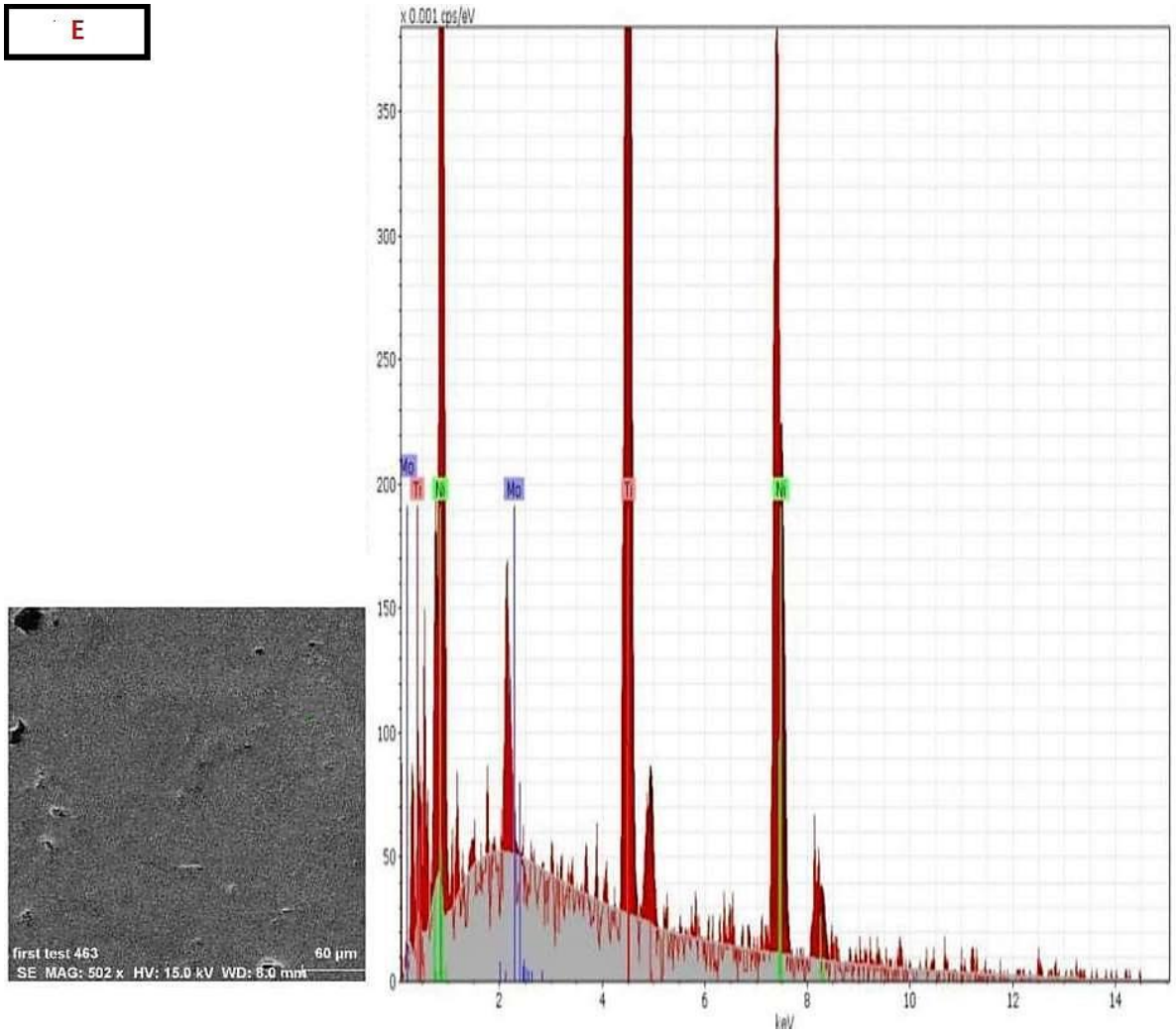

Figure (4-11): EDX for (E) alloy

Table (4-5) illustrated the chemical composition for E alloy.

Element	Wt%	At%	Wt%
Ti	36.14	41.01	1.09
Ni	63.47	58.76	2.37
Mo	0.39	0.22	0.10

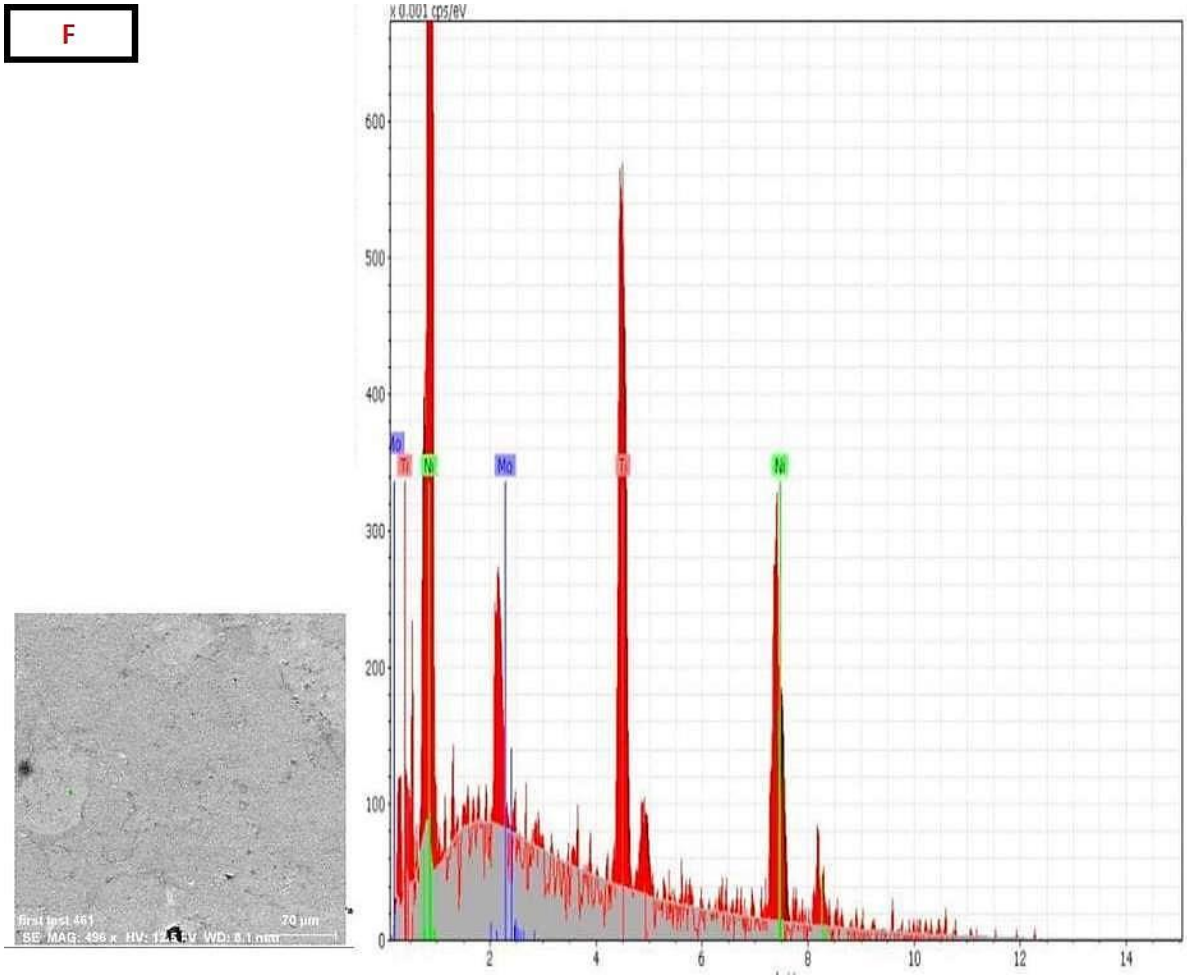

Figure (4-12): EDX for (F) alloy.

Table (4-6) illustrated the chemical composition for F alloy.

Element	Wt%	At%	Wt%
Ti	30.69	35.27	1.08
Ni	68.66	64.36	3.35
Mo	0.65	0.37	0.13

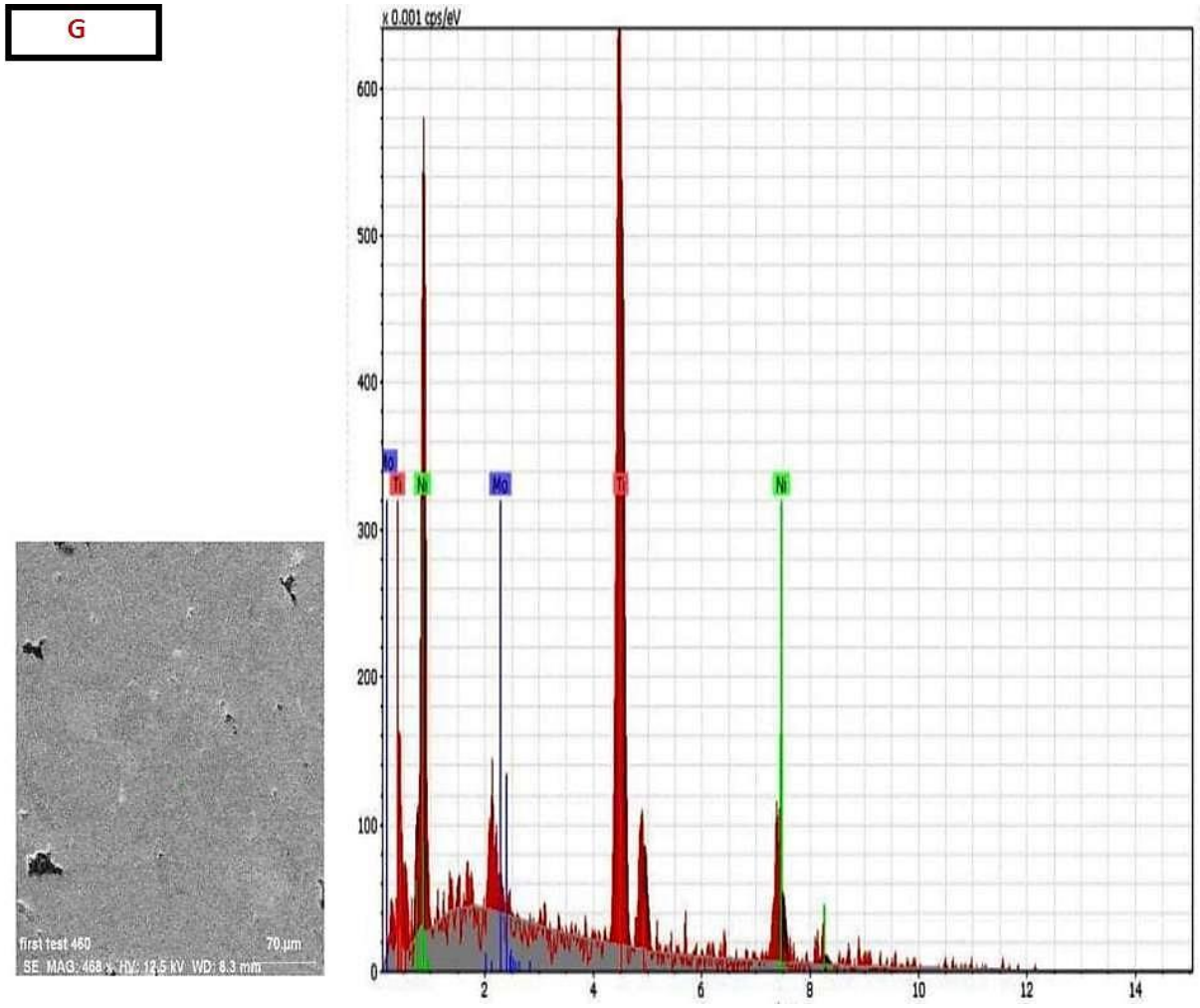

Figure (4-13): EDX for (G) alloy

Table (4-7) illustrated the chemical composition for G alloy.

Element	Wt%	At%	Wt%
Ti	64.08	68.97	2.09
Ni	34.41	30.21	2.68
Mo	1.51	0.81	0.21

Such results were conclusive in determining the applicability of the (A,B,C,D,E,F and G) alloy as a biomaterial.

4.3 Results Mechanical Tests

4.3.1 Hardness Test

The microhardness measurements have been made for the samples produced by powder metallurgy by taking the average of 3 readings at each point. The results obtained are represented graphically in figure (4-14).

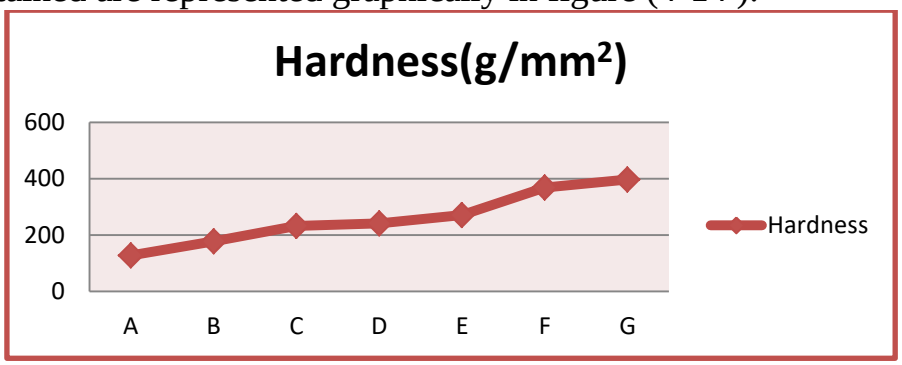

Figure (4.14): Hardness test for alloys (A,B,C,D,E,E,F and G).

hardness test was conducted using Brinell hardness machine. It was observed that as the Mo content is increased, the hardness values, increased. which increased significantly as Mo content was increased to 40at%. The hardness of the base alloy (Alloy A) equal to 127.05 increased when Zr was added by (1% B alloy, 2% C alloy and 3% D alloy) equal to(177.4,232.005,241.615). While when Mo was added by (1% E alloy, 2% F alloy, and 3% G alloy), the hardness increased, respectively, to(270.23,368.24,396.35).

4.3.2 Wear resistance for prepared specimens

Specimens with (13.24) mm diameter and thickness (6.16)mm subjected to dry wear test under load (15) N and with different times (5,10,15) min at constant sliding speeds of 6.5 cm Figures (4-15),(4-16) show the relationship between Volume loss weight & with (1, 2, and 3wt% at Zr and Mo) with time different . From these figures, it's clear that weight loss increased with increasing applied time. In general, the weight loss increased slightly with load for all alloys .These results may be attributed to the presence of carbonaceous layer on the surface of all alloys at normal load of 15N which may Aid lubrication and reduction of wear. The alloys Mo added (E,F and G alloys)had a lower weight loss than that Zr added alloys (B,C and D alloys), could be attributed to higher

hardness. The result is shown in the Figure (4.15, 4.16): This is Attributable to the hardness of this alloy, so, it is subjected to Archard's law which States "weight loss for materials that is inversely proportional to the material hardness value", Also, the thickness of the oxide film formed on the surface of the specimen due to high hardness which is difficult to remove during the time [118].In addition, The wear rate in the base alloy is higher than the wear rate when molybdenum and zirconium are added ,The wear rate of the base alloy was equal to (0.609mV), it decreased when zirconium was added by (1%,2% and 3%) to (0.293mV,0.387mVand0.377mV), While the addition of molybdenum in a percentage of (1%, 2%, and 3%) decreased by more percentages to (0.546mV, 0.230mV and 0.251mV), respectively . The wear rate of NiTi improved when adding zirconium by 1%, 2% and 3% to 51%, 36% and 38%, respectively, while the wear rate improved when adding molybdenum by 1%, 2%, 3% to 10%, 62% and 58%, respectively.

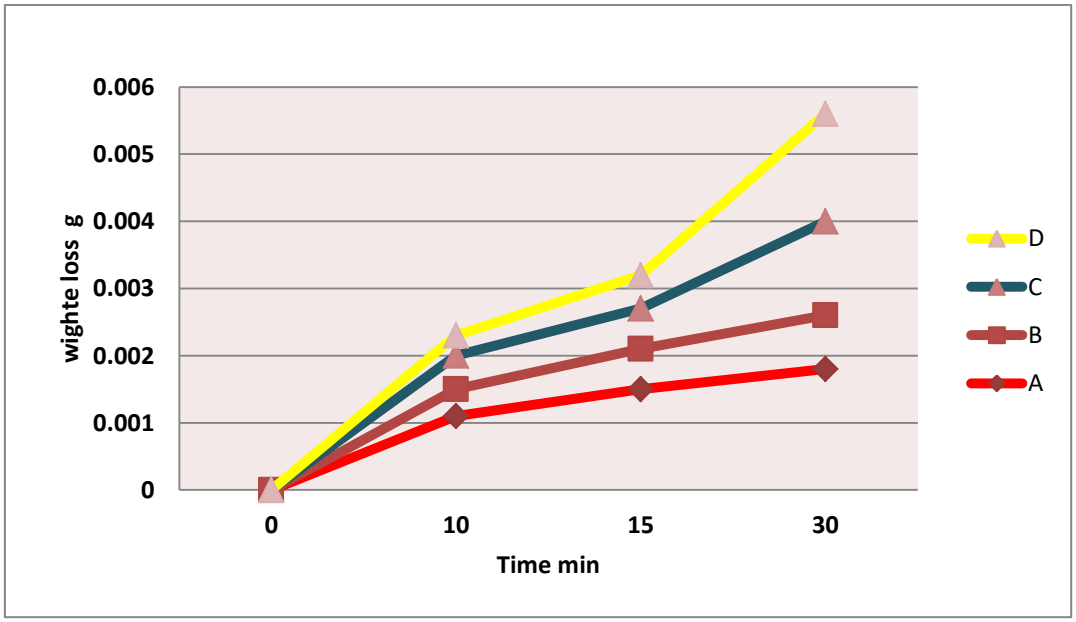

Figure (4.15): Wear resistance weight loss (g) test for alloys (A,B,C and D).

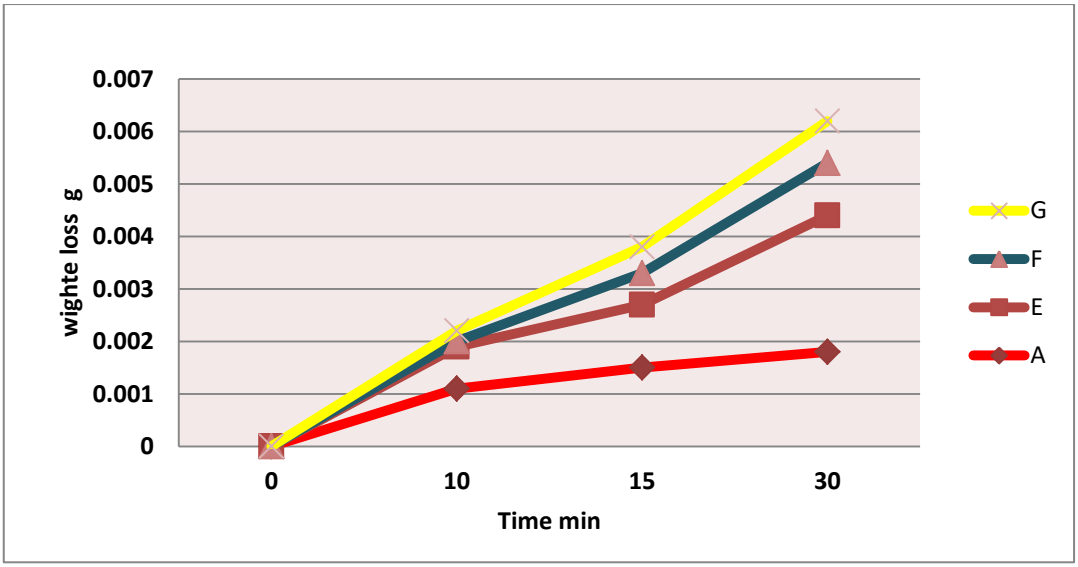

Figure (4.16): Wear resistance weight loss (g) test for alloy (A,E,F and G).

4.4 Electrochemical Tests

4.4.1 Open Circuit Potential (OCP)-Time Measurement.

The OCP-time is measured concerning SCE in Ringer Solution at (37) oC±1 for tested alloys. Figures (4.17) display the evolution of the alloys' corrosion potential throughout time. The time from (0 up to 240 min) and with an interval of 5 min were potentially reported. The values of the OCP were recorded by using all specimens for each alloy . The open circuit corrosion potential measurements were carried out to examine the variation in time of corrosion behavior of the materials in simulated human body conditions. Figure (4.17) shows the variations of potential with time of immersion and the tendency to a steady-state value. The examples are shown in this figure; the stable behavior in simulated body fluid can be attributed to the formation of oxides. From Figure (4.17), all starting potentials are in the negative direction.

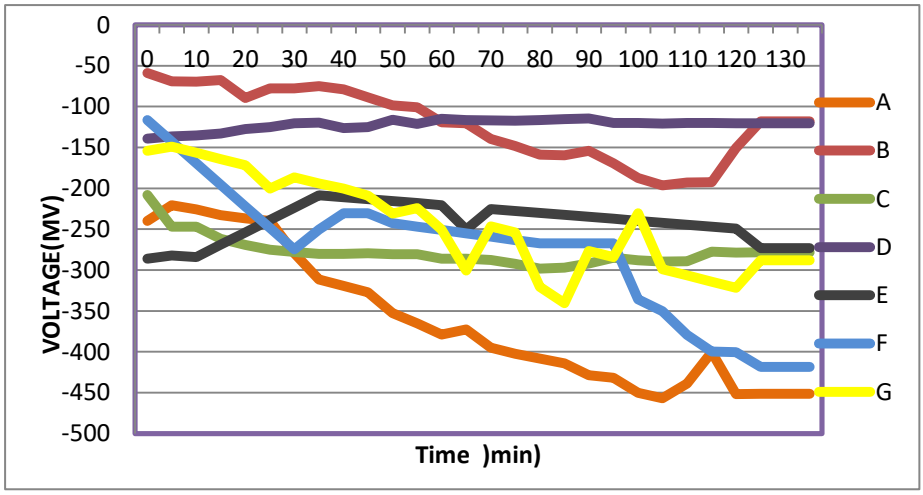

Figures (4-17): The OCP-Time of (A,B,C,D,E,F and G) alloys in Ringer Solution.

4.4.2 polarization

The corrosion behavior of (A,B,C,D,E,F,G) alloys in Ringer solutions has been studied using Potentiodynamic polarization to give estimation about the corrosion behavior of alloys. The corrosion parameters are corrosion current (Icorr.) , and corrosion rate (C.R.) resulted from corrosion test for samples in Ringer solution at 37±1^{o}C were illustrated in table (4- 8) .

Table (4-8): Corrosion Current (Icorr.), and Corrosion Rate (C.R.) for All Alloys in Ringer Solution at 37±1^{o}C

Samples	OCP mV	Ecorr. Mv	Icorr. µA/cm^2	Corrosion rate (C.R.)mpy	Improvemnt Percentage %
A	-451.1	-242.6	2.51	0.0145	-
B	-111.9	-334.4	0.417	0.0018	87
C	-278.2	-818.6	0.428	0.0015	89
D	-120.1	-486.2	1.70	0.0061	57
E	-273.2	-313.1	1.28	0.0072	50
F	-418.5	-329.8	2.09	0.0121	16
G	-288.1	-247.2	2.46	0.0132	8

Table (4-8) shows that there are significant improvements in corrosion resistance of the alloys with different additives of Mo and Zr in Ringer solution. The Icorr. for specimens with Zr (B ,C and D)alloys ranges from (0.417μA/cm^2) to (1.70μA/cm2) which are lower than Icorr. For A alloy, which is (2.51 μA/cm2). Zr addition, the Ecorr. value for alloys with Zr addition is ranged from (-334.4 mV) to (-486.2mV) which are lower than Ecorr. for A alloy which is (-242.6 mV), which means that Zr addition made the A alloy nobler. The same behavior can observe in (F,E and G)alloys; the Icorr reduce from 2.51μA/cm^2 for the A alloy to 1.28 μA/cm^2 when the Mo addition reached to 1wt.%, reached to 2.09 μA/cm^2 When the Mo addition to 2wt.% and reached to 2.46 μA/cm^2 When the Mo addition to 3wt.%,Also the Ecorr. increase from -313.1 Mv When the Mo addition to 1wt.% to -247.2Mv When the Mo addition to 3wt.%.in Ringer solution, From Table (4-8), it can be noted that the improvement of corrosion resistance for A alloy when increasing the addition of Mo and Zr. Icorr for (B,C and D) specimens alloy are graded from0.417 to1.70(μA/ m^2) which are lower that (E,F and G) alloys that graded from1.28 to 2.46 (μA/ m^2) , and both of specimens its lower that the base alloy (A alloy),which is around 2.51(μA/ m^2).However, the Ecorr value for the alloys (B,C,D)is lower than the other alloy that content Mo or base alloy, and graded from -334.4to -486.2MV ,and Ecorr value for (E,F and G)alloy was range from -313.1to -247.2 MV which is also lower than the base alloy(A) value that was -242.6 Mv .Figures (4-18),(4-19)and(4-20) show the polarization curve for (A,B,C,D,E,F and G) alloys in Ringer solution . In cathodic polarization, the corrosion current density decreases with increasing voltage until it reaches the lowest possible value. In anodic polarization, the corrosion current increases with increasing voltage indicating active anodic polarization [119].

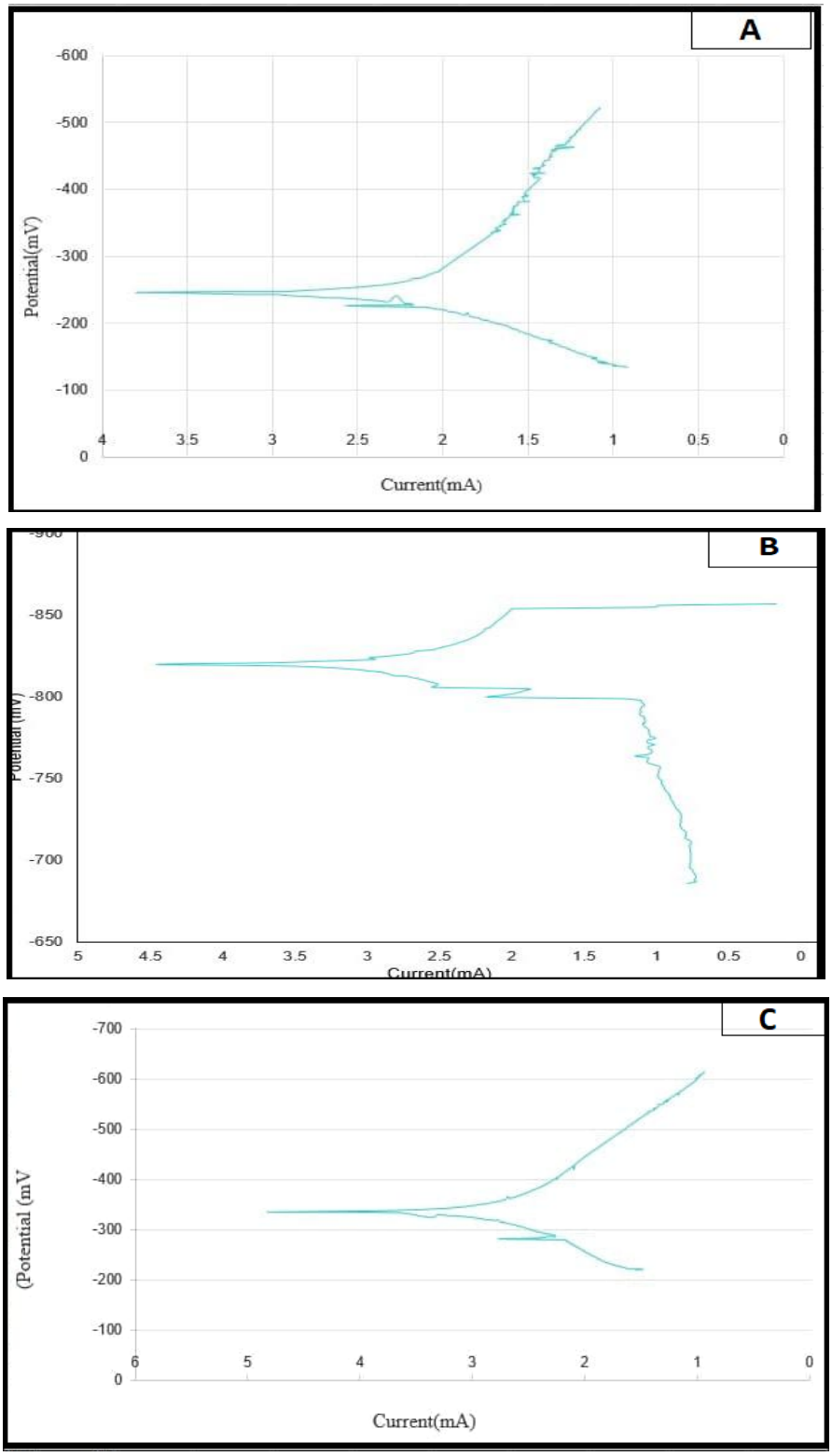

Figure (4-18): Potentiodynamic Polarization for the alloys(A,B,C)in Ringer Solution .

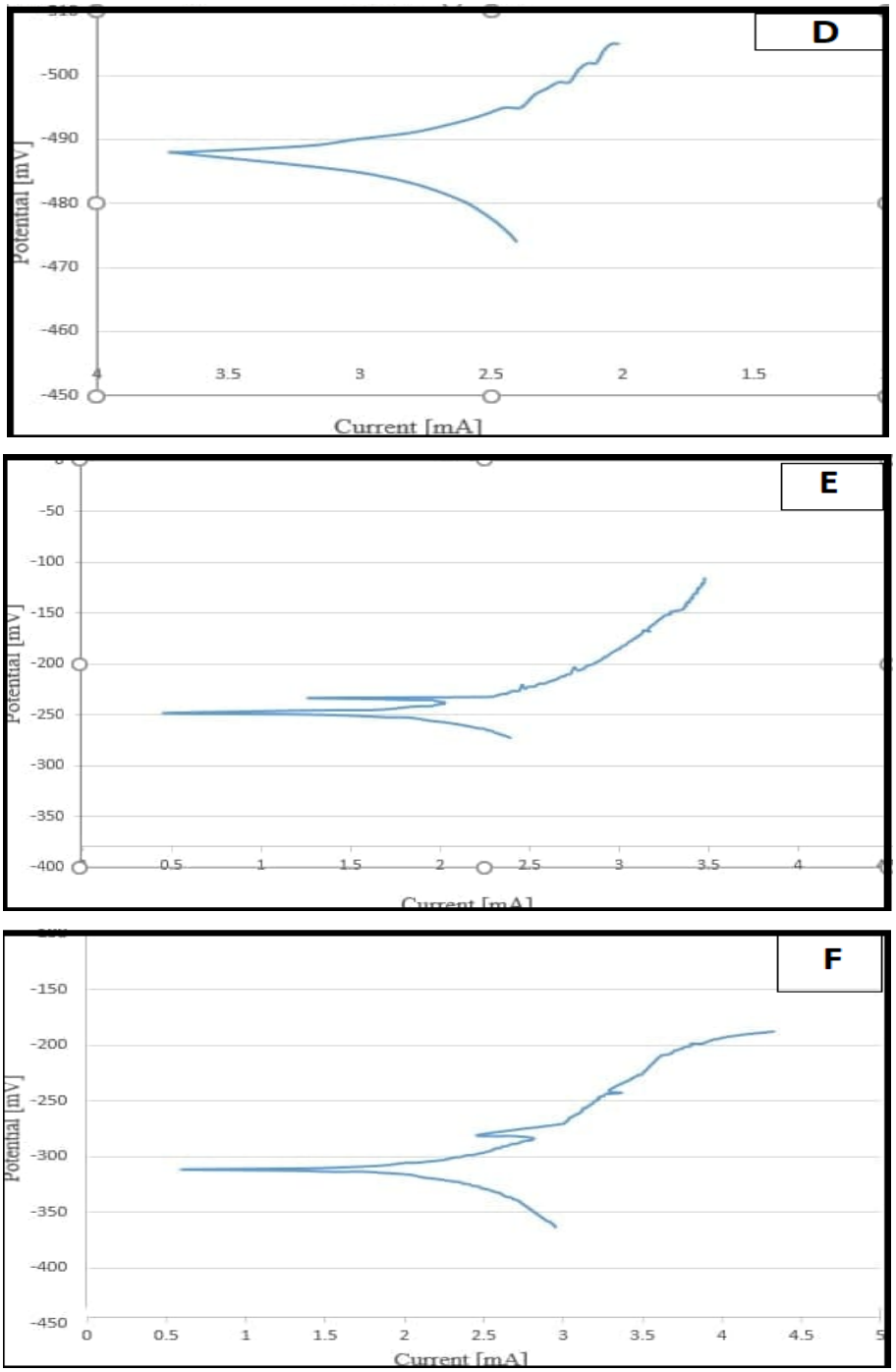

Figure (4-19): Potentiodynamic Polarization for the alloy(D,E,F) in Ringer Solution .

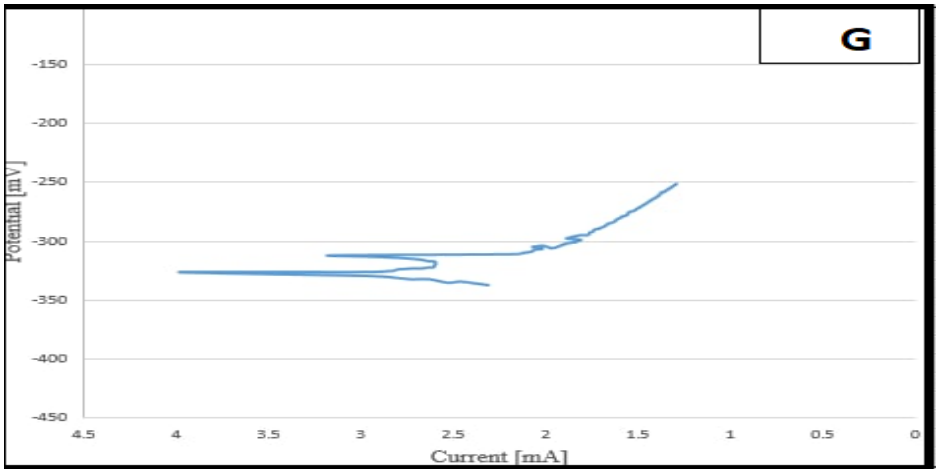

Figure (4-20): Potentiodynamic Polarization for the alloy(G) in Ringer Solution.

In addition, the corrosion resistance increases as the Zr and Mo content increase in Ringer Solution, this can be attributed to the collective effect of Zr and Mo, such as passivity, oxide film, and noble elements which will lead to protection corrosion in the surface layer However, for the specimens to tend to passivation, they must undergo several active-passive transitions. Therefore, until the low current density is obtained, the submerged specimen's protective layer must be sufficiently integrated [120]. Accordingly, as alloying elements (Mo &Zr) increase, the protective layer increases.

4.5 Shape Memory Effect

In the present study the method used to determine the shape memory effect properties of the prepared samples is Macro Brinell hardness test. Figure(4.21) for all prepared alloy samples. The value obtained equal to 8.23% at compacting pressure 800MPa.This value close to the those of dense nitinol compacts which reach to (8-10%) [121].

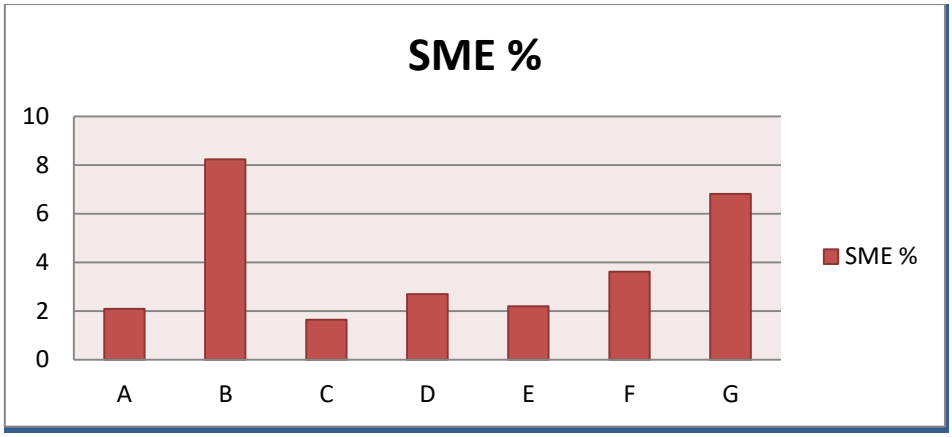

Fig. (4.21) Effect of alloys on SME properties obtained from Brinell Hardness test.

Chapter Five

CONCIUSIONS&RECOMMENDATIONS

5.1 Conclusions

Where the results obtained from the research appeared, where we reached the following conclusions:-

1-It was found that sintering the alloy at a temperature of 950 ° C for a period of 6 hours is effective to fully satisfy the sintering and converting Ni Ti into alloy structure.

2-The sample (cooling in furnace) compressed at 800 MPa and sintering at 950°C for 6 hours caused in a three phase structure (hexagonal Ni3Ti phase, NiTi monoclinic phase and NiTi cubic phase) at room temperature .

3-The microstructure was obtained explain accuracy the phases that found in X-ray analysis.

4- The corrosion of NiTi alloy showed significant improvement with addition of mo and Zr in ringer solution It was shown that higher improvement with the addition of the 1wt%,2wt%and 3wt% Zr was87%, 89% and57% in ringer solution, respectively. while with addition of 1wt%,2wt%and 3wt% of Mo, the improvement percentage in ringer solution was 50% ,16% and 8% respectively .

5- The improvement of wear rate for NiTi alloys under load15N when adding Mo than with alloys which zr added Because of the high hardness of Mo

5.2 Recommendations

1-Using other ratios of added elements and studying their effect on properties.

2- Transmission electron microscopy is necessary for detailed analysis.

3-Studying the other properties to alloys that used in this study such as creep and fatigue property.

4-Conducting the casting process for this alloy and comparing the results obtained from powder metallurgy.

Table of Content

Abstract..... I

Table of Content..... I I I

Chapter one: Introduction ……. 1

1.1. Introduction …….....1

1.2. Processing of Nitinol ……..……..…….....2

1.3 Biocompatibility …….....3

1.4 The objectives of the current study ……...5

Chapter Two: Theoretical Part & Literature Review.....6

2.1. Introduct.....6

2.2. The Memory Alloys ……6

2.3. Properties of SMA:……..……8

2. 3.1 Shape memory effect: …….....8

2.3.2 Pseudo elasticity:…….……10

2.3.3 Damping properties:……...……12

2.4. Applications of Shape Memory Alloys ……...……..13

2.4.1 Biomedical Applications…….....14

2.4.2 Robotic Applications……...16

2.4.3 Automotive Applications …….…….……..18

2.4.5 Aerospace Applications…….20

2.5. Phase Diagrams for NiTi Alloy ……..,…….....21

2.6. Transformation temperatures.…… …….....22

2.7. Mechanical properties of NiTi SMA……...……24

2.8. the effect of alloying elements on the shape memory alloys……25

2.8.1 Molybedum (Mo)……..……..25

2.8.2 Zirconium(Zr)……..26

2.9 Literature Review…….……27

Chapter Three: Experimental..... 36

3.1.Introduction……..……..36
3.2. Program of the Current Study ……..…..36
3.3. Materials in Current Study……..…37
3.4. Equipments ……37
3.5. Particle size analysis ……..……40
3.6. Samples Preparation ……..41
3.7. Mixing of Powders ……..…….…….42
3.8. Compacting of Powders ……...42
3.9. Sintering Process …….…….....42
3.10. Scanning electron microscope (SEM)…….……....43
3.11. X-Ray Diffraction…….……44
3.12 Optical Microscope…….……...44
3.13 Mechanical Tests……45
3.13.1. Hardness Test …….……..45
3.13.2 Dry Sliding Wear Test …….……45
3.14 Corrosion Tests……..47
3.14.1 Open circuit potential…….……47
3.14.2 Potentiodynamic polarization……48
2.15 Shape Memory Effect……..……..49
Chapter Four: Results & Discussion.....50
4.1 Introduction.....50
4.2 Results The Metallography……..50
4.2.1 X-Ray Diffraction …….……..50
4.2.2 Optical Microscope……..55
4.2.3 Scanning Electron Microscopy……..……..57
4.2.4 E energy Dispersive X-Ray Analyzer (EDX……60
4.3 Results Mechanical Tests……..……...68
4.3.1 Hardness Test……68
4.3.2 Wear resistance for prepared specimens…… ..……..68
4.4 Electrochemical Tests…….…70
4.4.1 Open Circuit Potential (OCP)-Time Measurement…….70
4.4.2 polarization…….……71

4.5 Shape Memory Effect…….……75
Chapter Five: Conclusions & Recommendations 77
5.1. Conclusions..... 77
5.2. Recommendations for Future Works..... 77
References 79
Appendix 91

REFERENCES

1. ASM Handbook, "Properties and selection Nonferrous Alloy and special Purpose Materials, Fifth edition, Vol. 2, (1998), pp. (897-901).
2. GF. Andreasen & Fahl JL, "Shape Memory.In", Encyclopedia of medical devices and instrumentation, Volume 2.Wiley, New York, (1987), pp. (15-20).
3. Lunenfeld, B., et al., *The clinical consequences of an ageing world and preventive strategies.* 2013. **27**(5): p. 643-659.
4. Al-Humairi, A.N.S., et al., *BIOMATERIALS: A Multidisciplinary approaches and their related applications*. White Falcon Publishing.
5. Vallet-Regí, M.J.C.R.C., *Evolution of bioceramics within the field of biomaterials.* 2010. **13**(1-2): p. 174-185.
6. Jablokov, V.R., et al., *Influence of oxygen content on the mechanical properties of Titanium-35Niobium-7Zirconium-5Tantalum beta titanium alloy*, in *Titanium, Niobium, Zirconium, and Tantalum for Medical and Surgical Applications*. 2006, ASTM International.
7. Long, M. and H.J.B. Rack, *Titanium alloys in total joint replacement—a materials science perspective.* 1998. **19**(18): p. 1621-1639.
8. Guimaraes, Z.A., et al., *A Novel Porous Diamond-Titanium Biomaterial: Structure, Microstructure, Physico-Mechanical Properties and Biocompatibility.* 2017. **89**(4): p. 3111-3121.
9. da Rocha, D.N., et al., *Production and characterization of niobate apatite.* 2013. **2**(1): p. 24-29.
10. Wang, K.J.M.S. and E. A, *The use of titanium for medical applications in the USA.* 1996. **213**(1-2): p. 134-137.

11. WJ. Buehler &Wang FE, "A summary of Recent Rsearch on the Nitinol Alloys and their potential Application in Engineering". Ocean Eng. 1, (1978), pp. (105-120).
12. K. Shimizu &Tadaki T, "Shape Memory Effect Mechanism", Gordon and Breach Science, New York, (1978), pp. (1-60).
13. V. N. Khodorenko et.al., "Exothermal and Endothermal Effects in Porous Titanium-Nickel Alloys", Institute of Medical Materials and Shape Memory Implants, Vol.27, No.22, (2001), pp. (80-85).
14. Istvan Mihalcz "Fundamental characteristics and design method for nickel-titanium shape memory alloy" periodic polytechnic ser. Mechanical engneering.vol.45, No.1, (2001), pp. (75-86).
15. Krone et al "The Potential of Powder Metallurgy for the Fabrication of Biomaterials", Advanced Engineering Materials, No.7, (2005), pp.(613-619)
16. Catherine et al. "Stress-Induced Transformation Behavior of a Polycrystalline NiTi Shape Memory Alloy" Submitted to JMPS, Mechanical Engineering Department, Northwestern University (2003)pp.(1-33)
17. H. Otsuka et.al., "International Conference on Martensitic Transformations", Sydney, Australia, (1989)
18. Y. Liu et al. "On the deformation of the twinned domin in NiTi shape memory alloys" Philosophical Magazine (JOM), Vol.80, No.8, (2000), pp. (1935-1953).
19. Kazuhiro et.al., "Scince and Technology of Shape-Memory Alloys: New Developments", MRS Bulletin, February (2002).
20. L.G. Machado1& M.A.Savi "Medical applications of shape memory alloys", Brazilian Journal of Medical and Biological Research 36, (2003), pp. (683-691)

21. FJ. Gil &Planell J, "A In Vitro Thermomechanical Ageing of Ni-TiAlloys", (1998), pp. (237-248).
22. J.T. Hong , T. J. Kim , S. N. Hong , Y.H. Kim , D. K. Chang & E. R. Kim “Uncovered self-expandable metal stents for the treatment of refractory benign colorectal anastomotic stricture “(2020) 10:19841.
23. E. Darel Hodgoson, "Shape Memory Alloys- Applications and Commercial Aspects", Memory Technologies, shape Memory Alloys,(1999).
24. T.W. Duerig, pelton A.R. & Stockel D, "TheUtility of Superelasticity in Medicine", Biomed. Mater .Eng. (1996), pp (255-266),
25. S. Nemat&J.Y. Choi "Strain rate dependence of deformation mechanisms in a Ni–Ti–Cr shape-memory alloy", Acta Material, 53, (2005), pp. (449–454).
26. Y. Li, et al "Constrained Phase-Transformation of a TiNi ShapeMemory Alloy" Metallurgical and Materials Transactions, Vol.34A,February (2003), pp. (219-223).
27. K. Otsuka &Wayman, "Mechanism of Shape Memory Effect and Superelasticity", Cambridge University Press, Cambridge, (1998), pp.(27-48).
28. S. Nemat-Nasser et al. "Very high strain-rate response of a NiTi shape-memory alloy" Mechanics of Materials, No.37, (2005), pp.(287–298).
29. S.W. Robertson et al "Effect of Product form and heat treatment on the Crstallographic texture of Austenitic Nitinol" Journal Materials Sciences,No.41,(2006), pp.(621-630).
30. S. Nemat -Nasser et al "High Strain-Rate, Small Strain Response of a NiTi Shape-Memory Alloy" Journal of Engineering Materials and Technology JANUARY, Vol. 127, (2005), pp (83-89)

31. J. Van Humbeeck & Stalmans R, "Characteristics of shape memory alloys", Shape memory materials, Cambrige University Press, Cambridge, (1996) pp. (149-183).
32. Y. Zhao et al. "Compression behavior of porous NiTi shape memory alloy" Acta Material, No.53, (2005) pp. (337–343)
33. Y. Sekiguchi, "Applications of Shape Memory Alloys, Medical Applications", Shape memory alloys, Volume 1. Gordon and Breach Science Publishers, New York, (1998) pp. (226-269).
34. T. W. Duerig et.al, "Engineering Aspects of Shape Memory Alloys", Butterworth- Heinemann, London (1990), pp (15, 97, 207, 295-296, 394-395, 446).
35. J.Y. Choi & S.Nemat Nasser "Effect of annealing and initial temperature on mechanical response of Ni-Ti-Cr shape-memory alloy" Materials Science Engineering, A 432, (2006), pp. (100-107)
36. D. CUBELA "The Research of Technological Parameters Influence on the Process of Nitinol Fabrication and Plastic Deformation" Metalurgija Vol.45, No.1, (2006), pp. (61-66).
37. Kaushik et al. "Symmetry and reversibility of martensitic transformations "Division of Engineering and Applied Science, California Institute of Technology, January 15, (2004), pp. (1-11).
38. K. Otsuka, X. Ren "Physical metallurgy of Ti-Ni based shape memoryalloys" progress in materials science 50 (2005),pp. 511-678.
39. SMA Inc., "Shape Memory Applications", 1999.
40. N.B.Morgan" Medical shape memory alloy applications-the market and its products", Materials Science and Engineering, A 378, (2004), pp. (16-23).
41. Y.S. Kim et al "Nitinol Spring rod dynamic Stabilization System and Nitinol memory Loops in Surgical Treatment for Lumber disc Disorders " Neurosurg Focus, Vol.22, January, (2007), pp. (1-9)

42. Lizhen et al "Biocompatibility Improvement of NiTi with a Functionally Graded Surface" Society for Experimental Mechanics, Annual Conference Proceedings, Milwaukee, (2002).
43. R. Hernandez et al. "Characteristics of Porous nickel-titanium alloy for medical applications" Bio-Medical Materials and Engineering, No.12, (2002), pp.(37-45).
44. M. Scott &Christian Greiner, "High strength, low stiffness, porous NiTi with superelastic properties" Acta Biomaterialia, 1, (2005), pp. (705716).
45. A.L. McKELVEY & R.O. RITCHIE "Fatigue-Crack Growth Behavior in the Superelastic and Shape-Memory Alloy Nitinol" Metallurgical and Materials Transactions, No.32, March (2001) PP.(731-738)
46. .N.I.Zahari et al. "Amicrocrystallpgraphic Study of Fatigue Damage inTi-Ni Shape Memory Alloy" Ti-2003 Science and Technology, Vol.3,(2003), pp. (1903-1910).
47. X. Wang, & J.J. Vlassak "Crystallization kinetics of amorphous NiTi shape memory alloy thin films" Scripta Materialia, Vol.54,(2006) pp.(925-930).
48. C. Chan, C. Trigwell and T. Duerig, "Oxidation of an NiTi Alloy", (1990) .pp. (349-354).
49. F. Villermaux et.al., "Laser Treatment of NiTi Shape Memory Alloy Biomaterials", (1997), pp. (62-66).
50. L. Tan &W.C. Crone "Surface characterization of NiTi modified by plasma source ion implantation", Acta Material, 50, (2002), pp. (4449-4460).
51. P. Filip et. Al., "Physics of Hydroxyapatite Plasma Coatings on NiTi Shape Memory Materials", Mater. Sc. Eng. A234-236, (1997), pp. (422-425).

52. D. Wever, et. Al., "Electrochemical and Surface Characterization of aNickel-Titanium alloy", Biomaterials 19 (1998), pp. (761-769).
53. V. Chuprina, "A Study of the Process of Oxidation of Titanium Nickelied", (1989), pp. (57-61).
54. I. Olefjord, S. Hansson and L. Eng, "Surface Analysis of Four Dental Implant Systems", (1993), pp. (32-40).
55. C. Trepanier, et. al., "Effect of Modification of Oxide Layer on NiTi Stent Corrosion Resistance", J. Biomed. Mater. Res. 43, (1998), pp. (433-440).
56. S. Shabalovskaya, et.al. "Surface and Corrosion Aspects of NiTi Alloys", in: Third Int, Conf. Shape Memory and Superelastic Technologies, Pacific Grove, CA, May (2000).
57. S. Shabalovskaya and J. Anderegg, "Surface Spectroscopic Characterization of TiNi Alloys for Implants", J. Vac. Sc. Tech. A13 (5), (1995), pp. (2624-2632).
58. C. Shih, et. al. "Increased corrosion resistance of stent materials by converting current surface film of polycrystalline oxide into amorphous oxide", (2000), pp. (323-332).
59. He, G., P. Liu, and Q.J.J.o.t.m.b.o.b.m. Tan, *Porous titanium materials with entangled wire structure for load-bearing biomedical applications.* 2012. **5**(1): p. 16-31.
60. Elias, C., et al., *Biomedical applications of titanium and its alloys.* 2008. **60**(3): p. 46-49.
61. Abd-elrhman, Y., et al., *Compatibility assessment of new V-free lowcost Ti–4.7 Mo–4.5 Fe alloy for some biomedical applications.* 2016. **97**: p. 445-453.
62. . Yao, C., J. Lu, and T. Webster, *Titanium and cobalt–chromium alloys for hips and knees*, in *Biomaterials for artificial organs*. 2011, Elsevier. p. 34-55.

63. Zaripova, F., A.Y. Eroshenko, and T. Petrashova. *BIOMATERIALS: APPLICATION OF METALS IN MEDICINE*. in *ВЫСОКИЕ ТЕХНОЛОГИИ В СОВРЕМЕННОЙ НАУКЕ И ТЕХНИКЕ*. 2013.
64. Scott, W.N., *Insall & Scott Surgery of the Knee E-Book*. 2011: Elsevier Health Sciences.
65. Vinarcik, E.J., *High integrity die casting processes*. 2002: John Wiley & Sons.
66. Callister, W.D. and D.G. Rethwisch, *Materials science and engineering*. Vol. 5. 2011: John wiley & sons NY.
67. Erdem, O.J.U.M.A.v.G.D., *The Development and Applications of Powder Metallurgy Manufacturing Methods in Automotive Industry.* 2017. **9**(3): p. 100-112.
68. Kipouros, G., et al., *On the advantages of using powder metallurgy in new light metal alloy design.* 2006. **37**(12): p. 3429-3436.
69. Groover, M.P., *Introduction to manufacturing processes*. 2011: Wiley Global Education
70. Sharma, P.J.S.C. and Co. Ltd. Publications, *Production Technology.* 2004
71. F. Auricchio, E. Boatti, and M. Conti. Sma biomedical applications. In L. Lecce and A. Concilio, editors, Shape Memory 145Alloy Engineering: for Aerospace, Structure and Biomedical Applications, chapter 11, pages 307–341. Elsevier Ltd., 2015.
72. Machado LG & Savi MA (2003) Medical applications of shape memoryalloys. Braz J.Med Biol Res 36: 683-691.
73. Ozeki K, Yuhta T, Aoki H, Asaoka T, Daisaku T & Fukui Y (2003) Deterioration in the superelasticity of Ti sputter coated on NiTi orthodonticwire. Biomed Mater Eng 13:355-362.
74. Tarniţă, D., Tarniţă, D.N., Bîzdoacă, N., Mîndrilă, I., & Vasilescu, M. 2009. Properties and medical applications of shape

memory alloy, *Romanian Journal of Morphology and Embryology*, vol. 50, no. 1, pp. 15-21.

75. K. Otsuka and X. Ren, "Physical metallurgy of Ti-Ni-based shape memory alloys," Prog. Mater. Sci., vol. 50, no. 5, pp. 511–678, 2005.
76. C. P. Frick et al., "Thermal Processing of Polycrystalline NiTi Shape Memory Alloys," MRS Proc., vol. 855, 2004.
77. https://www.imoa.info/molybdenum-uses/molybdenum-metal-alloys.php Haldar, A., Suwas, S., Bhattacharjee, D.: Microstructure and texture in steels, Springer, 2009. ISBN: 978-1-84882-453-9.
78. Sahib M. Al-Saffar ,,Effect of Alloying Elements (Mo) on Biomaterials Ni-Ti Shape Memory Alloys,, Eng. & Tech. Journal , Vol.32,Part (A), No.4, 2014.
79. D. Mantovani "Shape memory alloys: Properties and biomedicalapplications" JOM 52, 10; ABI/INFORM Trade & Industry, PP. 36-44, 2000
80. D.A.porter" Phase transformations in metals and alloys" 2nd edition, Chapan L Hall, 2-6 Bormdary Row, London SEl m, LX,1992.
81. S.A. Thompson, "An overview of nickel-titanium alloys used in dentistry," International Endontic Journal, 33, 297-310, (2000).
82. J. Ryhänen" Biocompatibility evaluation of nickel-titanium shape memory metal alloy" Oulu University Library, 1999.
83. N.B. Morgan, "Medical shape memory alloy applications – the market and its products," Materials Science and Engineering, A 378, 16-23, (2004)
84. Elahinia H. M., Hashemi M.,Tabeshi M., & Bhaduri B. S., 2012, Manufacturing and Processing of NiTi implants:A review, Progress in Materials Science, 57(5), 911-946.

85. Otsuka, K., and Ren, X., 2005, Physical metallurgy of Ti-Nibased shape memory alloys, Progress in Materials Science, 50, pp. 511–678.

86. L. Mertz, "What Is Biocompatibility?: A New Definition Based on the Latest Technology," IEEE Pulse, vol. 4, no. 4, pp. 14–15, Jul. 2013.

87. C. Trepanier and A. R. Pelton, "Biocompatibility and corrosion resistance of NiTi," Nitinol Devices & Components, pp. 1–9.

88. S. A. Shabalovskaya, "On the nature of the biocompatibility and on medical applications of NiTi shape memory and superelastic alloys.," Biomed. Mater. Eng., vol. 6, no. 4, pp. 267–289, 1996

89. A. Holton, E. Walsh, A. Anayiotos, G. Pohost, and R. Venugopalan, "Comparative MRI Compatibility of 316L Stainless Steel Alloy and Nickel???Titanium Alloy Stents," J. Cardiovasc. Magn. Reson., vol. 4, no. 4, pp. 423–430, 2003.

90. D. Stoeckel, A. Pelton, and T. Duerig, "We are Nitinol. TM Self-Expanding Nitinol Stents - Material and Design Considerations Self-Expanding Nitinol Stents - Material and Design Considerations," vol. 683, 1995.

91. Huang, K. Y., & Jane, C. J. (2009). A Hybrid Model for Stock Market Forecasting and Portfolio Selection Based on ARX, Grey System and RS Theories. *Expert Systems with Applications*, 36(3), 5387-5392.

92. Huang, S. J., Chiu, N. H., & Chen, L. W. (2008). Integration of the Grey Relational Analysis with Genetic Algorithm for Software Effort Estimation. *European Journal of Operational Research*, 188(3), 898-909.

93. Julong, D. (1989). Introduction to Grey System Theory. *The Journal of Grey*

System, 1(1), 1-24.

94. Kuah, C. T., & Wong, K. Y. (2011). Efficiency Assessment of Universities

through Data Envelopment Analysis. *Procedia Computer Science*, 3, 499-506.

95. Kung, C. Y., & Wen, K. L. (2007). Applying Grey Relational Analysis and

Grey Decision Making to Evaluate the Relationship between Company Attributes and its Financial Performance-A Case Study of Venture Capital Enterprises in Taiwan. *Decision Support Systems*, 43(3), 842-852.

96. Kuo, Y., Yang, T., & Huang, G. W. (2008). The Use of Grey Relational Analysis in Solving Multiple Attribute Decision-Making Problems. *Computers & Industrial Engineering*, 55(1), 80-93.

97. Lebas, M. J. (1995). Performance Measurement and Performance Management. *International Journal of Production Economics*, 41(1-3), 23-35.

98. Lin, C. L., Lin, J. L., & Ko, T. C. (2002). Optimisation of the EDM Process

Based on the Orthogonal Array with Fuzzy Logic and Grey Relational Analysis Method. *The International Journal of Advanced Manufacturing Technology*, 19(4), 271-277.

99. Elahinia, M.H.; Hashemi, M.; Tabesh, M.; Bhaduri, S.B. Manufacturing and processing of NiTi implants: A review. Prog. Mater. Sci. 2012, 57, 911–946.

100. Sun, L.; Huang, W.M.; Ding, Z.; Zhao, Y.; Wang, C.C.; Purnawali, H.; Tang, C. Stimulus-responsive shape memory materials: A review. Mater. Des. 2012, 33, 577–640.

101. E. Zanaboni, " One way and two way–shape memory effects: thermomechanical characterization of Ni–Ti wires" M.Sc. Thesis, biomedical engineering department, Pavia University, 2008.

102. E . patoor , D . C. Lagoudas and P. B. Entcheve , " Shape memory alloys , part I : General properties and modeling of single crystals " , Mechanics of Materials , Vol . 38, 2006, PP. 391 - 429.

103. Z. J. Ridha , " Preparation and studying properties of NiTi SMA coated with biocompatible layer ", MSC. Thesis, Material engineering, university of Babylon, 2016.

104. G. Olender, R .Pfelfer and C. W. Muller " A preliminary study of bending stiffness alteration in shape changing nitinol plates for fracture fixation", Biomedical engineering, Vol. 39, No. 5, 2011, PP. 1546 - 1554.

105. S. Lombard and P. Poncet , " Metallurgical principles of Nitinol and its use in interventional device " Any key words : Nitinol , shape memory , superelasticity , medical device , 2005 .

106. C. Dimities and Lagoudas," Shape memory alloys modeling and engineering application ", Texas AZM University, USA, 2008.

107. S.L. Angionic , M. Meo and A. Foreman ," Impact damage resistance and damage suppression properties of shape memory alloys in hybrid composites - a previous " smart Mater . Strut. , Vol 20, 2011, PP. 1 - 24

108. T. Yoneygma and S. Miyazaki, " Shape memory alloys for biomedical application" Cam Bridge, England, 2009.

109. A. Biscarini, G. Mazola and A. Tuissi," Enhanced Nitinol Properties for Biomedical application ", Biomedical Engineering, Vol. 1, No. 3, 2008, PP. 180 - 196.

110. Naresh, N.; Vreeland, T.; Ahrens, T.J.: Microstructural modifications in a dynamically consolidated microcrystalline nickel–titanium alloy powder. J. Mater. Sci. 22, 4446–4452 (1987).

111. .S. Dilibal, H.Adanir "Comparison and Characterization of NiTi and NiTiCu Shape Memory Alloys" Marmara University, Istanbul/Turkey, 2013.

112. Nawal M. Dawood, "Preparation & Characterization of Coated & Cu alloyed Bio Nitinol", Ph.D. thesis, University of Technology, Department of Materials Engineering, Baghdad, 2014.

113. T. Goryczka and J. V. Humbeek, " Characterization of a Ni Ti Cu shape memory alloy produced by powder technology ", Journal of achievement in materials and manufacturing engineering, Vol.17, Issue. 1–2, 2006, pp.65 – 68.

114. M. A. Sadeq, " Corrosion behavior of biocompatible coatings of porous NiTi shape memory alloy ", ph. D. Thesis, production engineering and metallurgy department, university of technology, 2013.

115. X . Li , J . Wang and E. H. Han," Influence of fluoride and chloride on corrosion behavior of NiTi orthodontic wires ", acta biomaterial, Vol. 3 , 2007 , p . 807 - 815.

116. J. Cv jov ć-Alajić, I., Cv jov ć, Z., M ov ć, S., P n ć, V. n R k n, M. (2011) 'Wear and corrosion behaviour of Ti–13Nb–13Zr and Ti–6Al–4V alloys in simulated physiological solution', Corrosion Science, Vol. 53, No. 2, pp.796-808.].

117. N. Pessal and L. Liu, " Determination of Critical Pitting Potentials of Stainless Steel in Aqueous Chloride Environments", Electrochem. Acta, (1987).

118. M. Barbosa, "Corrosion Mechanism of Metallic Biomaterials", in: Biomat. Degrad. Elsevier Science Publisher, (1991), pp. (227-257).

119. C.Dimities and Lagoudas. "Shape memory alloys modeling and engineering application" ,Texas AZM university, USA,2008.

120. W. Carroll, M. Kelly and B. Brien, "Corrosion Behavior of Nitinol Wires in Body Fluid Environment", in: Int. Conf. on Shape Memory and Superelastic Technologies, Antverpen, (1999), pp. (240-249).

121. V. Gyunter, et. al. "Shape Memory Effects and Their Applications in Medicine", Nauka, Siberian Branch, Novosibirsk, (1992).

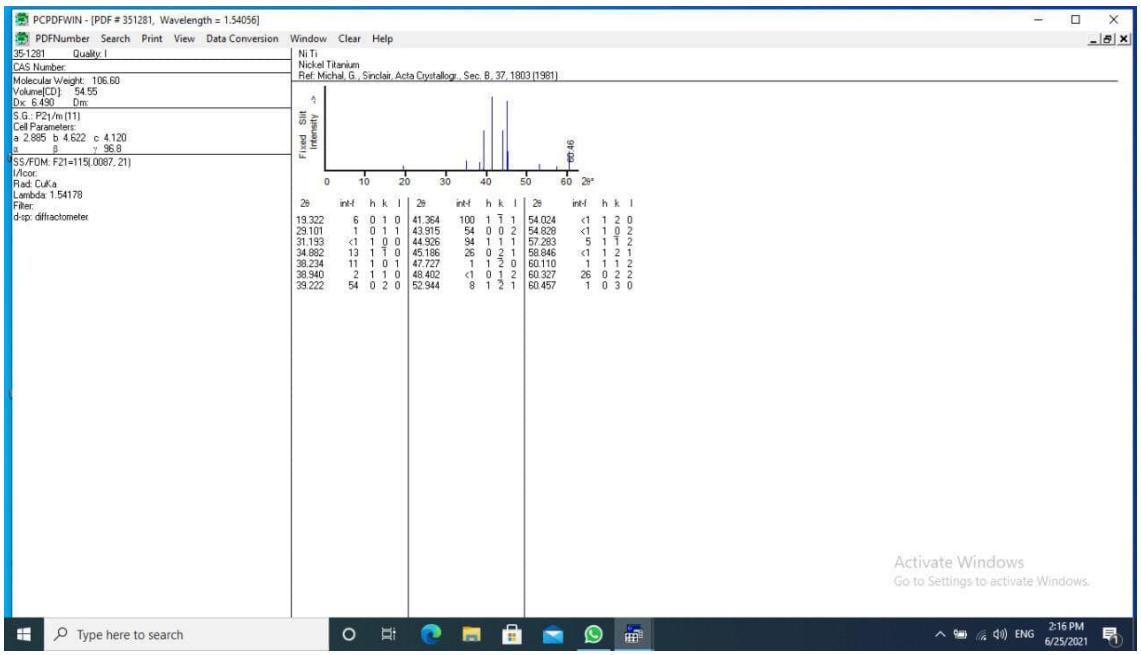

Fig. (1): X-Ray Diffraction of Phase NiTi standard

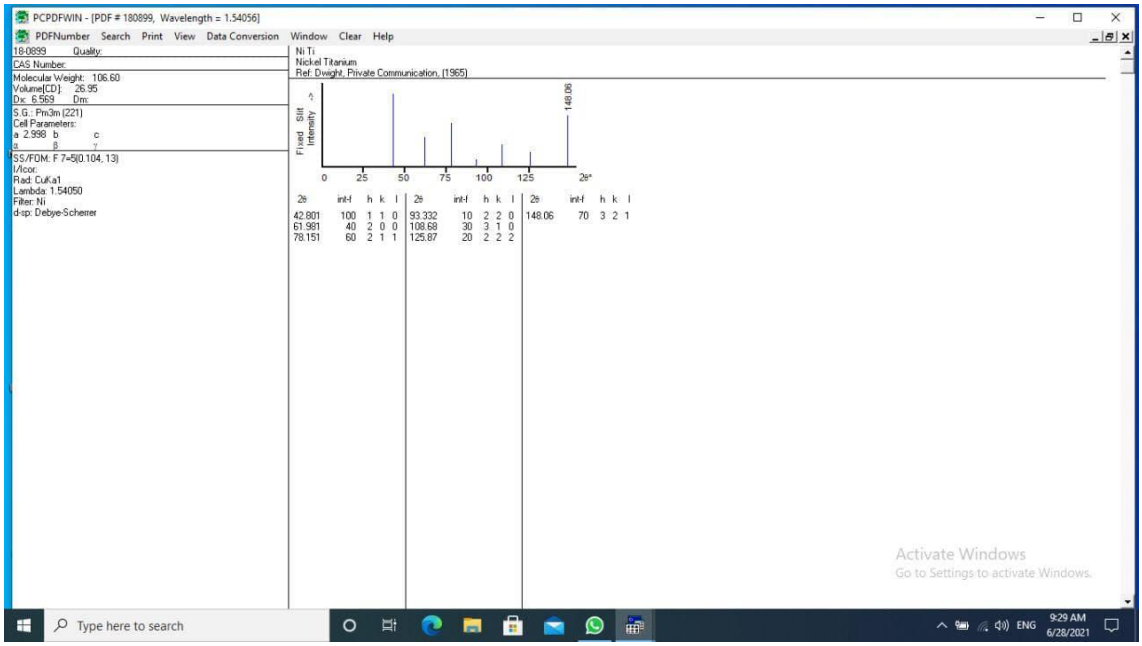

Fig (2): X-Ray Diffraction of Phase NiTi standard.

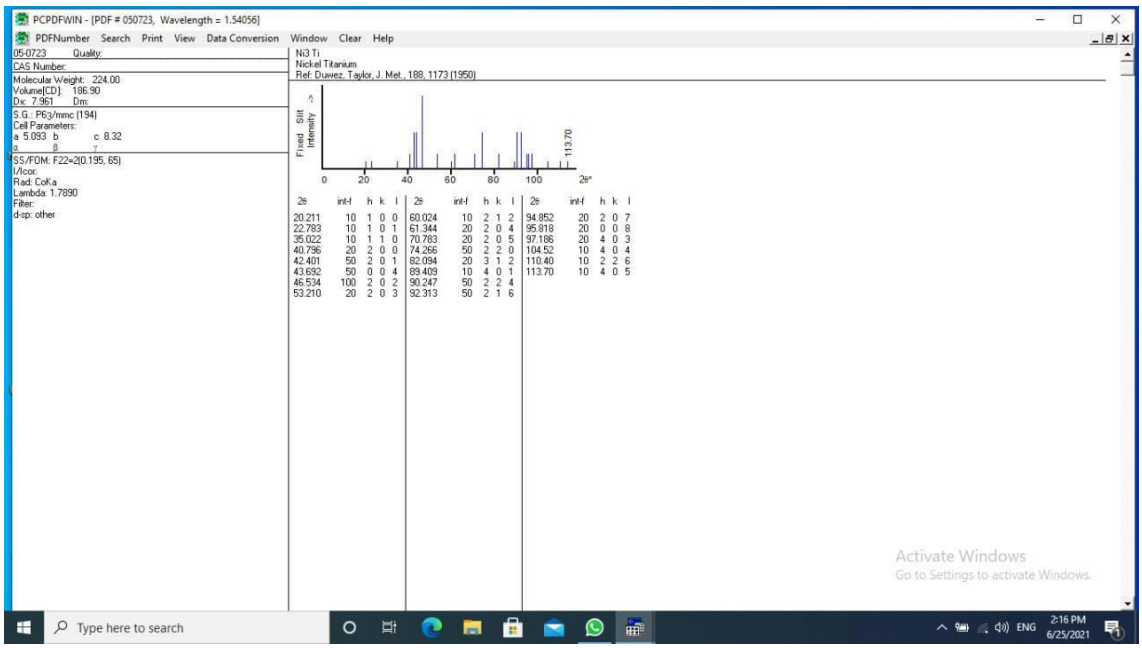

Fig (3):X-Ray Diffraction of Phase Ni3Ti standard.

وزارة التعليم العالي والبحث الـــعلمي
جـامـــعـــــــة بـابـــــــــل
كليـــــــة هنـــــــــدسة المواد
قسـم هنـــــــــــدسة المـعـادن

تأثير (Zr,Mo) على البنية المجهرية وخواص سبائك ذاكرة الشكل NiTi الطبية .

رسالة

مقدمة إلى قسم هندسة المعادن في كلية هندسة المواد/ جامعة بابل وهي جزء من متطلبات نيل درجة ماجستير في هندسة المواد /المعادن .

من قبل

نريمان ياسين علي عبود

بإشراف

ا.د. جاسم محمد سلمان المرشدي

2021م 1943 هـ

الخلاصة

تم اكتشاف خواص سبائك ذاكرة الشكل للنيكل تيتانيوم (NiTi) لأول مرة في أوائل الستينيات ، حيث كان لسبائك ذاكرة الشكل العديد من التطبيقات،تم استخدام سبائك NiTi بشكل متزايد في الأجهزة الطبية الحيوية الخارجية والداخلية ، على سبيل المثال أسلاك دعامة القلب ، وتقويم الأسنان ، وكسور الأوعية الدموية والعظام ، ولوحات التثبيت و مسامير المسالك البولية الذاتية التوسع. تم تحضير سبائك ذاكرة الشكل NiTi من مساحيق النيكل والتيتانيوم الأولية بواسطة ميتالورجيا المساحيق ، عند ضغط 800 ميجا باسكال ، ودرجة حرارة 950 درجة مئوية و10^{-3} تور في جو فراغ . من أجل تقييم أداء هذه السبيكه ، تم اعتماد على العديد من التوصيفات مثل تحليل حيود الأشعة السينية XRD والمسح المجهري الإلكتروني (SEM) باستخدام EDS والصلاده والاختبار الكهروكيميائي في محلول رنكر. كشفت النتائج عند تحليل XRD أن Ni-Ti قد تم تغييره بالكامل إلى NiTi (في الطور المكعب والاحادي) و Ni_3Ti ولكن عند إضافة الزركونيوم بمعدل 3٪ ظهر مركب وهو Ni_7Zr_2.

يتم طحن العينات في جو جاف ويتم صقل العينات بعد تلبيدها. الفحص المجهري البصري ، تقنيات حيود الأشعة السينية. تم إجراء اختبار الصلاده باستخدام آلة الصلاده برينل. لوحظ أنه مع زيادة محتوى Zr ، تزداد قيم الصلاده. على سبيل المثال ، تساوي 30٪ من NiTi حيث كانت صلاده قدرها 127.05 والتي زادت بشكل ملحوظ مع زيادة محتوى Zr إلى عند 03٪. زيادة الصلاده تشير إلى قابلية التشغيل. لوحظ أنه مع زيادة محتوى Mo ، تزداد قيم الصلاده. على سبيل المثال ، كان لدى NiTi صلاده قدرها 127.05 والتي زادت إلى 40٪. تظهر المناطق المضيئة والمناطق المظلمة في المجهر البصري و SEM. هذا يؤكد المراحل التي تظهر XRD، وهي في المناطق الفاتحة Ni_3Ti والمناطق الغامقه NiTi. وبسبب المولبيدينوم ، يكشف الفحص المجهري البصري عن خصائص السطح مثل المساميه المفتوحة وحدود الحبيبات ، بالإضافة إلى التمييز بين الاطوار NiTi و Ni_3Ti.

أظهر تآكل سبائك NiTi تحسنًا ملحوظًا بعد إضافة Mo و Zr في محلول رينجر. تم إثبات أن التقدم الكبير في التحسن عند 1٪ و 2٪ و 3٪ من وزن Zr كان 87٪ و 89٪ و 57٪ على التوالي في محلول رينجر. بينما عند إضافة 1٪ و 2٪ و 3٪ من وزن Mo ، كانت نسبة التحسن 50٪ و 16٪ و 8٪ على التوالي في محلول رينجر . ومع ذلك ، فإن نتيجه اضافه Zr للسبيكه الأساسية تعطي خصائص ممتازة. تحسين معدل البلى لـ NiTi عند إضافة Mo و Zr تحت الحمل 15N، عند إضافة Mo ، يكون فقدان الوزن أقل مما هو عند إضافة Zr ويزداد فقدان الوزن مع زياده الوقت.